DNA HELIX-STACK SWITCHING AS THE BASIS FOR THE DESIGN OF VERSATILE DEOXYRIBOSENSORS

by

Carlo Giovanni Sankar
B.Sc., Simon Fraser University, 2001

THESIS SUBMITTED IN PARTIAL FULFILLMENT OF
THE REQUIREMENTS FOR THE DEGREE OF

MASTER OF SCIENCE

In the Department of
Molecular Biology and Biochemistry

SIMON FRASER UNIVERSITY

Fall 2004

SIMON FRASER UNIVERSITY

PARTIAL COPYRIGHT LICENCE

APPROVAL

Name: **Carlo Giovanni Sankar**

Degree: **Master of Science**

Title of Thesis: **DNA Helix-Stack Switching as the Basis for the Design of Versatile Deoxyribosensors**

Examining Committee:

Chair: **Dr. N. Branda**

Dr. D. Sen
Senior Supervisor
Professor / Departments of Molecular Biology and Biochemistry and Chemistry

---

Dr. P.J. Unrau
Committee Member
Assistant Professor /Department of Molecular Biology and Biochemistry

---

Dr. H. Yu
Committee Member
Assistant Professor /Department of Chemistry

Dr. R. H. Hill
Committee Member
Associate Professor /Department of Chemistry

Dr. J. L. Thewalt
Public Examiner
Associate Professor/ Departments of Molecular Biology and Biochemistry and Physics

Date Approved: October 12th, 2004

ABSTRACT

The charge conduction properties of deoxyribonucleic acids (DNA) can be harnessed for monitoring the binding of a ligand to its receptor. Here, we show how DNA-based sensors (deoxyribosensors) consisting of a photo-activated oxidant tethered to a receptor-containing DNA molecule can be used to monitor the presence of a ligand. Phosphorescence measurements, reflective of changes in charge conduction to a targeted region in these deoxyribosensors are made in the presence and absence of the test ligand. The deoxyribosensors described here, exploit established rules for DNA helical stacking in three-way junctions and use previously selected aptamer sequences as receptors for target analytes. More specifically, a systematic investigation outlining the characteristics of a deoxyribosensor for the detection of the amino acid derivative, argininamide are presented. These results suggest a general design for deoxyribosensors for any molecular ligand for which an aptamer sequence can be obtained. Also, a new methodology for investigating helical stacking of nucleic acids of unknown tertiary structure, such as DNAzymes or RNAzymes is discussed.

DEDICATION

This thesis is dedicated to my family. Through our toughest times we have been there for each other and I could not have accomplished this with out your support, patience and motivation.

ACKNOWLEDGEMENTS

I would like to express my utmost gratitude to my senior supervisor Dr. Dipankar Sen for his relentless support, patience and guidance throughout my graduate studies. Dr. Sen has been an extraordinary mentor and friend; his passion for science, open mindedness and willingness to explore new frontiers, has given me the opportunity to be part of a very stimulating research environment.

Dr. Peter J. Unrau for helpful discussions, friendship and support throughout my graduate studies.

Dr. Hogan Yu for his helpful discussions, friendship, sense of humour and optimism throughout my graduate studies.

Dr. Ross H. Hill and Dr. Jenifer L. Thewalt for their patience and support in putting together this thesis.

Dr. Richard Fahlman for training me in the lab, his friendship and helpful discussions. Dr. Fahlman's input on the work presented in this thesis was invaluable.

Past and present members of the Sen Lab for their friendship and helpful discussions; Richard Fahlman, Anat Feldman, Dennis Wang, Dan Chinnapen, Yong Liu, Ed Leung, Kelly Cadiuex, Yi-Jeng (Y.J.) Huang, Becky Thorne and Hyun-Wu Lee.

My collaborators from the Yu Lab; Chuan-Yun Luo, Lily Su and Navanita Sarma.

Koman Joe for his and help with the HPLC, his friendship and helpful discussions.

Everyone in the MBB Department, especially: Leslie Mitchell, Dan Chinnapen, Himani Hutkhede, Ashvinder Bhogal, Carlo Artieri, Amit Goel, Will Hsiao, Jim Stewart, Laila Singh, Kush Dalal, Jillian Smith, Michael Ng, Luis Del Rio, Anat Feldman, Alfredo Menendez, Marinieve Montero, Melita Irving, Bari Zahedi, Minna Roh, Wendy Lee, Andrea Uetrecht, Yong Liu, Jackie Watson, Jay Cadiuex, Alex Ebhardt, Hani Zaher, Victor Lundin, Peter Stirling, Michel Leroux, Linda Pinto, Anna Gifford, Dev Sharma, Bruce Brandhorst, Willie Davidson, Evelyn Davidson, Ingrid Northwood, Andy Yim and Jenny Lum.

The Gang: Ferdinand Bancosta, Sheldon Hu, Rizwan Mohamed, Ramil Javerina, Hanna de Guzman and Ken Fung. You are my friends for life.

Last but definitely not least, my family; for their support, patience and motivation. Thank you mom, dad and Diana.

TABLE OF CONTENTS

LIST OF FIGURES

LIST OF TABLES

LIST OF ABBREVIATIONS

A	Adenine
Å	Angstrom (10^{-10} meters)
AQ	Anthraquinone
Arg	Arginine
ArgA	Argininamide
ATP	Adenosine Triphosphate
C	Cytosine
dA	deoxy-Adenosine
dC	deoxy-Cytidine
dG	deoxy-Guanosine
dH_2O	deionized H_2O
DMS	Dimethyl Sulfide
DNA	Deoxyribonucleic Acid
DNAzymes	DNA enzymes
dT	deoxy-Thymidine
E-8-17	DNA Enzyme 8-17
E-Bipartite	DNA Enzyme Bipartite
EDTA	ethylenediaminetetraacetic acid
FRET	Fluorescence Resonance Energy Transfer
G	Guanine
Lys	Lysine
NHS	N-Hydroxysuccinimide
NMR	Nuclear Magnetic Resonance
°C	degrees Celsius
PAPH	Phonon-Assisted Polaron-likeHopping
PCR	Polymerase Chain Reaction
R	Purine
RNA	Ribonucleic Acid
RNAzymes	RNA enzymes
rRNA	ribosomal RNA
SELEX	Systematic Evolution of Ligands with Exponential Enrichment
S-multi	Substrate to multiple enzymes via Watson-Crick base pairing
Spd	Spermidine
Theo	Theophylline
tRNA	transfer RNA
T	Thymine
U	Uracil
W.C	Watson-Crick
Y	Pyrimidine

CHAPTER 1: INTRODUCTION AND BACKGROUND

1.1 Chapter Overview

The material in this chapter is intended to give a brief background of the work presented in this thesis. The thesis work combines three well-studied areas of nucleic acids; nucleic acid aptamers, properties of three-way junctions and charge transfer through the DNA helix. These characteristics of nucleic acids are exploited to produce biosensors made of DNA (deoxyribosensors). This chapter takes DNA out of its typical biological role and describes it in an *in vitro* setting. Fundamental nucleic acid structures and properties are introduced to emphasize the structural variability of DNA giving rise to unique structures such as aptamers. Also, background information on the conformational variability of branched DNA, specifically of three-way DNA junctions, is described. The chapter concludes with a background on the phenomenon of charge transport in DNA, the key process for signal detection of the deoxyribosensors presented in this thesis.

1.2 The Biological Role of DNA

In the central dogma of molecular biology, the role that comes to mind for DNA is one for the storage of genetic information; which is the starting point for the passage of information: DNA→RNA→Protein. The ground-breaking discovery of the structure of DNA as a double helix in 1953 by Watson and Crick ultimately elucidated how DNA was replicated and transcribed (Watson and Crick 1953). The complemetary base pairing

between adenine and thymine (A-T) as well as guanine and cytosine (G-C) is the basis for DNA replication (Figure 1-1). During DNA replication, the two strands separate and are used by the replication machinery as templates for the synthesis of a newly synthesized strands. This feature makes DNA the ideal molecule for the storage of genetic information. Similarly in transcription, which is the generation of an RNA transcript from a stretch of genomic DNA, the copying process substitutes uracil (U) for thymine (T). This is the first process toward gene expression. In the cell DNA is generally present as long highly ordered and packed super-helices, which transiently undergo replication, transcription and recombination to suit the cell's needs.

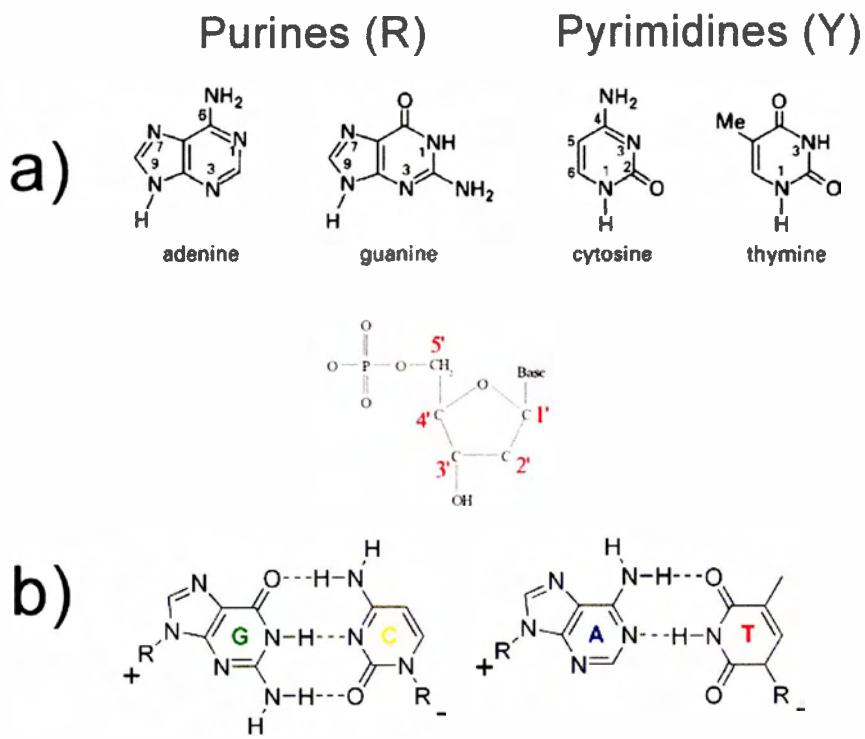

Figure 1-1 The elements of DNA: a) Nomenclature for the assignment of positions in the nitrogenous bases and sugar; b) Watson-Crick base pairing in DNA. Strand Polarity is indicated as (+) or (-), which represent the backbone going into or coming out of the plane respectively. Strand polarity is defined as the backbone going into the page in the 3'to 5' direction and is designated (+). R represents the deoxyribose sugar.

1.3 DNA Structure and Properties

Aside from being the molecule of choice for the storage of genetic material, DNA (as well as RNA) offers a plethora of structural and physical properties which can be exploited *in vitro*. Given the opportunity, DNA as a class of molecules, has the potential to offer structural variability by adopting complex three-dimensional conformations giving this family of molecules properties typically not associated with DNA. In the field of nucleic acids, *in vitro* selection, or SELEX (Systematic Evolution of Ligands with Exponential enrichment) has empowered researchers to obtain such complexly folded DNA molecules having properties typically not associated with them. Some of these DNA molecules that have been obtained through SELEX have catalytic properties (DNAzymes or if RNA, RNAzymes) and ligand binding sequences called aptamers. An aptamer is a DNA molecule that has the property of binding its cognate ligand with high specificity and affinity. This name is an amalgamation of the Latin word "aptus", meaning to fit and the Greek word "mer" meaning parts or units. A simplified example for the selection of a DNA sequence, which binds a Ligand (L), is described in Figure 1-2.

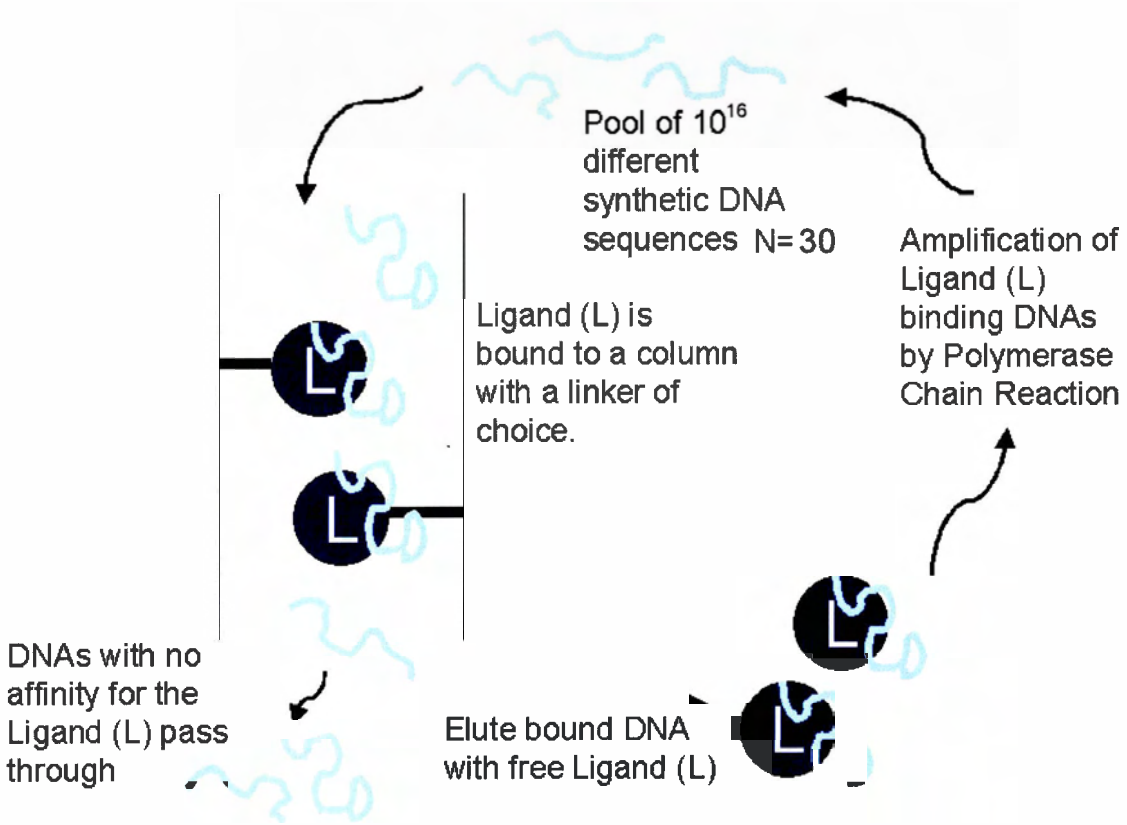

Figure 1-2 A simplified scheme for SELEX. This scheme outlines the steps involved in selecting a DNA molecule which binds Ligand (L). Nucleic acid molecules of this type are referred to as "aptamers".

For SELEX to be successful, a diverse amount of distinct DNA molecules is needed. Here we start with a pool of 10^{16} different single stranded DNA sequences. Each DNA molecule in the pool is designed such that it contains a random region (in this example the random region is made up of 30 nucleotides) flanked by known sequences, which serve as sites for primer binding during amplification by Polymerase Chain Reaction (PCR). The pool of DNA molecules is then subject to a selection pressure that discriminates for the ability to bind a specific ligand (L). In Figure 1-2, the DNA molecules are passed through a column containing an immobilized ligand (L). The successful molecules bind ligand (L) and the unsuccessful ones pass through the column. The ligand binding DNA molecules are then eluted from the column using free ligand and are the subject to amplification by PCR. This process is repeated and thus multiple

rounds of "selection" are performed to obtain a DNA sequence(s) that bind the ligand with high specificity and affinity.

In SELEX, a large number of different sequences are used in attempts to cover as much of the possible DNA sequence combinations in a random nucleotide region. For example, a random region of 30 nucleotides has 4^{30} or $\sim 10^{18}$ different possible sequences. Synthetic limitations confine most random pool libraries to at most 10^{16} different sequences and thus only a small percent of the total possible sequences are covered. This means that for the case of an N=30 nucleotide random region, only 1% of the sequence space is covered. Nevertheless, for most selection experiments, the important statistic is not the amount of copies of the different possible sequences or the coverage of sufficient sequence space, but the number of successful species present in the pool. The presence of successful species in a pool varies from $1{:}10^{6}$ to $1{:}10^{12}$, depending on the target and the stringency of selection. Generally the size of the random pool library is not an obstacle for the isolation of aptamers. For a detailed discussion on sequence space in SELEX see the following review by Osborne and Ellington (Osborne and Ellington 1997).

Another trait of DNA is its ability to self-assemble into multi-unit assemblies and arrays. This is due to the highly specific recognition of sequence complementarity by individual DNA strands and the fact that in aqueous solutions, a DNA double helix (of < 150 base pairs) has physical and hydrodynamic properties much like a rigid rod (Hagerman 1988). The assembly of DNA into multi-subunit structures has been used as a scaffold for organizing gold microbeads into ordered structures (Mirkin *et al.* 1996). Recent developments have shown that these nano-scale objects have lattice or crystalline

like structure (Paukstelis *et al.* 2004). For a more detailed discussion on nano-scale objects made of DNA see the following reviews by Seeman (Seeman 1999; Seeman 2003; Seeman 2003).

Beyond DNA's ability to form complex three-dimensional structures and ordered arrays, it also has the potential to form structures with conformational variability. Certain DNA structures have the ability to change conformation depending on their environment. These conformational changes can be in response to a specific molecule or stimulus. Much of these changes can be characterized as a toggling between one form and another, in a "switch" like fashion. This dynamic ability of DNA has been successfully exploited in regulating the activity of nucleic acid enzymes in an allosteric fashion (Soukup and Breaker 2000). Currently, the conformational variability of nucleic acids is being pioneered in the development of DNA based sensors and is the subject of the work presented here.

Designing conformationally variable DNA molecules entails combining common DNA motifs with ones that are not so common, such as the aptamers mentioned above. In the sections to follow, examples of common DNA motifs and their properties are discussed to provide a background for the work in this thesis.

1.3.1 Structure of the DNA Double Helix

In the cell, the most common structural motif that DNA is found in is the double helix. Here, the two complementary strands are stabilized by Watson-Crick hydrogen bonding and base stacking interactions. Under conditions of neutral pH and moderate (~physiological) salt concentrations, double helical DNA adopts a right-handed B-type

conformation as shown in Figure 1-3. The B-type helix is not dependent on sequence and any DNA molecule can form it provided that the complementary strand is available. Macroscopically, all B-type helices have a relatively similar structure; nevertheless variations in the fine local structure do occur and give rise to motifs that have special features, such as protein binding domains, and restriction sites.

Another type of right handed double helix that can be formed by DNA is the A-type helix also shown in Figure 1-3. The A-type helix is also formed when DNA and RNA are hybridized. Compared to the B-type helix, the A-type is a wider and shorter helix. In an A-type helix the axial rise per nucleotide is 2.56 to 3.29 Angstroms, where in a B-type helix the axial rise is significantly larger 3.03 to 3.37 Angstroms. When looking down the helix axis, the A-DNA has a hole down the center of the helix where as the B-type DNA does not. Another major structural difference is the base pair dislocation from the helix axis. In B-DNA the base pairs form a 90° angle with the helix axis, this is not the case for the A-type helix and as a result, it is not as well stacked as the B-type helix having poor electronic overlap.

A third type of double helix is the Z-type helix, which is different from the A and B type helix owing to its left-handed nature. Z-type helices require specific sequences such as alternating GC repeats and need relatively high salt conditions in order to form. (~2.5 M NaCl (Herbert and Rich 1999)). The concentration of salt required can be greatly diminished by the use of trivalent or tetravalent salts. The structure of the Z-type helix is shown in Figure 1-3. In the absence of a solution of high ionic strength, the GC repeats will simply adopt the B-type structure. Such a salt dependent transition from a B

to a Z –type helix has been exploited in the rational design of a DNA mechanical switch (Mao *et al.* 1999).

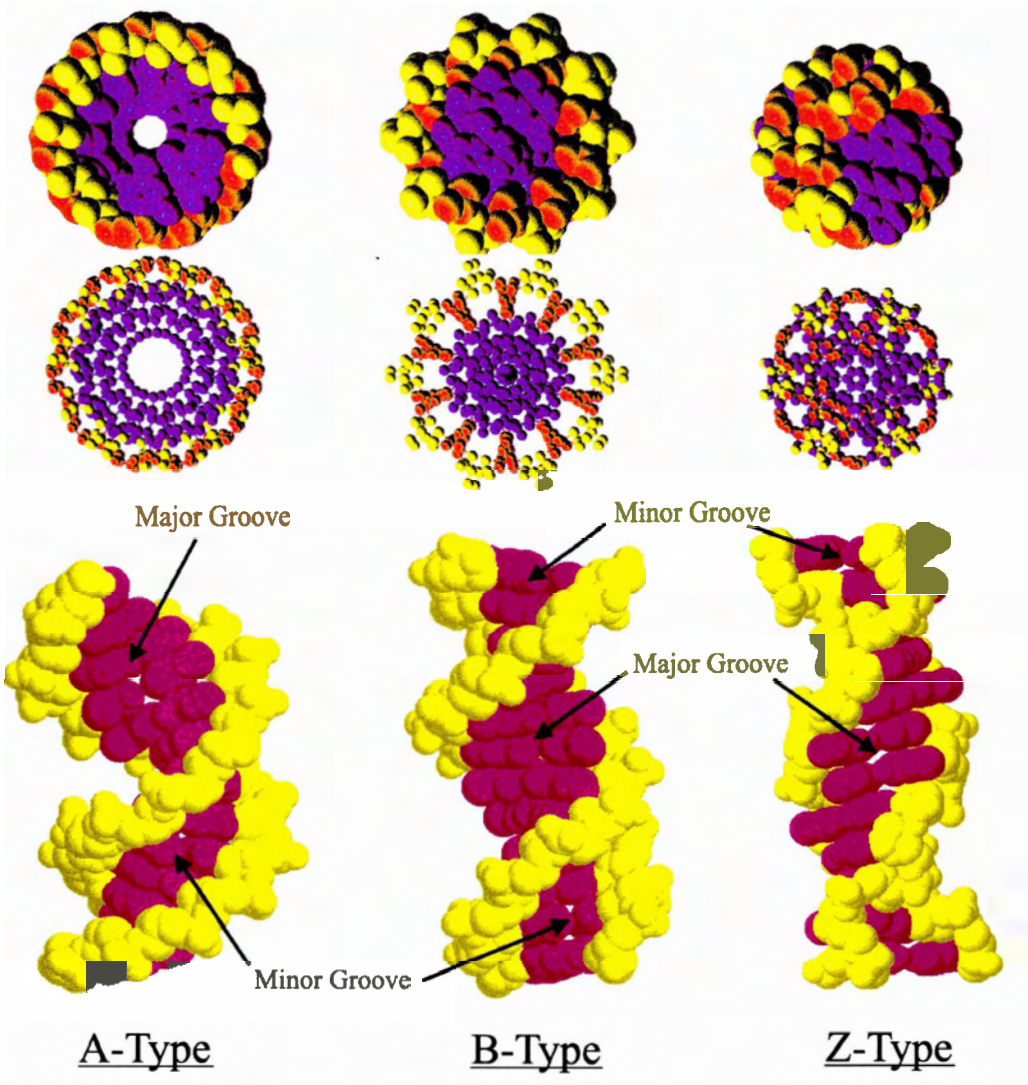

Figure 1-3 Models of double stranded DNA. The three families of double helices are shown; the A,B and Z-type helices. A view looking down the top of the helix is included above each model. Yellow represent the sugar and phosphate backbone and purple represent the nitrogenous bases. Models were constructed using the freeware program Jmol (http://jmol.sourceforge.net/).

1.3.2 DNA Structures of Higher Complexity

The structure of three different families of double helical DNA has been introduced. In the cell, DNA exists primarily as a double helix. The myriad of complex,

three-dimensional structures that DNA can form comes about when we incorporate "imperfections" to the DNA helix such as base pair mismatches or bulges. Typically these unique structures arise as a result of a single stranded DNA molecule folding upon itself. In the cell, most of the complex three-dimensional structures have been associated with RNA. A few examples of complexly folded RNA are structures like ribosomal RNA (rRNA) and transfer RNA (tRNA). The tRNA is a fascinating molecule that is a key component in protein synthesis. Due to its unique structure, tRNA can recognize a three nucleotide codon on one end and a protein building block (an amino acid) on the other.

Structures of higher complexity have been, in nature, associated to RNA primarily due to the 2'hydroxyl functionality. This extra functionality does not necessarily make RNA a better molecule for forming structures of higher complexity, since DNA, when given the chance, can accomplish comparable tasks if not the same. An example of where DNA and RNA were able to perform the same task arose when Szostak's group was isolating aptamer sequences specific for binding adenosine triphosphate (ATP) (Sassanfar and Szostak 1993) (Huizenga and Szostak 1995). The two aptamers that were isolated here, one made of RNA and the other of DNA, both exhibited similar binding affinities for their cognate ligand ATP (50 μM and 6 μM respectively).

Rare examples exist as well where the functional abilities of a nucleic acid molecule can occur whether composed of DNA or RNA. An example of this phenomenon is a nucleic acid enzyme displaying peroxidase activity when either made of RNA or DNA (Travascio *et al.* 1999). Another example where DNA has substituted for RNA is when DNA was used to reconstruct the anticodon domain of yeast $tRNA^{Phe}$

(Basti *et al.* 1996). For the resulting structure to be functional, some modifications had to be made to the DNA molecule. This lack of functionality shouldn't be regarded as DNA being inferior in its ability to form more complex functional structures because yeast $tRNA^{Phe}$ itself also needs the aid of some modified RNA bases, the most common of which are pseudouridine and inosine.

The folding of moderate length (~40 nucleotides) single stranded DNA upon itself can yield structures with novel functionalities. Examples of the most common structural motifs are shown in Figure 1-4.

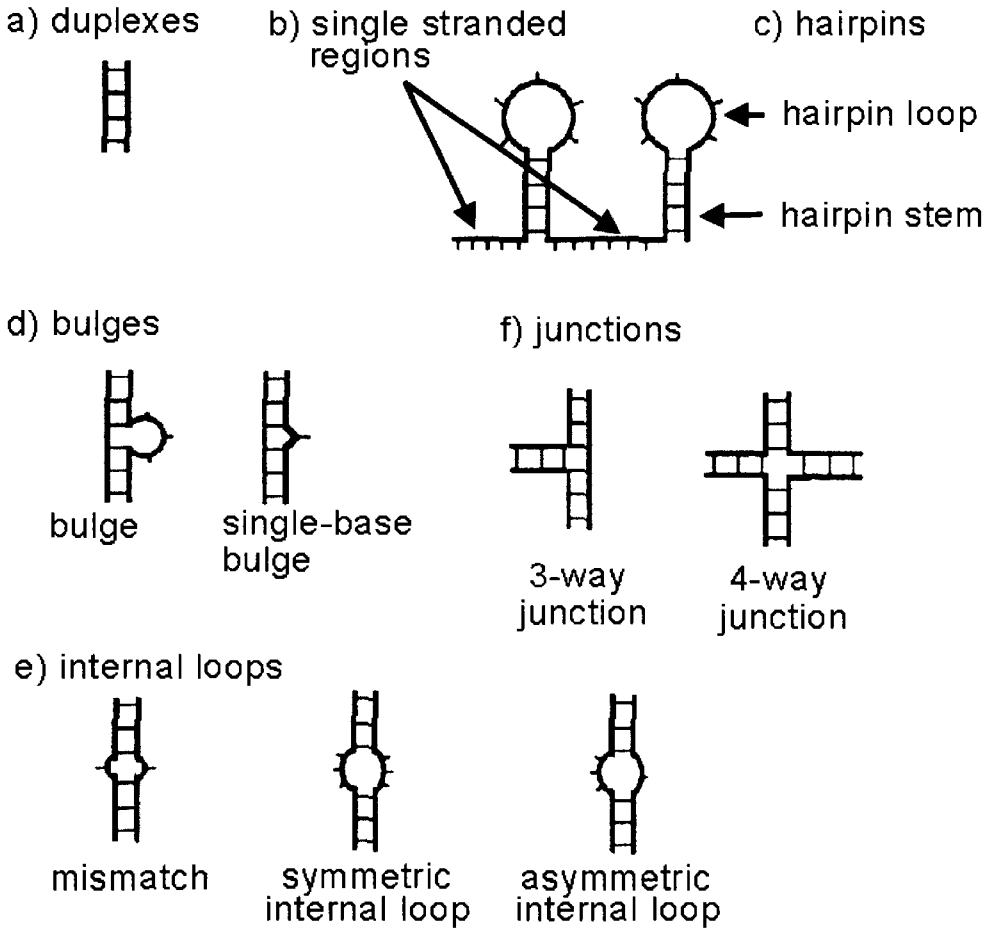

Figure 1-4 Common DNA (as well as RNA) secondary structure motifs.

1.3.2.1 Hairpins and Single stranded Regions

Single stranded regions, as the name implies, are regions in nucleic acids that do not base pair with any other part of the DNA molecule (Figure 1-4b). These single stranded regions can arise when certain sections of a single stranded DNA molecule contain internal complementary sequences and fold upon themselves making unique structures such as hairpins (see Figure 1-4c). The regions not involved in the hairpin stem are referred to as single stranded regions. Single stranded regions can serve as linking-structures, separating two DNA motifs (such as the two hairpins in Figure 1-4c). The actual hairpin loops themselves can also be referred to as single stranded regions, as well as bulges and internal loops (discussed below). It is also important to note that the bases in a single stranded loop can interact with themselves by the formation of intra-loop hydrogen bonds and base stacking interactions. Such interactions can influence the stability of the adjoining hairpin stem. One such example is that of tetra-loops, loops containing four nucleotides having sequence 5'-YYYR-3'(Santini *et al.* 2003).

1.3.2.2 Mismatches, Internal Loops and Bulges

DNA has the ability to form double helices even when not all of the nucleotides in the two strands are fully complementary. The local structures lacking complementarity can include base pair mismatches, bulges and internal loops. Not all mismatches interact with each other, but within this realm exist non-canonical base-pairs which do interact with each other, but in a much less efficient manner than the normal Watson-Crick interaction. In the cell, mismatches occur from time to time as a result of mutagenic processes and are corrected by a variety of repairing enzymes. *In vitro*, however,

mismatches and non-canonical base pairs can give rise to properties that are typically not associated with the regular, fully complementary B-type DNA.

The presence of mismatches and non-canonical base pairs generally perturbs the structure of the B-type duplex causing irregularities and destabilization to base stacking. Some examples of non-W.C. type base pair interactions are depicted in Figure 1-5. There have been many different possible types of these non-WC interactions documented, some involve base:sugar as well as base:phosphate backbone interactions, depending on the type of the mismatch.

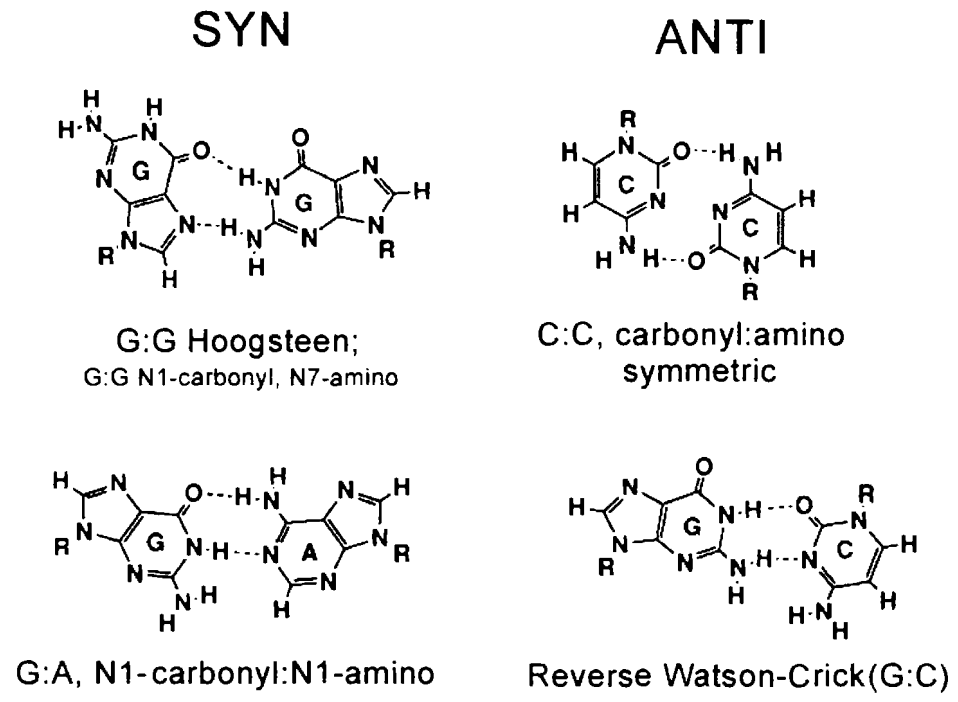

Figure 1-5 Some examples of non-Watson & Crick base pairs. Two columns are shown (SYN/ANTI), depicting the relative configuration of the bases about the glycosidic bond.

What gives rise to all these possible combinations is the ability of the base to rotate (to a certain degree) about the glycosidic bond. The glycosidic bond is the one between the sugar and the nitrogenous base, C1'-N9. In the conventional Watson-Crick type base pairing found in the B-type helix, the base and the sugar are found in the *anti*

conformation about the glycosidic bond. In structures such as Z-type DNA and some mismatches, the *syn* conformation can be found. This rotational variability about the glycosidic bond allows the base to use a non-Watson-Crick face in base pairing as well as other interactions (Figure 1-6).

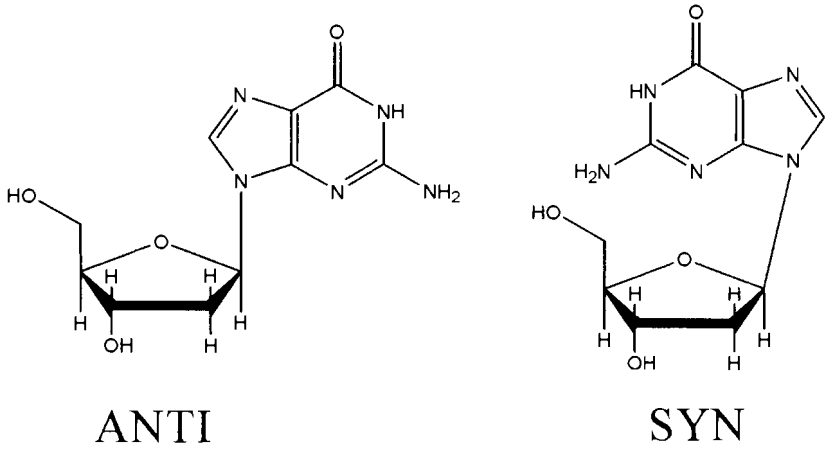

Figure 1-6 Variability of the Glycosidic Bond. The normal conformation about the glycosidic bond is the ANTI, found in the Watson-Crick base pairing conformation.

Mismatches can occur in many different scenarios: Symmetric internal loops contain mismatches of equal number of bases in each strand, these can be synthesized to however many tandem mismatch repeats as one requires. Similarly, asymmetric internal loops can occur where an unequal number of nucleotides occur in each strand of a duplex (Figure 1-4e). In the case where all the mismatches are on one strand of the duplex, as in Figure 1-4d, these structures are referred to as bulges, here a three base and a one base bulge are shown. As mentioned earlier, as mismatched bases are incorporated into duplex DNA they have the power to distort the helix causing kinks and bends that disrupt the coaxial stacking nature of the double helix. The extent to which additional bases can cause the helix to bend, whether in DNA or RNA has been reviewed (Lilley 1995).

1.3.2.3 Branched DNA

So far we have seen that DNA can form a variety of structures depending on its sequence and environment. Another set of special structures that DNA can form is that of branched DNA. In nature, one of the most common branched DNA structures is that of the four-way junction or Holliday Junction, which is an intermediate structure in genetic recombination. During meiosis, homologous chromosomes pair up and become pressed together at their centromeres. During this time of close proximity, the homologous chromosomes can physically exchange genetic material by the breaking and rejoining of their DNA molecules. This genetic recombination event, referred to as "crossing-over", is facilitated by enzymes, which break and rejoin the two DNA molecules. Initially both DNA molecules are nicked, and within the vicinity of the nick partial unwinding of the DNA strands occurs. This is followed by an event where a nicked strand from one duplex base-pairs with its unbroken complementary strand in the other duplex and vice versa. Upon enzymatic ligation a crossed-strand intermediate is generated, this is referred to as a Holliday junction or four-way junction. Since these are homologous DNA duplexes a high degree of complementarity exists between the junction branch points of this crossed-strand intermediate allowing the junction to "migrate" by unwinding and rewinding of the duplexes. This isomerization event known is known branch migration (Camerini-Otero and Hsieh 1993). When branch migration subsides, the crossed four-way junction structure can resolved back into two separate duplexes by the cleaving and ligating properties of enzymes, generating recombinant duplexes. *In vitro*, the four-way junction motif can be engineered such that each arm contains a different sequence and thus produces an "immobile" junction. In the presence of moderate ionic conditions, the extended four-way junction (Figure 1-4f) has been

shown to undergo coaxial stacking of its arms in a sequence dependant manner, resulting in X-like structure.

Another type of branched DNA is the three-way junction; and is the basis for the work described in this thesis. In a three-way junction with no unpaired bases, the structure is generally thought to be unstacked and extended. From simple model building, it can be deduced that it would not be possible for a perfect three-way junction with no unpaired bases (3H) to form a structure where two of its arms are coaxially stacked arms without actually breaking one of the strands; Recall from before that the axial distance between two stacked bases in a B-type helix is ~3.4 Å. This would mean that we would be trying to fit the width of a helix (~20 Å) in to a space only big enough for the space between two bases. Comparative gel-shift mobility assays (Duckett and Lilley 1990) and FRET studies (Stuhmeier *et al.* 1997) on the perfectly base paired three-way junction confirm that its overall global orientation is one that is unstacked and extended. Fluorescence resonance energy transfer (FRET) is a spectroscopy technique used to determine physical distances within a molecule, in this case the distances and inter arm angles branches of a DNA three way junction molecule. The spectroscopy technique involves the incorporation of a fluorophor molecule and a quencher molecule covalently attached at the branch endpoints of a three-way junction. The changes in fluorescence are measured, and by using a series of algorithms spatial features giving insight into the structure of a molecule are revealed.

Generally, for a perfectly base paired three-way junction, the inter-helical angles are similar, ranging from 60-90°. Also, the structure does not typically fold by pair-wise coaxial stacking and does not undergo any major conformational changes upon

increasing the ionic strength of its environment, as seen for Z-DNA or 4-way junctions. However, some perfectly base paired three-way junctions have been found to be quite asymmetrical in their global structure, suggesting that the simple "Y" unstacked structure may be an oversimplification for some sequences (Lu *et al.* 1991).

When unpaired bases are incorporated between two stems of a perfect three-way junction (3H), the structural constraints with respect to flexibility about the junction are relaxed. Preliminary experiments of incorporating a single stranded region or a bulge between the helical arms showed that the resulting structure had increased stability in gel electrophoretic studies (Leontis *et al.* 1991). It was later shown that such three-way junctions were able to undergo a conformational change upon addition of magnesium or other multivalent ions (Welch *et al.* 1993). The resulting structure was thought to be one where two arms became coaxially stacked while the third was subtended at an angle which was dependent on the number of unpaired bases, this was confirmed by FRET studies (Stuhmeier *et al.* 1997).

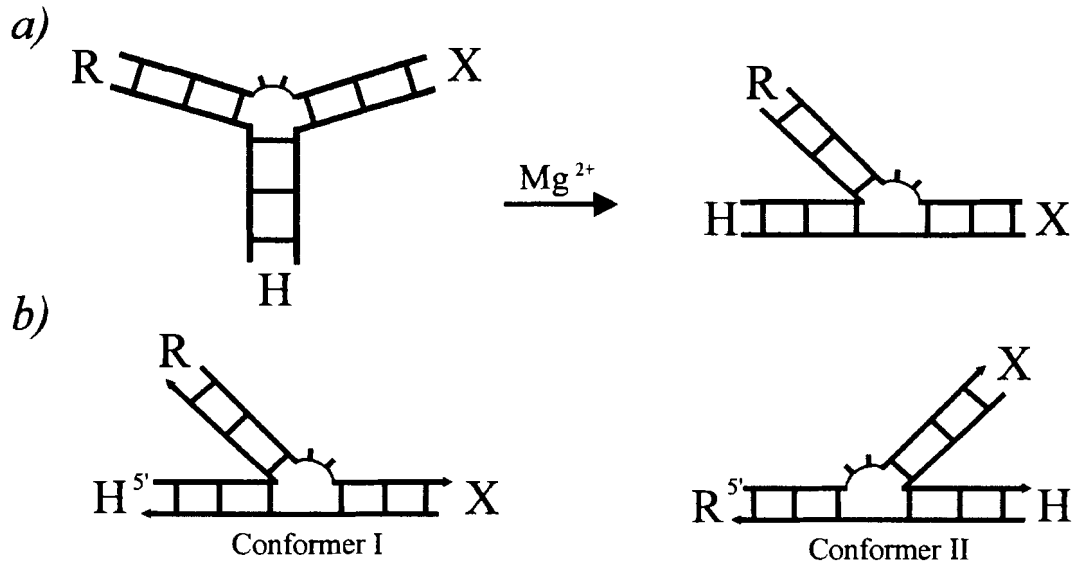

Figure 1-7 Schematic of a three-way junction with two unpaired bases and its conformers. a) Upon addition of divalent cations, the bulged three-way junction undergoes a conformational change where b) two conformers are possible. Model is based on (Lilley 2000).

One of the most well studied three-way junctions containing a single stranded region is the "$3HS_2$" type junction, having a 2 nucleotide bulge between two helices (Figure 1-7). Here, upon addition of moderate amounts of divalent cations, the $3HS_2$ junction undergoes a conformational change resulting in a structure having two stacked helices with a third helix extended away from the point of strand exchange. Here, two conformers are possible, differing in stacking partners and in the polarity of the bulge-containing strand, interpreted in a direction moving away from the two stacked helices. In conformer I the polarity is 3' to 5', while in coformer II the polarity is 5'-3' (Figure 1-7). The preference for stacking partners in these junctions is sequence dependent and involves the identity of the bases about the junction branch point. More specifically, it is the identity of the penultimate base pairs on the stem opposite the two base bulge that dictate which arms stack on which (van Buuren *et al.* 2000). This is referred to as the pyrimidine rule and is depicted in Figure 1-8. The pyrimidine rule was determined

empirically by systematic analysis of 24 different three-way junctions containing 2 unpaired nucleotides at the junction.

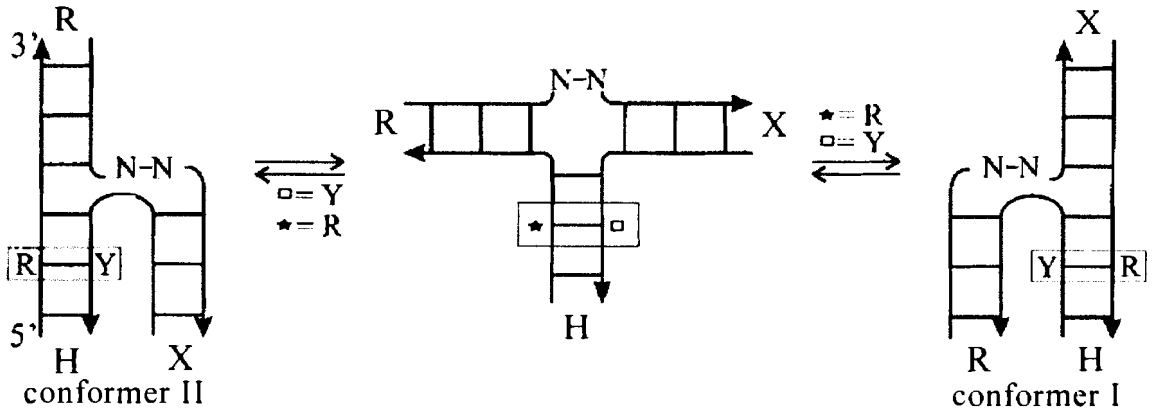

Figure 1-8 The Pyrimidine Rule for defining stacking partners in a three-way junction with a two nucleotide bulge. The identity of the penultimate base pair on the stem opposite the two base pair bulge determines which arms stack on which. Model is based on (van Buuren *et al.* 2000).

1.3.2.4 Other Structures

The structures described in the previous sections are only a sampling of the many different characterized folded structures that exist for nucleic acids. Other structural motifs not discussed in this manuscript include pseudoknots, guanine quadruplexes, and triplexes, to name a few.

1.3.3 Charge Transfer in DNA

One of the many characteristics of DNA is its ability to behave as a conducting medium for electrons and thus have properties much like a semiconductor. A semiconductor by definition is a substance conducting only a slight electrical current at room temperature, but showing increase conductivity at higher temperatures. This property in DNA is attributed to the structure of the B-DNA double helix and its electron rich bases. The idea that DNA or nucleic acids, could serve as conductive species first

arose over 40 years ago (Eley and Spivey 1962). The topic was then revived and supported in the 1990's when it was demonstrated that photo-induced charge transfer could occur over distances of more than 40 Å between metallo-intercalators tethered at opposite ends of a 15 base pair duplex (Murphy *et al.* 1993). This observation and many others that followed led to a heated debate over the mechanism of this process (Turro and Barton 1998). Elucidating the mechanism in which DNA behaves as a semiconductor is relevant to many areas of nanotechnology research. From a biological standpoint, it is also beneficial to understand the mechanism of this process as oxidative damage to DNA *in vivo* can lead to mutations and cancer.

1.3.3.1 Mechanisms of Charge Transfer/Transport

The mechanism of electron transfer is a topic of intense research, with different groups having different opinions on the details of the process (Turro and Barton 1998). The two main models for DNA charge conduction that are generally accepted are; the 1) super-exchange model and the 2) hole hopping model. A variation of the hole-hopping model has been described by Schuster and coined "phonon-assisted polaron-like hopping" (Liu *et al.* 2004). These contrasting models are believed to occur in different charge transport scenarios, particularly, those that affect the distance of charge separation between the donor and acceptor molecules; particularly the length and sequence of the bridging DNA (Jortner *et al.* 1998) . These models offer characteristic distance and sequence dependences for charge transport as well as different rates for the process. The super-exchange model holds true for short distances of up to three base pairs, while the hole hopping model and the phonon-assisted polaron like hopping model appears to be applicable for charge transport over longer distances (~200 Å). The views on this issue

are evolving such that it is now accepted that both models (super exchange and hole hopping) work in synergy, depending on the driving force of the reaction and the sequences being tested. The terms "transfer" and "transport" are frequently used in the literature; charge transfer refers to the single step tunnelling and is appropriate for describing the super exchange mechanism. Charge transport on the other hand, is a multistep hopping reaction, with each step of the hopping process being a transfer reaction (Giese 2000); (Jortner *et al.* 1998). For a more detailed review on charge transport/transfer, please see reviews by Giese (Giese 2002) and Barton (Delaney and Barton 2003).

1.3.3.2 The Super Exchange Mechanism

The super exhange mechanism was one of the first ways that electron transfer in DNA was conceived to occur. In this model, the π-orbitals of the bases form delocalized molecular orbitals, sometimes referred to as the DNA π -way (Murphy *et al.* 1993). Here, the π-orbitals of a given base are in direct contact with the π -orbitals of a neighbouring base. This would allow for rapid electron transfer from donor to acceptor, depicting DNA as molecular wire. This process is believed to occur when the donor and acceptor molecules are in very close proximity and decays exponentially with distance (Jortner *et al.* 1998).

DNA is a dynamic molecule, with its constituent atoms, corresponding counter ions, and solvating water molecules, having motions in time-scales ranging from femtoseconds to milliseconds or longer (Beveridge and McConnell 2000) (Braun *et al.* 1998). For these reasons it is conceivable that super-exchange occurs only over short

distances, as longer stretches of DNA tend to be more dynamic and offer less favourable conformations for super-exchange to occur.

1.3.3.3 The Hole Hopping Mechanism

As the name implies, this model depicts an electron hole, or radical cation, to migrate through DNA by a "hopping" mechanism. In the hole-hopping mechanism, the radical cation uses the nucleobases with the lowest oxidation potential as resting spots. In DNA, the purines (primarily guanines) are the carriers of the positive charge owing to their relatively lower oxidation potentials (Seidel *et al.* 1996). The reduction potential of the free bases are as follows: dG (1.29 V), dA (1.42 V), dC (1.6 V) and dT (1.7 V) (Steenken and Jovanovic 1997). The radical cation migration process is initiated by an oxidation event to the DNA where a single electron is robbed creating a radical cation ($G^{\cdot+}$). The electron hole is allowed to rest on these bases (Gs) of relatively lower energy and hop from G to G in a random walk, robbing electrons from neighbouring guanines (Meggers *et al.* 1998). Thus, for efficient charge transport to occur in such a system, consisting of an electron acceptor and donor separated by a DNA bridge, sufficient guanines must be present to provide "stepping stones" for the migration of the radical cation. As a rule of thumb, when constructing DNA sequences for the purpose of long-distance hole hopping, G:C base pairs should be separated by no more than one or two A:T base pairs. If the DNA bridge only consists of an (A:T) tract, as the length of the bridge increases, the adenines also become carriers of the positive charge (Giese *et al.* 2001). Giese has shown that when the DNA bridge only consists of (A:T) base pairs, there is actually a change in mechanism from the rapid super exchange to hole hopping mechanism by varying the length of the (A:T) DNA bridge between the donor and

acceptor molecules (Giese *et al.* 2001). As the length of the DNA bridge increased from 1-3 base-pairs, a sharp decrease in the efficiency of electron transfer was observed indicating a strong distance dependence. When the DNA bridge was greater than 4 base-pairs the efficiency of electron transfer becomes nearly independent of distance (Giese 2002).

In addition to having sufficient guanines as stepping stones for the radical cation, it is generally accepted that the higher the degree of base stacking that a DNA bridge has, the more efficient the transport of the radical cation will be from donor to acceptor. Perturbations to the axial stacking of the DNA bridge, such as bulges, mismatches and single strands, all attenuate the efficiency of charge transport. In the cases where perturbations to the helix caused little or no effect on the efficiency of charge transport, such as certain G:A mismatches (Boone and Schuster 2002), or abasic sites (Gasper and Schuster 1997), it is believed that the resulting structure was stacked, thus permiting charge transport.

1.3.3.4 Other Mechanisms

The scenarios for electron transfer that have been discussed in the previous sections all describe a general system where a single electron (an electron hole) travels through oxidized DNA. Electron transfer through an oxidized DNA medium is the system used to describe the work in this thesis. Much less is known about electron transfer through reduced DNA, where the electron now is in excess. Here the excess electron would migrate through the bases which are most easily reduced, C and T, owing to their reduction potentials (Steenken and Jovanovic 1997). Also, because their potentials are so similar, electron migration would occur in both of these bases, making

every base pair a carrier of the excess electron. The mechanisms that govern these processes, whether hopping or tunnelling, is at an early stage, but it is conceivable that because every base pair can carry the excess electron (radical anion), the electron migration process would be well coupled and efficient. Several systems have been used to explore this process, including electron injection into DNA by γ-irradiation in ice, and electron injection by photo activated flavins (Anderson and Wright 1999; Debije *et al.* 1999), (Razskazovskii *et al.* 1997), (Schwögler *et al.* 2000).

1.3.4 Monitoring Charge Transport

Several methods have been developed to monitor charge transport in DNA. The ideal situation would be to directly attach electrodes at ends of a DNA molecule and measure changes in current. Unfortunately, technical limitations make this task impossible at the current time. The most direct measurements have been on "600 nm ropes" consisting of a few DNA molecules twined into single structure of at least 600 nm in length (Eley and Spivey 1962), (Fink and Schonenberger 1999). Measurements of electrical current as a function of the potential applied across these 600 nm ropes showed that efficient conduction through DNA was possible. Fink and Schonenberger measured a resistance of 2.5 MΩ across the 600 nm DNA ropes indicating that DNA transports electrical current as efficiently as a good semiconductor.

The most commonly studied systems involve chemical modifications to DNA where an oxidant and/or reducing agent is covalently attached to the DNA at specific positions, spanning a region where charge transport is monitored. These covalently tethered compounds are typically light sensitive so that electron transport can be turned on or off by irradiation with the correct wavelength of light. Several compounds have

been described as possible candidates as oxidants/reductants depending on whether one wishes to monitor charge transport over long (~200 Å) or shorter distances (~20 Å). The different compounds that have been incorporated into DNA for the purpose of monitoring charge transport, have been reviewed by Grinstaff (Grinstaff 1999).

1.3.4.1 Monitoring Electron hole Migration in DNA

The most typical way to monitor electron hole migration/phonon-assisted polaron hopping in DNA is performed by injection of a radical cation into the DNA by photo-excitation of a tethered oxidant. The tethered oxidant or electron acceptor used in this work is an anthraquinone (AQ) derivative. A simplified scheme outlining electron hole migration is depicted in Figure 1-9 below. The electron donor is the 5' most G of a GG run or a GGG run in the DNA sequence. Upon irradiation of the anthraquinone-linked DNA sample with ultraviolet light, a ground state electron in the anthraquinone moiety gets excited into the singlet state. For the case of AQ, an intersystem crossing to the triplet state may then follow. The excited AQ* then rapidly removes an electron from the DNA resulting in a G·+ radical cation and an AQ·- radical anion. Anthraquinone is an electron deficient, hydrophobic molecule that stacks well on top of the DNA by way of dispersion forces. Depending on which system is being discussed, upon radical cation injection, the radical cation localizes on either the first purine closest to the AQ (in the phonon-assisted polaron hopping model) or on the first guanine, as a result of tunnelling (in the hole hopping model). Here the radical ions can undergo different side reaction, the two most interesting of which are explained below (see Figure 1-9).

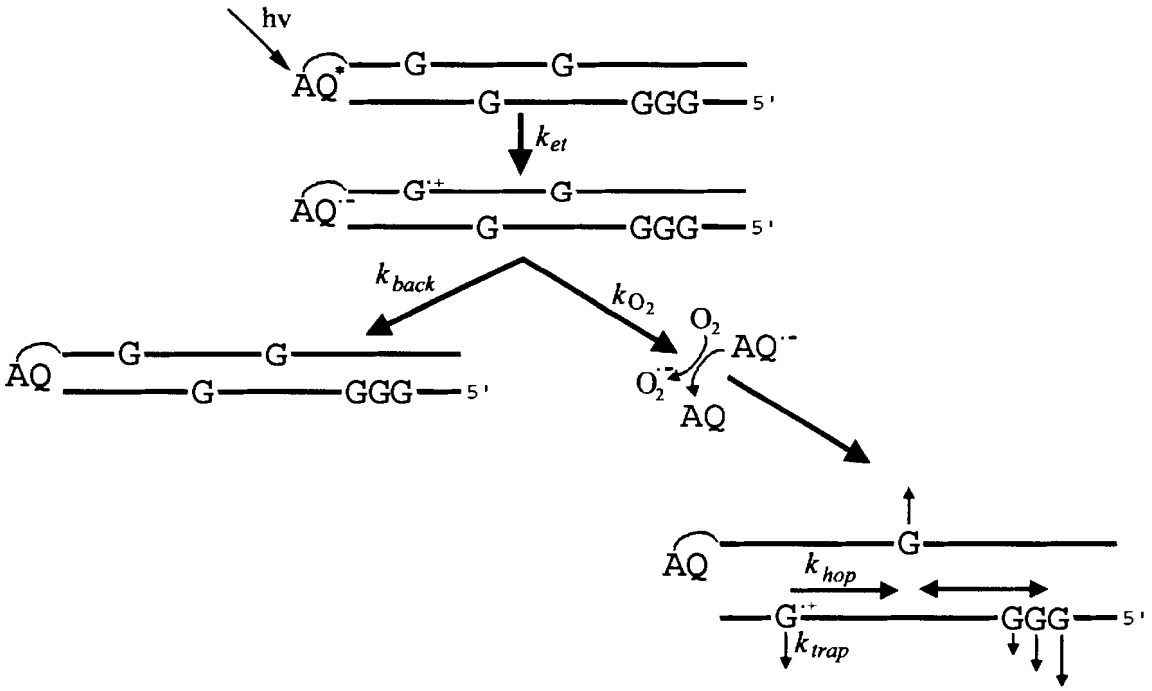

Figure 1-9 A Simple Scheme for monitoring electron transfer. Upon radical cation injection one of two side reactions can occur: a) annihilation of the radical ion b) radical cation trapping and migration.

One of the possible side reactions is the annihilation of the radical ions. Here, a simple back reaction having rate k_{back} occurs and involves the return on an electron to its donor resulting in the initial ground state. The magnitude of k_{back} depends on many factors, such as the electron withdrawing properties of the solvent, or the electron donating character of the local sequence adjacent to the AQ moiety. The efficiency of radical cation injection into the DNA helix has been addressed by Schuster's group. They propose that the back reaction can be minimized by excluding a guanine in the first four bases at the end of the DNA helix where the anthraquinone is tethered. AQ-DNA constructs having this design required only 1% of the irradiation time to see comparable guanine damage at sites along the DNA duplex (Sanii and Schuster 2000).

The second side reaction occurs when the $AQ^{\cdot-}$ radical anion loses its excess electron to molecular oxygen (O_2) in the solvent, resulting in a superoxide ($O_2^{\cdot-}$) and

ground state AQ, leaving the base radical cation G·+ with no local partner for annihilation. The rate of this process is described by kO_2 in Figure 1-9. At this point, the guanine radical cation can migrate in a random walk along the DNA double helix to other guanines. This process is referred to as "hole hopping". This base radical cation migrates/hops along the DNA helix with rate described by k_{hop} (Figure 1-9). Migration of the G·+ radical cation could terminate by undergoing a side reaction with water or molecular oxygen resulting in a base labile guanine lesion in the DNA strand. This is referred to as radical cation trapping and its rate is described by k_{trap}. Radical cation trapping can be visualized as breaks in the DNA using gel electrophoresis after treatment of end-radiolabelled DNA samples with hot piperidine.

Although all guanines have the potential to react under oxidative stress to form the oxidized G lesion, not all guanines react with the same efficiency. This is due to base sequence effects about the single guanine. It has been demonstrated that due to the π-stacking interactions of a 5'-GGG-3' run in a Watson-Crick DNA helix, the 5' most guanine becomes the most electron donating and thus is more readily oxidized than the any G residue on the 5'-GGG-3' run or any other G along the double helix (Saito *et al.* 1995), (Sugiyama and Saito 1996). The 5' G reactivity of a 5'-GG-3' run has become a signature of oxidative damage caused by electron hole migration and is used widely for studies of long-range hole transport (Meggers *et al.* 1998) (Giese *et al.* 1999). In addition to this, other sequence effects have been shown to modulate the oxidative reactivity of the 5' guanine. Experimental evidence from Saito and co-workers has shown that the efficiency of GG cleavage has the following hierarchy, (read 3'-NNN-5'): GGG > CGG > AGG = TGG > TGT (Saito *et al.* 1998).

Another topic of interest and debate is the identity of the oxidized product. Several heterocyclic compounds have been proposed, for a detailed discussion see the following references: (Burrows and Muller 1998), (Cadet *et al.* 1997), (Kino *et al.* 1998). Although many structures have been proposed, two major compounds have been generally accepted as major oxidation products under oxidative stress to guanines, they are 7,8-dihydro-8-oxoguanine (8-oxo-G) and 2-amino-imidazolone (Giese 2002). The ionization potential of 8-oxo-G is slightly lower than a regular guanine (Sheu and Foote 1995) and can be used as a marker of oxidative stress or as an electron-sink in studies of long-range hole transfer (Schuster 2000). From a biological standpoint, these two oxidative products can produce mutations to the DNA sequence: 8-oxo-G can base pair with adenine in a Hoogsteen fashion, and upon DNA replication in the cell, it would induce a G:C to T:A transversion mutation (Shibutani *et al.* 1991). The imidazolone can base pair with guanine and can cause a G:C to C:G transversion mutation upon DNA replication (Duarte *et al.* 1999) (Kino and Sugiyama 2001). Ongoing research into characterizing the oxidation products of guanine and their mutations will give more insight into how oxidative damage in DNA occurs (Duarte *et al.* 2001).

CHAPTER 2: GENERAL ELECTRICAL BIOSENSORS MADE OF DNA

2.1 Introduction

Since charge transport in DNA can be modulated by its conformational state, it is this dependence that is used to design biosensors made of DNA. The idea of exploiting charge transfer in DNA to monitor ligand-receptor binding events was first described by Fahlman and Sen (Fahlman and Sen 2001). In their work, they successfully incorporated a ligand-binding receptor to a conducting DNA molecule such that ligand binding to the receptor changes the conformation of the conductive path. The resulting receptor-DNA construct would constitute a biosensor for the ligand/analyte in question. Such deoxyribosensors for the ligand adenosine have been described by Fahlman and Sen (Fahlman and Sen 2001). In theory, any ligand-binding receptor, of biological or other origin could potentially be used in such deoxyribosensors. For the receptor component of these deoxyribosensors, the most obvious choice was to utilize receptors made of nucleic acids, or "aptamers". In nature, certain nucleic acids are known to bind a myriad of different molecules small or large for many cellular processes. An example is riboswitches, which are segments of mRNA that can regulate the metabolites they sense. Riboswitches for adenine, guanine, S-adenosylmethionie (SAM), lysine, thiamine pyrophosphate (TPP), flavins mononucleotide (FMN) and coenzyme B12 have be recently identified (Mandal *et al.* 2003). Recent advances in *in vitro* selection technology (SELEX) have empowered scientists to obtain nucleic acid aptamer sequences (whether DNA or RNA) which are capable of binding their target ligands with high affinity and

specificity. The ligands for which one wishes to obtain an aptamer for, could be any molecular species of choice, including many that do not normally interact with DNA or RNA (Gold *et al.* 1995). Another feature of nucleic acid aptamers is that they exhibit an induced-fit folding behaviour, where the aptamer by itself is unstructured in solution, it can undergo significant compaction and structural stabilization upon binding to its cognate ligand (Hermann and Patel 2000).

Fahlman and Sen have described two related but distinct designs of deoxyribosensors for the detection of the trial analyte, adenosine, which binds poorly, if at all to double-stranded DNA but for which a moderate affinity ($K_d \sim 1$ μM) DNA aptamer sequence has been *in vitro* selected (Huizenga and Szostak 1995) (see materials and methods section for definition of K_d). Nuclear Magnetic Resonance (NMR[1]) in combination with molecular modelling have revealed that this aptamer binds two adenosine molecules and undergoes adaptive folding and compaction, resulting in a tightly hydrogen bonded and stacked helical structure (Lin and Patel 1997).

Figure 2-1 below illustrates the two designs for the adenosine deoxyribosensors. Figure 2-1a depicts the integrated ligand sensor in its off and on conformations. Here, the aptamer region, a direct component of the electron transfer path to the detector stem is

[1] NMR spectroscopy is a valuable analytical technique that can be used to determine the three-dimensional structure and dynamics of macromolecules in solution with the aid of molecular modelling. Nuclear magnetic resonance results from the absorption of energy by a nucleus changing its orientation in a magnetic field. Protons (^1H) are the most commonly studied nuclei in NMR. The resonance spectrum that is produced by these nuclei is representative of the various groups and their relative orientations within molecule. The intramolecular distance information that can be obtained using NMR, can be grouped into two general classes of distance information; "through-bond" connectivity and "through-space" connectivity. The former is referred to as COSY for correlation spectroscopy and the latter is referred to as NOESY for Nuclear Overhauser Effect spectroscopy. NMR spectroscopy can become especially useful when studying the structure of nucleic acids; nucleobases contain aromatic ring systems where the π-electrons are free to move in an orbital not associated with any one atom. Ring currents can be set up in these delocalized electron systems giving rise to signature spectra for the resonating protons associated with the aromatic rings.

unstructured in the absence of ligand making it a poor DNA bridge for charge transport. Upon binding of the ligand adenosine, the structure compacts and becomes stacked permitting charge transport to the 5'GGG'3 containing electron sink in the detector stem, where the signal is measured. In Figure 2-1b, a more versatile construct for the adenosine deoxyribosensor is depicted, the coupled ligand sensor. Here, the aptamer region is not part of the conduction path; instead it is adjacent to it. In the unbound form, the aptamer region is unstructured and disturbs the co-axial stacking of the AQ-stem and the detector stem, resulting in a sub-optimal DNA bridge to the detector stem. This is rectified upon binding of the target analyte adenosine. These constructs as well as the ones in the work to follow all use the light-activated photo-oxidant anthraquinone for initiation of charge transport. Both of these deoxyribosensor constructs gave high levels of charge transfer to their detector stems upon binding adenosine. The signal observed was 10-20 fold for the integrated ligand sensor and 10-15 fold for the three-way junction based coupled ligand sensor (Fahlman and Sen 2001).

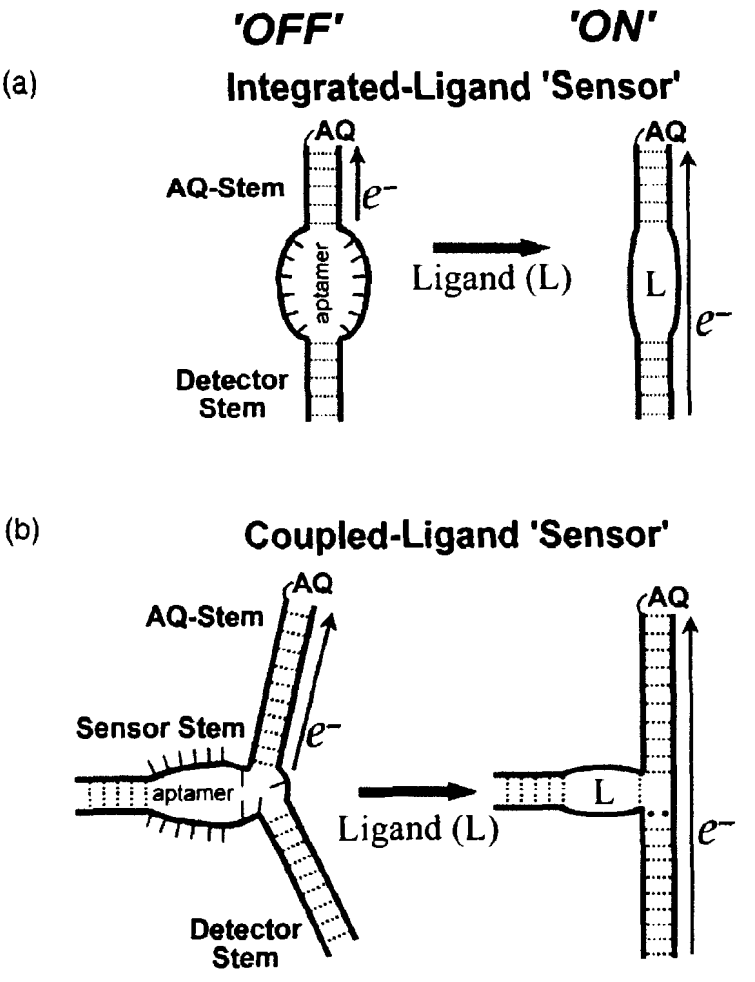

Figure 2-1 Design for two classes of deoxyribosensors.

Here, we wished to investigate whether the three-way junction based, "coupled-ligand sensor" could be generalized for the detection of other analytes. Adenosine is an uncharged molecule containing the heterocyclic adenine base. It is an essential component of nucleic acids and does not experience charge repulsion from the negatively charged aptamer backbone. Also, as revealed by the NMR structure, adenosine has the advantage of hydrogen bonding and stacking with elements within the aptamer component (Robertson *et al.* 2000). These characteristics of the analyte adenosine make

it a good test analyte of choice because it easily incorporates into DNA in a manner to be supportive of charge transfer.

As a next step, we wanted to test how robust nucleic acid sensors could be when the analyte in question didn't have such desirable properties for neatly interacting with DNA, as in the case for adenosine. We sought out to design a three-way junction based, coupled-ligand sensor for a small molecule ligand that was not an aromatic heterocycle and which contained a substantial positive charge. This positive charge may give the ligand the undesired property of interacting non-specifically with the DNA backbone. As a starting point we wished to investigate whether the existing coupled–ligand sensor for adenosine could be converted into a sensor for a different analyte simply by replacing the aptamer component of the sensor with a different aptamer of choice. The question was to see to what extent aptamers of diverse secondary structure could, in modular fashion be incorporated into a standard design of deoxyribosensors.

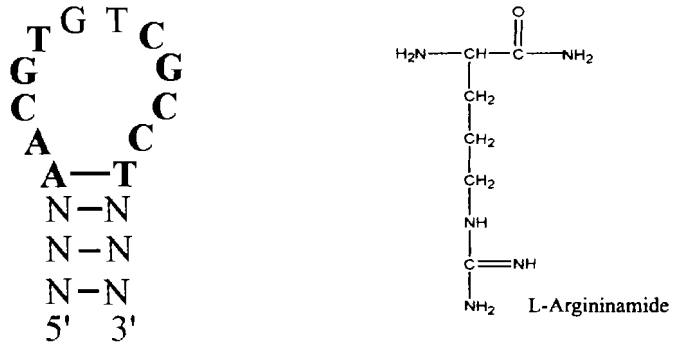

Figure 2-2 Secondary structure of the argininamide aptamer and its ligand L-argininamide.

The aptamer chosen for this investigation was one for the binding of amino acid derivative L-argininamide, a positively charged (2+) and non-heterocyclic analyte. This DNA aptamer had been selected by Harada and Frankel and the affinity of the aptamer

for argininamide was measured to be ~ 100 μM (Harada and Frankel 1995) (Robertson *et al.* 2000)(see Figure 2-2). The initial part of the research started out on the premise that the existing coupled ligand sensor for adenosine could be converted into one for argininamide by simple replacement of the aptamer sequence. Subsequent investigation focussed on whether established rules for helical stacking in DNA three-way junctions could be utilized for the design of better (having higher signal and specificity) deoxyribosensors.

2.2 Materials and Methods

2.2.1 DNA Oligonucleotides

All DNA oligonucleotides were purchased from the University of Calgary Core DNA Services. Treatment and handling of unmodified DNA sequences, and the procedures for coupling of AQ to 5' amino modified DNA and subsequent purification were carried out as described by Fahlman and Sen (Fahlman and Sen 2001).

2.2.1.1 Treatment of Crude Oligonucleotides

All treatments of oligomers are based on a 0.2 micromole synthesis scale. Amine coupled oligonucleotides containing a C6-NH_2 modification on their 5'-end were treated as follows: The lyophillized DNA pellet from the synthesis was resuspended in 100 μl of deionized H_2O (dH_2O) and extracted three times with chloroform. The chloroform extractions were carried out to remove nitrogenous contaminants from the original oligonucleotide synthesis as they will compete the amine labelled DNA during the AQ coupling reaction. The remaining aqueous solution containing the DNA was precipitated by the addition of 30 μl of 1M NaCl and 340 μl of 100% ethanol. The resulting pellet

was washed two times with 70% ethanol and subsequently resuspended in 100 µl of dH_2O where the concentration was determined by measuring the optical density. All unmodified oligomers were dissolved in 50 µl of denaturing loading buffer, heated at 90°C for 3 minutes and run on an 8% denaturing polyacrylamide gel. Denaturing loading buffer consisted of formamide, containing 1 mM EDTA pH 8.0 and trace amounts of xylene cyanol FF and bromophenol blue as tracking dyes. DNA was visualized by UV shadowing and the appropriate band was cut out and eluted in 10 mM Tris-Cl pH 8 and 0.1 mM EDTA. The eluent was filtered through a 0.2 µm microfilter (Gelman Sciences), concentrated by butanol extraction and ethanol precipitated by topping up the concentrated DNA solution to 300 mM sodium acetate and adding 2.5 equivalents of 100% ethanol.

2.2.1.2 Anthraquinone Coupling

Approximately 5 mg of AQ-NHS ester was weighed out and resuspended in DMSO (1 ml DMSO: 20 mg AQ-NHS ester). The majority of the mixture will not dissolve and has a yellowish cloudy appearance. This mixture is vortexed and 7 µl of the suspension is immediately transferred to a separate 0.6 ml Eppendorf tube to which 75 µl of Sodium Borate pH 8.5 is added. Then 10 nanomoles of the chloroform extracted amino-derrivatized oligonucleotide is added. The reaction vessel is covered in foil and shaken overnight on a bench top vortex. The reacted DNA was then ethanol precipitated by the addition of 27 µl of 1M NaCl and 280 µl of ethanol. This is followed by another ethanol precipitation by the addition of 100 µl 300 mM NaCl and 250 µl of 100% ethanol. The pellet is then washed with 70% ethanol and resuspended in 50 µl of 100 mM triethyl ammonium acetate (TEAA) pH 7.0 and 100 µl chloroform. Here, a

chloroform extraction is performed to remove excess uncoupled AQ-NHS ester that has not reacted with the amine group tethered to the 5' end of the DNA. This is then shaken slowly for several hours until the pellet dissolves (it is important to note that the pellet will look a chalkish yellow). This can be expedited by soaking the reaction vessel in a 37°C water bath and periodically vortexing the solution. Once the pellet has dissolved the aqueous fraction is removed and placed in a speed vac to remove any residual chloroform. This takes approximately 15 minutes under vacuum. The resulting solution of TEAA would contain the AQ-coupled oligo ready for purification by HPLC.

2.2.1.3 DNA Assemblies

DNA assemblies were formed by annealing mixtures of constituent DNA oligomers (1 μM each) in 100 mM Tris–HCl (pH 8.0), 100 mM NaCl, 100 μM EDTA. DNA solutions were heated to 85°C for two minutes and allowed to cool slowly until the final temperature was 20 °C. These solutions were then diluted two-fold with $MgCl_2$ and L-argininamide or other analytes, as appropriate; L-arginine, L-lysine and spermidine were added to their final concentrations, as described in the text. Following mixing, the solutions were incubated for 15 minutes at room temperature (20 °C) prior to photoirradiation.

2.2.2 Photoirradiation

All irradiations were carried out at room temperature (20 °C). Samples pre-incubated at 20 °C were irradiated using a UVP Black-Ray hand-held lamp (model UVL-56 with a 366 nm wavelength maximum, at 18 W) for 90 minutes or for 35 minutes with a distance of 4.0 cm between the bulb and the sample solution surface (Fahlman and Sen 2001).

Following irradiation, samples were precipitated in 300 mM sodium acetate and 2.5 equivalents of 100% ethanol and the DNA pellets dissolved in 10% (v/v) piperidine and heated for 30 minutes at 90 °C in sealed tubes. The samples were then lyophilized, dissolved in a standard denaturing loading buffer (pH 8.0) containing 10 mM EDTA, heated to 90 °C, cooled, and loaded on 12% (w/v) polyacrylamide sequencing gels. The band patterns from gels were analyzed using a Molecular Dynamics Typhoon 9410 Variable Mode Imager.

2.2.3 Data Analysis

All densitometry measurements were carried out using the Typhoon™ 9400 Variable Mode Imager and Molecular Dynamics Image Quant 5.2 software for Windows NT. Densitometry traces of entire lanes in a gel were obtained. The density of a peak of interest, corresponding to damage at a particular nucleotide (e.g. G8) was taken as a percentage (X) of the total signal contained within that particular lane. Such a normalization was required to compensate for slightly uneven loading in different lanes. The signal obtained from the addition of a particular concentration of analyte to the relevant deoxyribosensor was then calculated as the percentage cleavage of the band in the presence of analyte ($X_{analyte}$) divided by the percentage cleavage of the corresponding band in the complete absence of analyte ($X_{no\ analyte}$).

Calculation of the dissociation constant (K_d) was carried out using Graph Pad Prism 4.0 assuming single site binding:

$$Y = B_{max} \cdot X / (K_d + X)$$

Where;

X = concentration of analyte
Y = observed G-damage at a particular analyte concentration
B_{max} = maximal observed G-damage at a particular analyte concentration
K_d = concentration of ligand to reach half-maximal binding

The equation above describes the binding of a ligand to its receptor and follows the law of mass action. In simple terms, when referring to the dissociation constant (K_d) for all the work described in this thesis, it is defined by the following equilibrium expression:

$$[DNA] + [L] \rightleftharpoons [DNA:L]$$

Thus;

$$K_d = \frac{[DNA]\,[L]}{[DNA:L]}$$

Where;

[DNA] = Concentration of unbound DNA
[L] = Concentration of unbound Ligand
[DNA:L] = Concentration of DNA bound to Ligand

2.2.4 Experimental Error

2.2.4.1 Error Associated with Densitometry Measurements

According to the Typhoon™ variable mode imager specifications, there exists a uniformity error of +/- 5% over the entire scan area (relative error). For this reason, the magnitude of the measurement is important in determining the number of significant figures. For this reason the number of significant figures varies depending on which set of experimental data is in question. As a default, the Typhoon™ gives densitometry data to three decimal places. For example, the magnitude of densitometry measurements for the ArgA 1.0 and 2.0 families was relatively large and required showing the data to only one decimal place. Here, densitometry measurements had values as high as "12.342 % raw signal", with 5% error, the error in the measurement is +/- 0.617, and the data is only represented to one decimal place. In contrast, when the magnitude of the densitometry

data was relatively small the data was presented to 2 decimal places. For example; when measurements were in the realm of "0.552 % raw signal", with 5% error, the error in the measurement is +/- 0.027, and the data is only represented to 2 decimal places. For the dissociation constant determination of the ArgA 2.0 deoxyribosensor and its cognate ligand argininamide, 5 replicates were used to obtain the K_d value. The K_d given is 1.3 +/- 0.4 mM. The error described in this particular case is standard error.

2.2.4.2 Error Associated with Analyte concentrations

The initial high concentration (relatively) stock solutions of test analytes, such as those for argininamide, arginine, lysine and spermidine were made using a Sartorius CP2245S analytical balance and Class A volumetric flasks from Kimax. The Sartorious analytical balance reads to the fourth decimal place and has a linearity error of +/- 0.0002 g. For making high concentration magnesium chlorides stocks a BP2100S balance from Sartorius was used, this balance reads to the second decimal place and has an error of +/- 0.02 g. Subsequent dilutions and experimental work was carried out using Gilson Pipetman P pipetors, specifically, Pipetman P10, P20, P200, and P1000 were used. These pipetors deliver volumes in the micro liter range and they are the standard tools for volume delivery in the biosciences. For a full description of the tolerances and errors associated with Gilson pipetors refer to the Gilson website. An example of analyte concentrations including significant figures and errors are given for the argininamide concentrations used in this work and represent the final concentrations in the reaction vessel, Table 2-1. Similarly, for concentrations of magnesium chloride used in this work a table including significant figures and errors is given, see Table 2-1 below.

Table 2-1 Error associated with analyte concentration. Concentrations of analytes and salts used in this thesis including significant figures and errors are shown in tables a) and b). a) argininamide concentrations and their errors, b) magnesium chloride concentrations and their errors.

a)

Argininamide Concentration in mM	Error (+/-) mM
100	4
25	2
10	0.6
5.0	0.4
2.0	0.2
1.0	0.08
0.50	0.05
0.10	0.01
0.025	0.003

b)

Magnesium Chloride Concentration in mM	Error (+/-) mM
100	5
50	2
30	1
10	0.5
3.0	0.2
1.0	0.07
0.10	0.008
0.010	0.001

Generally, the error in the concentrations throughout the work presented in this thesis and in Table 2-1 is between ~5% and ~10%. The higher concentrations have the lowest relative error and as concentrations progressively decrease the relative error in the concentrations increase. Thus a concentration of 100 mM is the most reliable as opposed to a concentration of 0.010 mM with 10% relative error.

2.3 Results and Discussion

2.3.1 An electrical Switch modulated by Argininamide: The ArgA 1.0 Family

As a starting point, the oligonucleotide sequences of the three-way junction based deoxyribosensor for adenosine (as described by Fahlman and Sen) were used. The immediate junction sequences (in red, Figure 2-3) had been selected for optimal performance by trial and error and included a G:A mismatch as well as A:T and T:A base pairs. Also the bridging sequences of the AQ-stem and detector stem, flanking the aptamer region, were left intact. The adenosine aptamer sequence was removed and replaced with the argininamide aptamer sequence; the resulting construct was named ArgA 1.0. In addition to the initial construct ArgA 1.0, variants of this construct were made by varying the junction sequences (in red) to test if any of these would give higher

signals in response to argininamide binding (Figure 2-3 below). The signal being measured was oxidative damage to a GGG sequence (specifically G8) in the detector stem of the aptamer-containing strand, which was ^{32}P end-labelled on its 5' end.

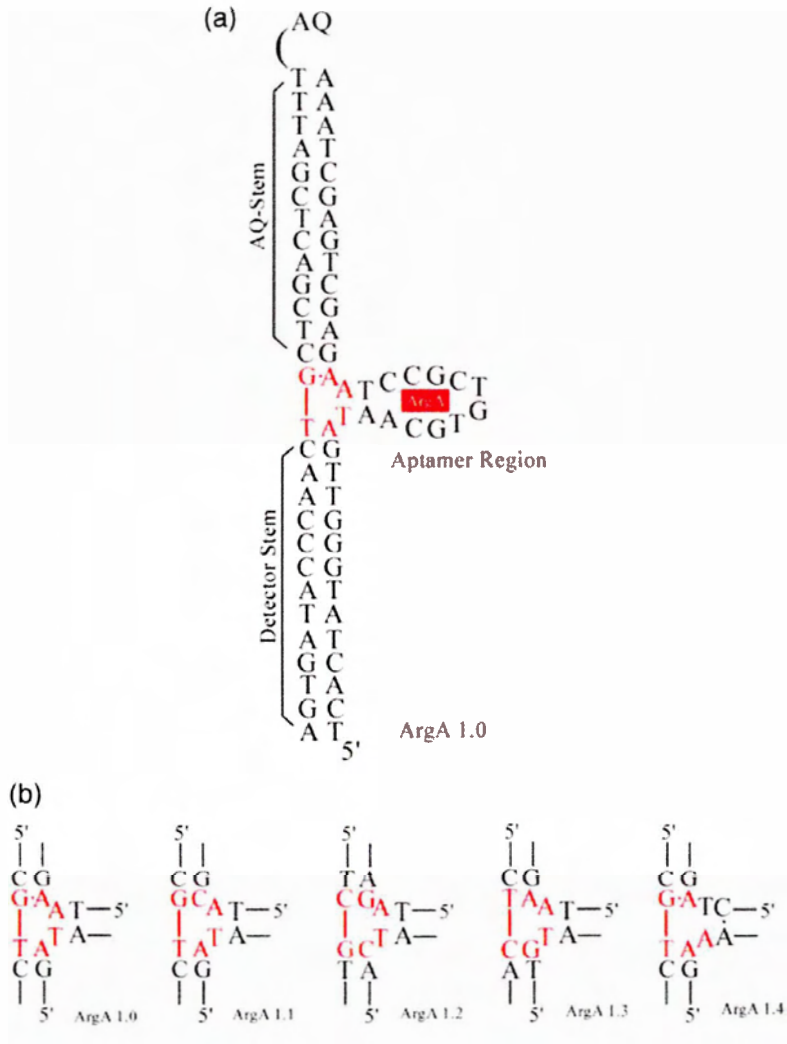

Figure 2-3 The ArgA 1.0 Family. a) The secondary structure of the coupled deoxyribosensor construct ArgA1.0, incorporating the DNA aptamer for ArgA. b) Junction base pairs for variant members of the ArgA 1.0 family sensors.

The ArgA 1.0 construct and its variants did not provide a strong signal to noise ratio at the detector stem. Ligand binding and irradiation were carried out at 19 °C in 50 mM Tris–HCl (pH 8.0), 50 mM NaCl, 20 mM $MgCl_2$, 50 μM EDTA. The relatively high concentration of magnesium was included to minimize any non-specific, charge-based

interaction of the positively charged argininamide with the deoxyribosensor. For constructs ArgA 1.0 and ArgA 1.4, a signal (see Materials and Methods) of ~1 was measured at G8. This meant that for these constructs, the addition of the target ligand did not invoke a conformational change to the deoxyribosensor structure such that a significant change in the amount of G damage at the detector stem would be observed. The other constructs, ArgA 1.1- 1.3 showed higher signals topping out at a 3-fold increase over the background signal (no analyte) for construct ArgA 1.3. The signals obtained at different guanine residues for the various constructs of the ArgA 1.0 family are summarized in Table 2-2 below.

Table 2-2 Damage signals at specific guanine residues in the ArgA 1.0 family, in the presence of 10 mM Argininamide. Reported signals contain 5% error.

Residue	ArgA 1.0	ArgA 1.1	ArgA 1.2	ArgA 1.3	ArgA 1.4
G35	11.2	5.0	8.7	7.3	6.2
G30	8.0	5.1	9.5	9.0	6.0
G20	4.5	2.7	3.7	7.1	1.7
G18	1.7	1.8	4.0	4.4	2.7
G13	1.5	2.8	3.0	8.1	2.2
G8	1.2	1.8	2.7	2.9	1.0

Although the ArgA 1.0 family as a whole did not give strong signals for the detection of argininamide, interesting features about the overall structural conformation of these deoxyribosensors could be learned by observing the breakdown pattern in the gels. The damage patterns for the most responsive sensor, ArgA 1.3, are illustrated in Figure 2-4 below. Here we note that the majority of the breakdown is occurring at G20 in the detector stem. From 0 mM to 10 mM added argininamide, the signal at G20 (within the aptamer arm) of ArgA 1.3 rose by 7.1-fold (by contrast, the signal at G8 in the detector arm rose by only, 3-fold). The responsiveness of the aptamer region to the addition of argininamide suggests that it may be base stacking with the AQ stem and

forming a conductive path. This was not the desired effect that we wanted to see, the ideal situation would have resulted in a structure where the AQ-stem and Detector stem are stacking upon the binding of argininamide.

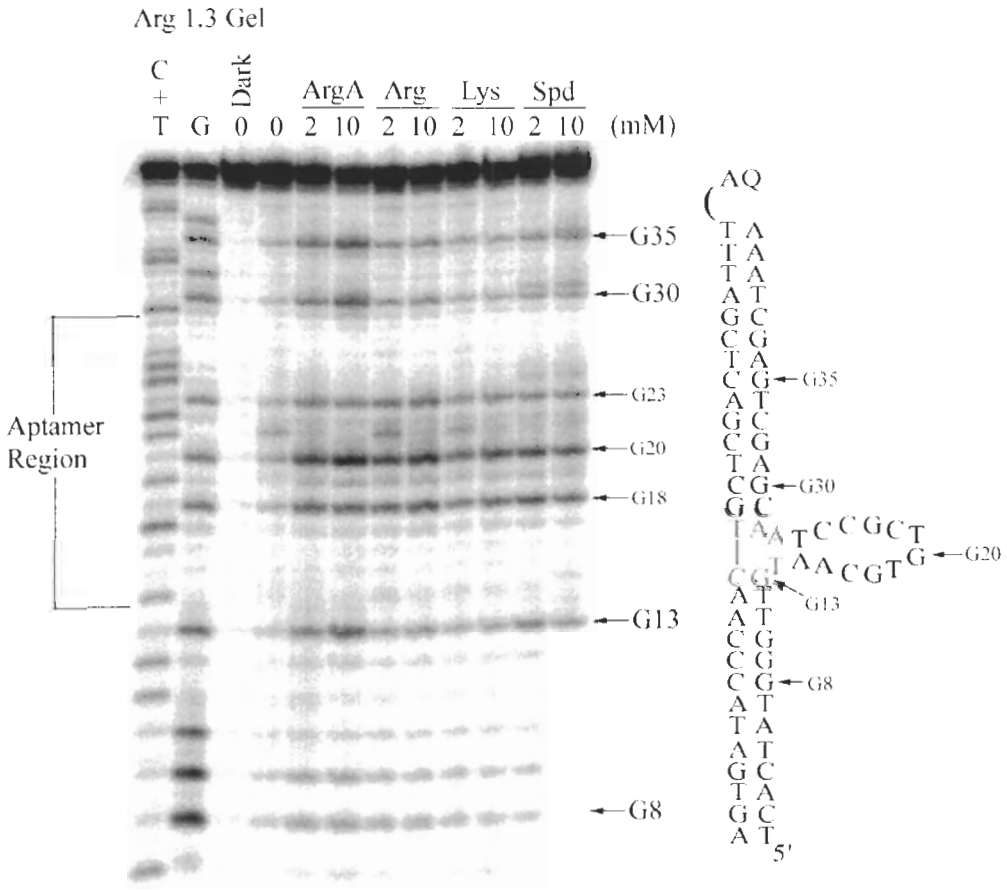

Figure 2-4 Electrophoretic gel for construct ArgA 1.3. Guanine damage patterns for the deoxyribosensors ArgA1.3 in the presence and absence of light as well as of different analyst, including L-argininamide (ArgA); L-arginine (Arg); L-lysine(Lys); and spermidine (Spd). Reference C+T and G ladders are shown to the left. Dark indicates a sample not exposed to either analyte or light; 0 indicates a sample not incubated with analyte but exposed to light like the other samples shown in the gel. To the right, construct ArgA 1.3.

However looking at Figure 2-4 above, damage at G20 appears to be non-specific as titration of the construct with structurally unrelated, but positively charged analytes L-lysine (+1) and spermidine (+3) gave the same high signal at G20. Given that neither

lysine or spermidine have any affinity for the aptamer, as the argininamide aptamer is specific for the guanidinium group of argininamide (Harada and Frankel 1995), the signal observed at G20 was probably a consequence of an overall, yet non-specific charge stabilization and compaction of the deoxyribosensors that the high amount of $MgCl_2$ present could not normalize.

Another key feature of ArgA 1.3, (see Figure 2-4 above) is the substantial signal increase at residues G30 and G35 located on the AQ-stem, out of proximity from the aptamer region. The increase in damage at these residues is specific for the binding of argininamide in contrast to lysine and spermidine. As the Argininamide concentration is increased to 10 mM, a strong increase in the oxidative damage is observed at these residues (G30 and G35). This demonstrates that argininamide binding to the aptamer region can stabilize the entire construct, including areas far from the site of argininamide binding (the AQ-stem) to a degree greater than the 20 mM Mg^{2+}present in the reaction buffer. As predicted, the presence of the amino acid L-arginine, which has a lower affinity for the argininamide aptamer (~20 fold lower), gave lower signals than did argininamide. This could be attributed to the difference in charge between the two amino acids, L-argininamide having a +2 charge and L-Arginine having a +1 charge (Harada and Frankel 1995). Table 2-3 below summarizes the signals measured at guanine residues at different locations in construct ArgA 1.3 in response to different ligands.

Table 2-3 Damage signals from ArgA 1.3 guanine residues in response to different ligands. Reported signals contain 5% error.

	ArgA		Arg		Lys	
Residue	2.0 mM	10 mM	2.0 mM	10 mM	2.0 mM	10 mM
G35	4.7	7.3	1.6	2.6	1.5	1.6
G30	4.9	9.0	1.9	3.4	1.6	2.1
G20	5.1	7.1	3.2	5.5	2.8	4.3
G18	4.4	4.4	3.1	5.3	3.0	4.4
G13	4.6	8.1	2.0	3.0	1.9	2.4
G8	2.7	2.9	1.7	1.9	1.7	1.3

Control analytes were incorporated in these experiments to show that the positive signal increases that were being observed were only due to the addition of the argininamide, which has high affinity and specificity for the aptamer region of the construct and little or no affinity to random sequence DNA (Harada and Frankel 1995). The three control analytes tested, arginine and L-lysine are similar in chemical structure and geometric shape in comparison to argininamide (see Figure 2-5). At pH 8, the pH at which all experiments were performed in, argininamide has a 2+ charge, arginine a 1+ charge, lysine a 1+ charge and spermidine a 3+ charge. The similar properties of these controls provide a means to demonstrate the high specificity and affinity for the cognate ligand among related molecules. Also the control analytes show that the signal increase at the GGG run is not due to general structure stabilization by way of non-specific binding or increase in ionic strength but as a result of binding the correct molecule only at the aptamer region.

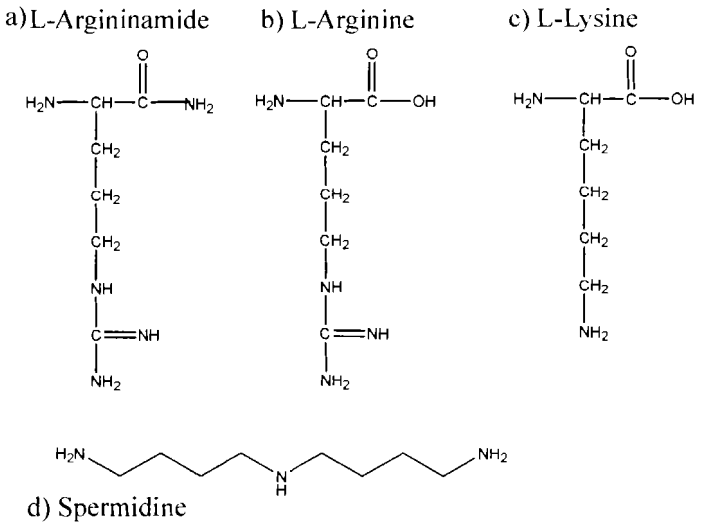

Figure 2-5 Chemical structures of a) L-argininamide, b) L-arginine, c) L-lysine and d) spermidine.

The argininamide aptamer region is characterized by a K_d value of 100 μM for argininamide. The arginine control is very similar and its inferior affinity is attributed to the guanidinium group of argininamide. According to Frankel and Harada, arginine has 20-fold lower affinity for the aptamer sequence, thus the increase in affinity for argininamide must be due to the replacement of the hydroxyl group in arginine by an amine group. This slight variation in chemical structure causing a major loss in binding affinity demonstrates the level of sensitivity of nucleic acid aptamers. An example where the use of these controls come into play is in validating whether the signal at specific guanine is non-specific or a true effect, as seen for G20 in construct Arg 1.3 (Figure 2-4). The controls confirm that the signal at G20 cannot be used as the analytical signal as it is also present when the control analytes are added. Also in a more general sense, the controls show that an increase in signal at G8 is not due to analyte binding at some random area on the deoxyribosensor construct. If this were the case, we would be able to distinguish the non-specific binding effect with the characteristically similar analyte controls.

2.3.2 The ArgA 2.0 Family

The difficulties that arose with the ArgA 1.0 family, in regard to the low signal, rooted from the fact that we did not have control over which stem of the three-way junction based deoxyribosensor would stack with the photo-oxidant containing AQ-stem. Unfortunately, it appeared that most of the charge transport was occurring between the AQ-stem and Aptamer region. To obtain a better handle on this matter we needed a system where we could control the stacking of the stems. For regular DNA three-way junctions, consisting of three fully base-paired helical stems of DNA (rather than two helical stems and an aptamer loop, or arm) certain empirical rules have been established to predict the overall conformation of the junction as a function of the identities of the base-pairs immediately bordering the junction. Welch (Welch *et al.* 1995), as well as van Buuren (van Buuren *et al.* 2000) established that the presence of a two nucleotide bulge at the junction leads to preferential stacking of two of the three stems of the three-way junction, and determined the role of specific junction base pairs in this process.

Based on their rules, a redesign of the ArgA 1.0 family of deoxyribosensors was undertaken. These rules would give us control over the final stacked structure of the deoxyribosensors in the presence of its cognate ligand, argininamide, that being one where the AQ-stem and Detector stem are stacked. The stacking rules, however, strictly hold where three fully base-paired helices (along with the unpaired two-nucleotide bulge) constitute a three-way junction. In our case we had two helical stems and an aptamer loop. The rules for preferential stacking dictate that it is the identity of the penultimate base pairs of the in each stem where the junction is formed that determine which arms

stack on which. In this regard, we conjectured that replacing one of the three helical arms by a very short stem of two base-pairs terminating in the aptamer loop (in addition to maintaining the two unpaired nucleotides at the junction) may satisfy the rules for maintaing control over helical stacking partners. Thus in the unbound form, the deoxyribosensors might result in conformation which exhibits sub-optimal stacking and general structural destabilization in the two remaining helical stems, and that stacking between the two stems might be restored by the binding of argininamide to the aptamer loop. Thus upon binding argininamide, the aptamer loop would under go structural stabilization and compaction, promoting the formation of the two base pairs, crucial to maintaining stacking control. Here the aptamer component would behave as a "pseudo-stem".

A new family of deoxyribosensors (the ArgA 2.0 family) was therefore designed, based directly on the junction sequences described by Welch (Welch *et al.* 1995). Figure 2-6a below shows the junction sequences for these constructs, and Figure 2-6b, shows the complete secondary structure of a member of this family, ArgA 2.0. Table 2-4 below, summarizes the signals obtained at different guanine residues within the different constructs in response to saturation argininamide binding. Of this family, ArgA 2.01 gave the highest signal at G8. From Table 2-4, as well as from the gel shown in Figure 2-6b, it is evident that ArgA 2.01 also conforms best to design expectations, in that the structural tightening of the aptamer (or R loop, using the terminology of Lilley(Welch *et al.* 1995)) upon argininamide binding leads to significantly improved stacking (and hence charge conduction) between the AQ and the detector stems. Table 2-5 and Table 2-6 summarize that the signal amplification in the detector helix, measured at G8, is, 5-fold

over background when measured in a buffer containing 20 mM Mg^{2+} and, 10-fold in 5.0 mM Mg^{2+} (all in the presence of saturating concentrations (10 mM) of argininamide).

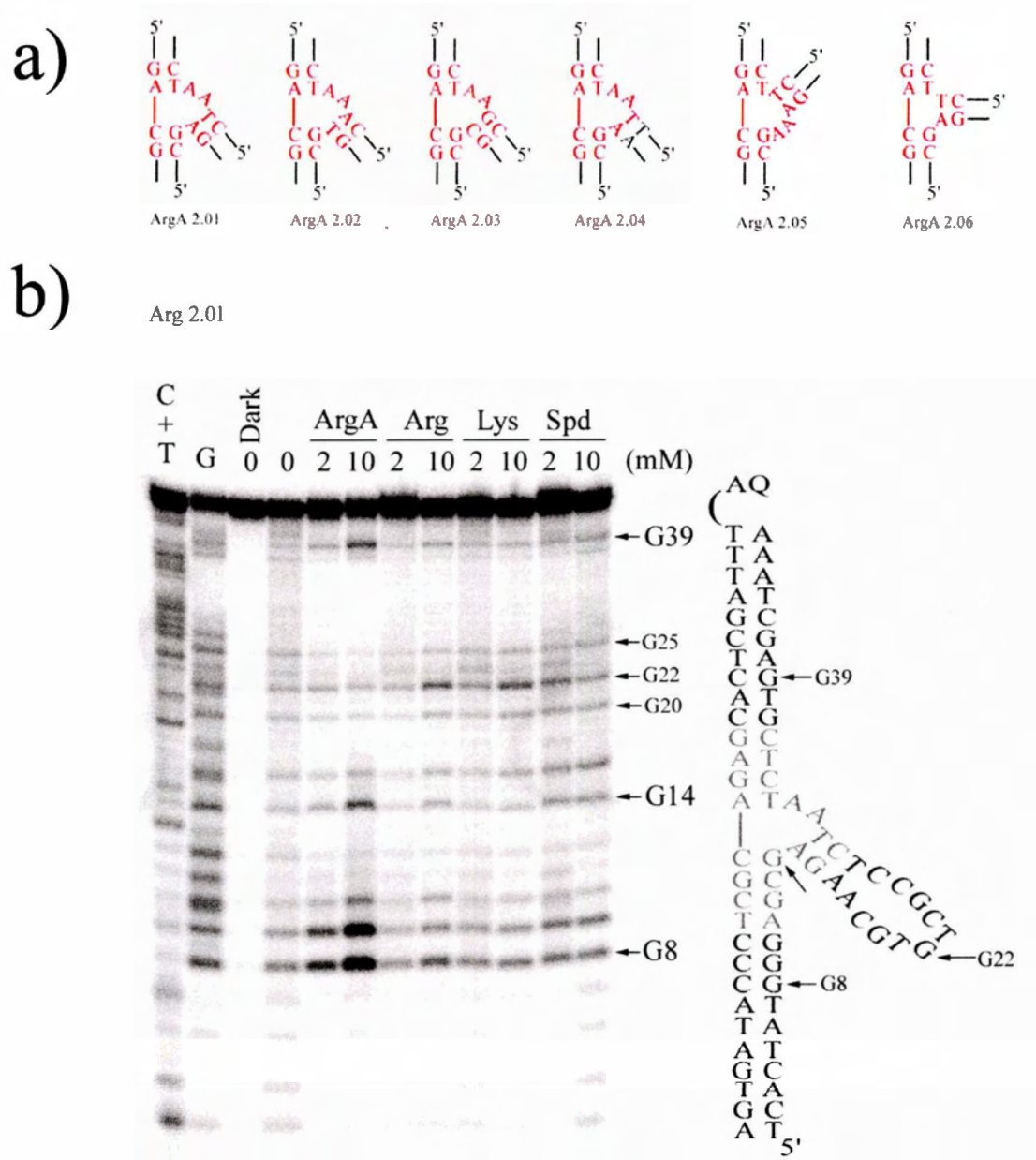

Figure 2-6 The ArgA 2.0 Family. (a) Junction base-pairs for variant members of the ArgA 2.0 family of sensors. (b) Left, gel showing guanine damage patterns in the deoxyribosensor construct ArgA 2.01, in the presence and in the absence of light as well as of different analytes, including L-argininamide (ArgA); L-arginine (Arg); L-lysine (Lys); and, spermidine (Spd). Reference C + T and G ladders are shown to the left. Dark indicates a sample not exposed to either analyte or light; 0 indicates a sample not incubated with any analyte, but exposed to light like the other samples shown in the gel. Right, the secondary structure of the deoxyribosensor, ArgA 2.01.

Furthermore, the large signal increase observed for ArgA 2.01 was also ligand specific. Figure 2-6b as well as Table 2-5 and Table 2-6, show that the large increase in signal at G8 of construct ArgA 2.01 was only produced by the cognate ligand, argininamide, but poorly by the weak ligand arginine and the structurally similar ligands L-lysine and spermidine. In contrast with the constructs of the ArgA 1.0 family, the ArgA 2.0 family constructs gave relatively low levels of ligand-induced signal at the guanine residues of the aptamer loop (for instance, G22). It can be concluded that the aptamer region in these constructs is not the preferred stacking partner for the AQ stem under all concentrations of ligand tested.

Table 2-4 Damage signals at specific guanine residues in the ArgA 2.0 family, in the presence of 10 mM argininamide. Reported signals contain 5% error.

Residue	ArgA 2.01	ArgA 2.02	ArgA 2.03	ArgA 2.04	ArgA 2.05	ArgA 2.06
G22	0.8	1.4	1.1	1.1	2.0	0.8
G14	2.7	4.5	4.4	10.5	4.9	4.2
G8	5.1	3.3	2.5	4.3	3.7	2.6

Table 2-5 Damage signals at ArgA 2.01 guanine residues in response to different ligands in the presence of 20 mM magnesium. Reported signals contain 5% error.

	ArgA		Arg		Lys		Spd	
Residue	2.0mM	10 mM	2.0mM	10 mM	2.0mM	10 mM	2.0mM	10 mM
G22	1.1	0.8	1.0	2.3	1.5	2.1	2.1	1.6
G14	1.0	2.7	0.4	0.9	0.4	0.5	1.2	1.4
G8	2.2	5.1	0.7	1.3	0.7	0.8	0.8	0.8

2.3.2.1 Magnesium Dependence on ArgA 2.01

The signal at G8 in the ArgA 2.01 construct was studied as a function of magnesium concentration. Here, we wanted to see if varying the magnesium concentration while keeping all other factors constant, would give a higher signal at the G8 position. The gel of the magnesium dependence is shown in Figure 2-7 below. It was

found that at constant temperature (19°C), the G8 signal increased progressively in the presence of 0-5mM magnesium, but decreased beyond this concentration.

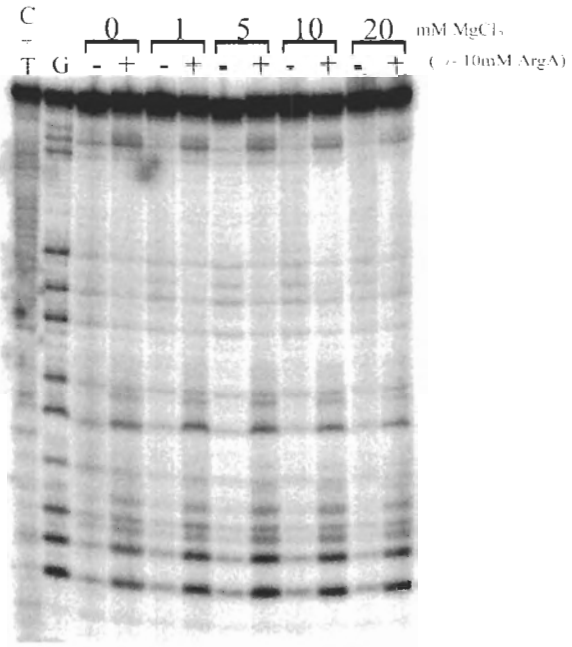

G8 Damage Dependence on Magnesium Chloride Concetration
(Holding Argininamide Constant at 10 mM)

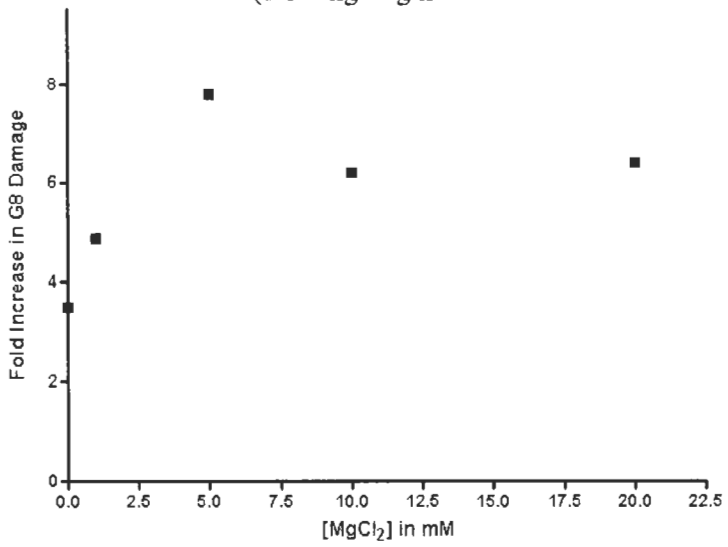

$[MgCl_2]$ in mM	Fold Increse in G8 Damage
0	3.5
1.0	4.9
5.0	7.8
10	6.2
20	6.4

Figure 2-7 G8 damage dependence on magnesium chloride concentration for construct ArgA 2.01. Damage signals for a particular concentration were obtained in the presence or absence of 10 mM ArgA and the fold increase in G8 damage is reported. Reported signals contain 5% error.

The magnesium titration was done in duplicate. There was not a very strong preference for a particular concentration of magnesium, nevertheless it was that 5.0 mM magnesium that gave the best signal to noise ratio, even by a small margin. For each of the five magnesium concentrations assayed, a pair-wise comparison of the signal before and after the ligand is bound is required to measure the "Fold-Increase" due to the addition of the ligand. This is taken into account, as the concentration of magnesium could have an effect on the initial conformation of the deoxyribosensor, and thus the initial background signal. As described in the materials and method section, the calculation of fold increase is as follows: a given band (G8) is taken as a percentage of the total breakdown products in a lane (for example a "plus" lane in Figure 2-7). This is subsequently divided by the percentage breakdown of the same G8 from a control sample where no argininamide is added (a corresponding "minus" lane in Figure 2-7), and the resulting "fold increase" value is obtained. Thus the "fold increase" value depends critically on the magnitude of the "minus" or background/noise signal. Therefore, small fluctuations in this value can have a big impact on the overall magnitude of the "fold increase" value.

Having established the best working magnesium concentration, the next step was to measure again the conduction signals of the ArgA 2.01 guanine residues in response to different ligands in the presence of 5.0 mM magnesium (Table 2-6). Here, the specificity, i.e. signal in response to argininamide versus spermidine, did not change substantially as a function of magnesium concentration (Table 2-6 below).

Table 2-6 Damage signals at ArgA 2.01 guanine residues in response to different ligands in the presence of 5.0 mM magnesium. Reported signals contain 5% error.

	ArgA		Arg		Lys		Spd	
Residue	2.0 mM	10 mM	2.0 mM	10 mM	2.0 mM	10 mM	2.0 mM	10 mM
G22(Gapt1)	1.3	0.6	0.9	1.8	1.8	1.5	2.3	2.8
G14	3.7	6.7	1.0	3.4	1.2	1.1	3.1	7.0
G8	4.8	10.3	0.9	1.7	2.4	1.5	2.6	4.3

2.3.2.2 Temperature Dependence on ArgA 2.01

In efforts to maximize signal to noise ratio of the deoxyribosensors, the signal at G8 in the ArgA 2.01 construct was studied as a function of temperature. The effect of three different temperatures is described, 4°C, 19°C and 37°C, see Figure 2-9 below. Ambient temperature (19°C) was found to be more optimal than 4°C, which gave very low signals. The lower signals obtained at 4°C can be attributed to decreased thermal motions in DNA at this temperature. One of the models describing the mechanism of charge transport in DNA, particularly the phonon assisted polaron like hopping model states that electron hole hopping is assisted by these thermal motions, thus lowering the temperature may reduce the rate of charge transport. At the same temperature (4°C), the irradiation times were varied. Increasing the irradiation time led to high levels of background cleavage at different sites in the deoxyribosensors, thus lowering the signal to noise ratio. At 37°C, too, the signal tended to be erratic, possibly owing to poor levels of ligand binding as well as to enhanced structural mobility of the three-way junction. The gels of these experiments are shown in Figure 2-8 below.

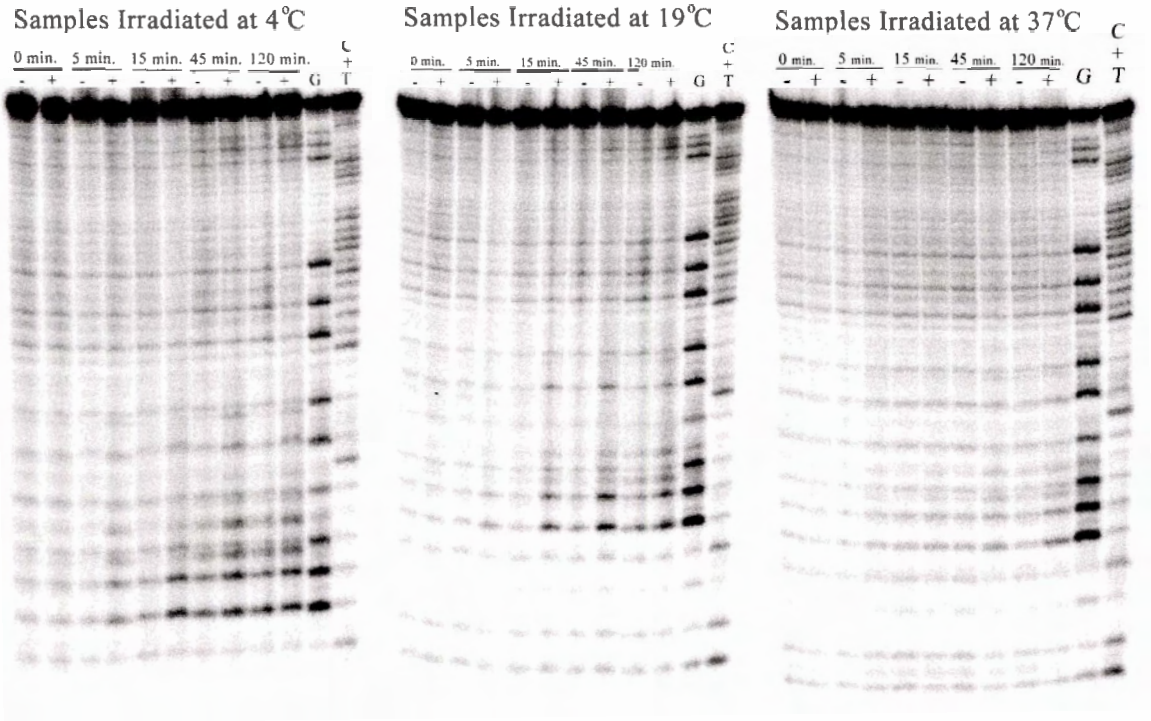

Figure 2-8 Gels of Temperature dependence on G8 Damage for Construct ArgA 2.01. Three different temperatures are represented, 4°C, 19°C and 37°C. Samples irradiated in the presence (+) or absence of argininamide (-).

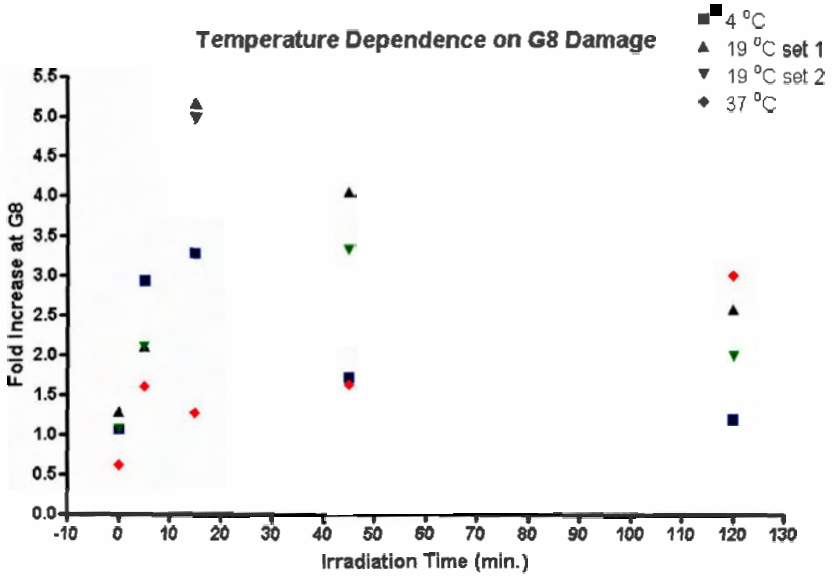

Figure 2-9 Temperature Dependence on G8 Cleavage in ArgA 2.01.

2.3.2.3 Signal Sensitivity and Specificity for the Cognate Ligand, Argininamide

The mode of interaction and binding affinity of the free DNA aptamer for argininamide, its ligand, have been studied extensively; the Kd for the aptamer–argininamide complex has been measured to be, 100 μM (Harada and Frankel 1995). We wished to investigate whether the sensitivity of these deoxyribosensors mirrored the intrinsic affinity of the free aptamer for argininamide. Figure 2-10 shows the signals obtained at various guanine residues within the ArgA 2.01 construct, measured in buffer containing 5.0 mM Mg^{2+}. It was found that at argininamide concentrations greater than 10 mM the signal at G8 plateaued at ~10-fold compared to the signal in the absence of analyte. The effective dissociation constant (K_d) for the deoxyribosensor–aptamer complex was 1.3 +/- 0.4 mM. This dissociation constant was deduced from five replicate experiments. The structural or other factors contributing to this lower sensitivity of the aptamer-containing sensor, relative to the free aptamer itself, remain to be identified; it is likely that the structure of the aptamer is less stable in the context of being structurally coupled to the bulky deoxyribosensor construct. In addition, ligand-binding is likely the sole fuel for the gross conformational rearrangement of the deoxyribosensor. The "energetic price" paid for this may be reflected in the weaker binding constant of ligand to aptamer within the construct versus the free aptamer.

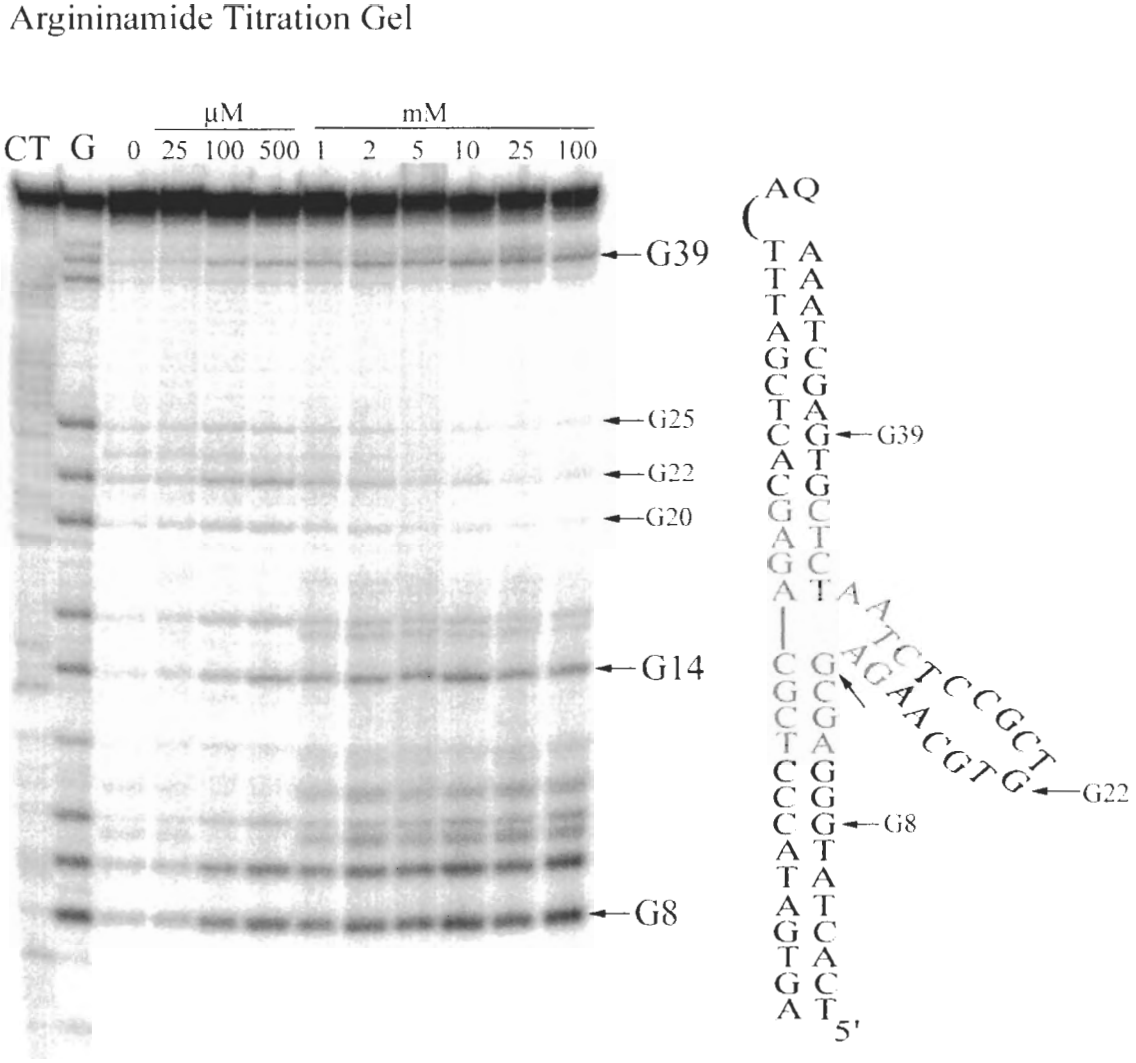

Figure 2-10 Guanine damage patterns in deoxyribosensor construct ArgA 2.01 in response to titration with increasing concentrations of L-argininamide (ArgA).

Curiously, the gel shown in Figure 2-10 suggested that the transition to the "final" folded/stacked conformation of ArgA 2.01 from its initial, "unstacked" state (i.e. in the presence of 5.0 mM magnesium but in the absence of argininamide) was not a simple, two-state transition. For instance, at low concentrations of argininamide (~25 μM – 1 mM) there was a substantial signal seen in the guanine residues within the aptamer loop; however, this signal disappeared at concentrations of higher argininamide. It appeared, therefore, that in the "early" stages of ligand stabilization, an equilibrium existed between

the AQ/aptamer and AQ/detector stacks, which was resolved, at higher concentrations of ligand, into the predominance of the AQ/detector stack. Curiously, with increasing concentrations of argininamide, a monotonic increase was seen in that signal at G39, in the AQ stem, remote from the junction itself. Thus, ligand-binding brought about a stabilization of the helical stack between the X and H (AQ and detector) stems and contributed to the overall stability of the helices themselves, even in the presence of the already stabilizing buffer concentration of 5.0 mM magnesium.

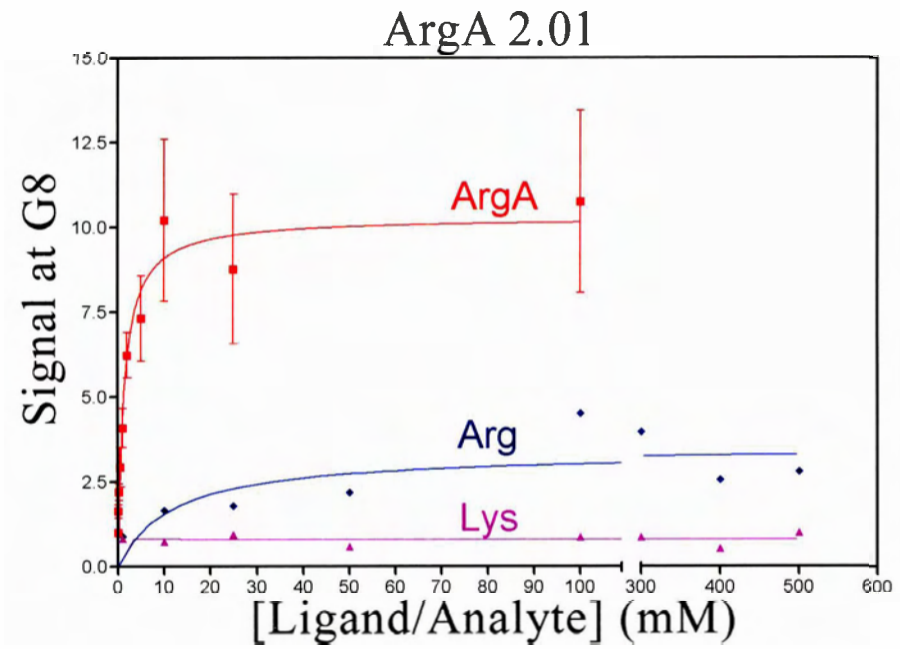

Figure 2-11 Response signals from analyte binding (measured as the ratio of oxidative damage at G8 in the deoxyribosensor construct ArgA 2.01 in the presence versus absence of added analyte) as functions of analyte concentrations

Figure 2-11 plots the signals measured in the ArgA 2.01 deoxyribosensor in response to the binding of L-argininamide, L-arginine, and L-lysine, respectively. The aptamer element has been shown to be specific for binding the guanidinium functionality of the ligand; nevertheless, the binding affinity of the aptamer for arginine is ~20-fold lower than that for argininamide (Harada and Frankel 1995). Correspondingly, Figure

2-11 shows that a significantly higher concentration of arginine (50 mM) was required to obtain the saturating arginine signal from the deoxyribosensor. Figure 2-11 shows clearly the specificity of the deoxyribosensor for its "natural" ligand, argininamide. The aptamer has no special affinity for binding the amino acid lysine; correspondingly, the signal response to lysine remains at the background level for the entire concentration range of lysine tested. Another interesting observation is that even at saturation, the peak signal from arginine binding is substantially lower than that obtained from argininamide binding. The high-resolution NMR structure reported for this aptamer has been solved with bound argininamide (Robertson *et al.* 2000). It may very well be that arginine does not bind to the aptamer in exactly the same way. Moreover, conformational change induced in the aptamer by arginine binding may not be identical with or, indeed, as pronounced as that produced by argininamide binding. Changes in the overall deoxyribosensor conformation, as monitored by changes in damage signal intensities, may thus be different for saturation binding of argininamide and arginine.

2.3.3 Expanding the versatility of the ArgA 2.0 Deoxyribosensor

At this point, a working biosensor made of DNA for the detection of argininamide had been established and the results were published in the Journal of Molecular Biology (Sankar and Sen 2004). The original goal of the project was to see if a general construct could be designed such that replacement of only the aptamer domain by a different aptamer would change the specificity of the sensor. This is what was attempted in this section, and the RNA aptamer for theophylline was chosen as the new recognition element. Theophylline is a small, uncharged xanthine based molecule and differs from caffeine by only a methyl group at the N-7 position (Figure 2-12 below). The aptamer

has a K_d of 0.1 μM for theophylline, and this binding affinity this 10,000 fold greater than the aptamer's affinity for caffeine (Jenison *et al.* 1994). Theophylline is a biomedically important compound, as it is used widely as a bronchodilator in the treatment of asthma, bronchitis and emphysema (Hendeles and Weinberger 1983). Theophylline has a narrow therapeutic index; not enough and the drug has no noticeable effect, too much and it becomes toxic. Dosages vary from patient to patient depending on how they metabolize the drug, one person may require a dosage 4 to 5 times higher than another (Hendeles and Weinberger 1983). Thus, a patient wishing to make this drug work for them safely and effectively must have their blood tested for the amount of theophylline present in order to decide on a dosage that is right for them. Levels of theophylline in the blood must be monitored carefully, as chemically similar compounds like theobromine (3,7-dimethylxanthine), which like caffeine can be found in the blood stream. The RNA theophylline aptamer does just that, it provides high specificity and affinity for its cognate ligand (Jenison *et al.* 1994).

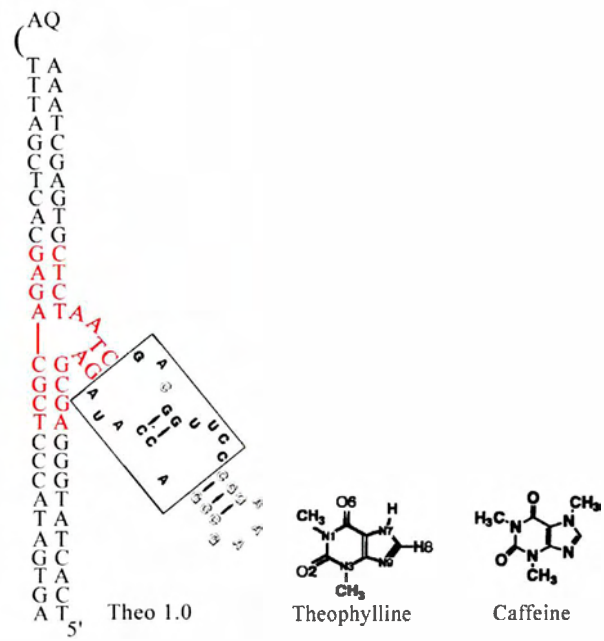

Figure 2-12 Structure of the theophylline deoxyribosensor, Theo 1.0 along with the structure of its cognate ligand and closely related analog, caffeine.

We incorporated the theophylline aptamer into the two stranded, three-way junction based deoxyribosensor motif to test if the core of this sensor could serve as a universal platform for many different aptamers, the resulting construct was accordingly named Theo 1.0. In contrast to what we were working with before (the all DNA ArgA construct) the aptamer containing strand was now a chimeric molecule, where the middle part of the molecule in which the aptamer was situated was made of RNA and the flanking detector and AQ pairing regions were DNA. This is depicted in Figure 2-12, where the boxed region and its stabilizing terminal loop make the RNA component of the strand. The boxed region represents only the theophylline-binding domain. The 5' end of the aptamer-containing strand is once again ^{32}P end labeled on its 5' hydroxyl in order to visualize guanine damage.

Numerous experiments to make Theo 1.0 function as a deoxyribosensor were tried. Unfortunately, visualization of the data was very poor, which lead to unreliable

quantitation, having very (background levels) weak and erratic signal. An example of this poor signal is seen in the following gel for the titration of theophylline on Theo 1.0 (Figure 2-13). Here the reaction conditions are as follows: 0.5 μM DNA (each strand), 5.0 mM $MgCl_2$, 50 mM Tris Cl pH 8.0, 50 mM NaCl, 50 μM EDTA.

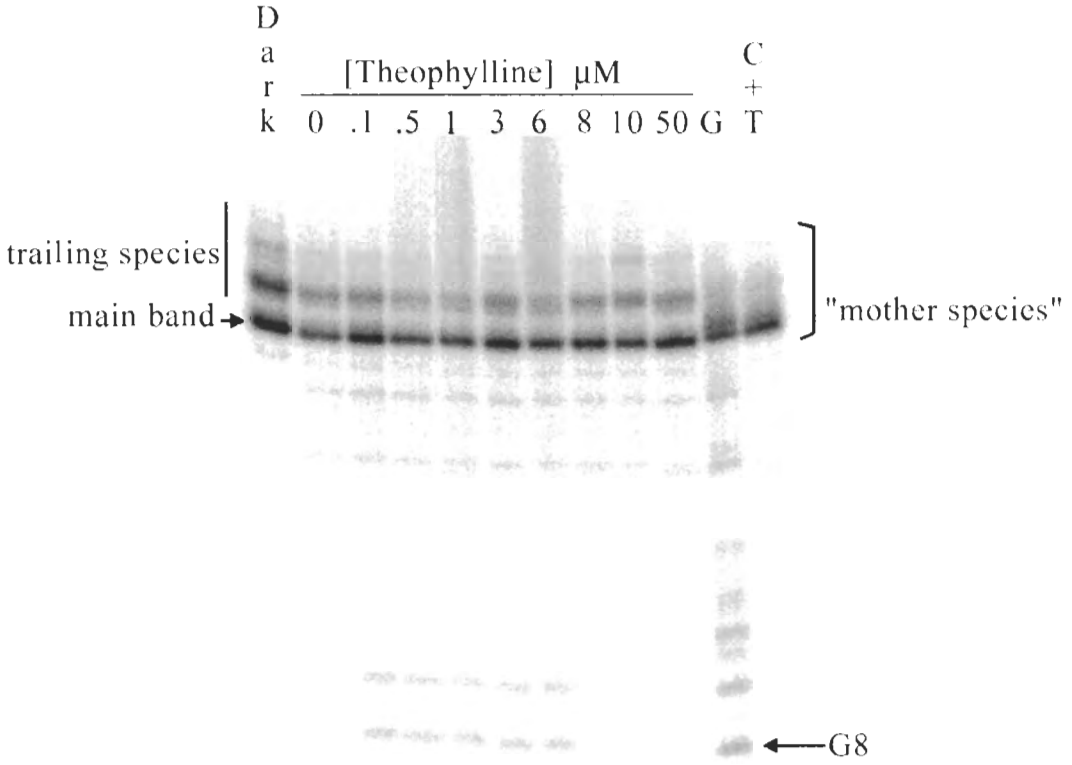

Figure 2-13 Theophylline titration on construct Theo 1.0.

Detection of a lesion on a 5' most guanine on a GGG run is visualized as a break in the DNA strand after treatment of the sample in a 10% piperidine solution at 90°C for 30 min. Because the RNA region (the theophylline aptamer is made of RNA) of the strand that contains the GGG run is also piperidine labile, this posed complications in establishing the "mother species" from which breakdown is measured. This also skewed the amount of breakdown products loaded in a lane of an electrophoresis gel from lane to lane as the complete removal of the RNA region varied greatly. Three different

quantitation methods were employed in order to better interpret the data; Method A: the damage at G8 was taken as the percentage of the breakdown products that included the main band and the breakdown products below it; Method B: the damage at G8 was taken as the percentage of the breakdown products that included the main band, the most prominent trailing species above it and the breakdown products below it; Method C: the damage at G8 was taken as the percentage of the total breakdown products in the entire lane, (this included the main band and any trailing species above it) see Figure 2-13 above. Results of the densitometry analysis are shown in Table 2-7. From Table 2-7, all of the three methods of quantitating the data showed that very little damage, ~ 1% breakdown (background) was occurring in all lanes, regardless of the amount of theophylline added to the sample. From the gel we could see that very little signal, if any, was getting through to the detector stem, as the bands in this section were extremely faint. From the chemically modified reference ladders the effect of trailing species was still there but the effect appeared attenuated, this is because the ladders are modified with harsh chemicals to force a cleavage products, namely DMS for the G ladder and Hydrazine for the C+T ladder, followed by treatment with hot base (piperidine) (see Materials and Methods). We then increased the incubation time from 30 minutes in hot piperidine to 60 minutes in the Theo 1.0 samples in attempts to reduce the amount of trailing species, as they are suspected to be uncleaved segments of the RNA aptamer region. Unfortunately this had very little or no noticeable effect on the presence of the trailing species.

Table 2-7 Quantitated Data from Theophylline titration on Theo 1.0. Methods A, B and C are shown. Reported signals contain 5% error.

Method A : G8 As a Fraction of Main Peak

Theophylline(μM)	Relative damage at G8 within lane (%)	Damage at G8 due to addition of Theophylline
0	2.56	1.00
0.1	2.12	0.83
0.5	2.76	1.08
1	2.69	1.05
3	1.94	0.76
6	2.66	1.04
8	2.11	0.82
10	1.83	0.71
50	1.92	0.75

Method B: G8 As a Fraction of Main Peak Plus Trailing Peaks

Theophylline(μM)	Relative damage at G8 within lane (%)	Damage at G8 due to addition of Theophylline
0	1.43	1.00
0.1	1.44	1.01
0.5	1.77	1.24
1	1.74	1.22
3	1.31	0.92
6	1.62	1.14
8	1.40	0.98
10	1.02	0.72
50	1.25	0.87

Method C: G8 Damage As a Fraction of All Peaks in the Lane

Theophylline(μM)	Relative damage at G8 within lane (%)	Damage at G8 due to addition of Theophylline
0	1.28	1.00
0.1	1.29	1.01
0.5	1.56	1.22
1	1.59	1.24
3	1.19	0.93
6	1.45	1.13
8	1.23	0.96
10	0.92	0.72
50	1.15	0.90

After several attempts to optimize the reaction conditions of Theo 1.0, no improvement in the quality of the data was obtained. Although we did not have any success with the Theo 1.0 construct we still wanted to see if we could make a sensor for theophylline. We took our approach of making a universal three-way junction based sensor back to the drawing board and decided to incorporate the aptamer into the integrated ligand sensor as described by Fahlman and Sen (Fahlman and Sen 2001). In this scenario, the aptamer is placed directly in the path for charge transfer to the detector

stem. The theophylline aptamer has the ability to be separated in to two separate strands by removal of the terminal stem loop, making the task of incorporating this aptamer into a conducting duplex simple. This construct was named Thru Theo 1.0, its secondary sequence structure and control constructs are shown in Figure 2-14.

Figure 2-14 Constructs for the Theo Thru 1.0 sensor and their controls. In red are the aptamer regions, upper case represents DNA nucleotides and lower case represents RNA nucleotides, a brake in a line indicate where a strand nick is located.

For the Thru Theo 1.0 construct to function, both the "AQ-strand" and the "Detector strand" had to be DNA/RNA chimeras. In all the other constructs we could get away with making the AQ-strand all DNA because the electron sink (GGG) containing strand would also contain the entire aptamer. The reason that this poses a problem is that when coupling the Anthraquinone moiety to the "AQ-strand" the coupling conditions, coupling time, coupling temperature and the impurities in the Anthraquinone-NHS ester synthesis, pose degrading conditions for the RNA component of the chimeric oligomer which would resulting in low yields (see Materials and Methods). For this reason Theo 1.0 is a "nicked construct" where a break in the AQ containing strand is required (Figure

2-14). Because charge transport was occurring through a nicked region in Thru Theo 1.0, control constructs were made to visualize what would be the maximal signal at the GGG run if the unstructured aptamer region was not present, the "nicked duplex control" provides a basis for this comparison (Figure 2-14). Another control, the "perfect duplex control" would provide a comparison for how the nick affected charge transport in this chimeric construct (Figure 2-14). Since charge transport has been observed in DNA duplexes that contained perturbations such as abasic sites (Gasper and Schuster 1997) and single stranded overhangs (Kan and Schuster 1999), we conjectured that a nick in the DNA helix may also permit charge transport through it. Also, evidence of charge transport through RNA/DNA hybrids has been observed to occur in hybrid duplexes of 19 and 30 base pairs in length but in much less efficient manner (Sartor *et al.* 1999). For these reasons we were hopeful that this construct would generate a functioning sensor for theophylline, having significant signal to noise ratio.

Unfortunately, the results obtained from the Thru Theo 1.0 experiments were no different from those in the three-way junction based Theo 1.0 experiments, the data was inconclusive, and very difficult to quantitate and analyze. In all experiments involving the Thru Theo 1.0 construct and its control variants, no appreciable G damage was visualized when the gels were quantitated. After repeated trials, these were the best gels obtained (Figure 2-15).

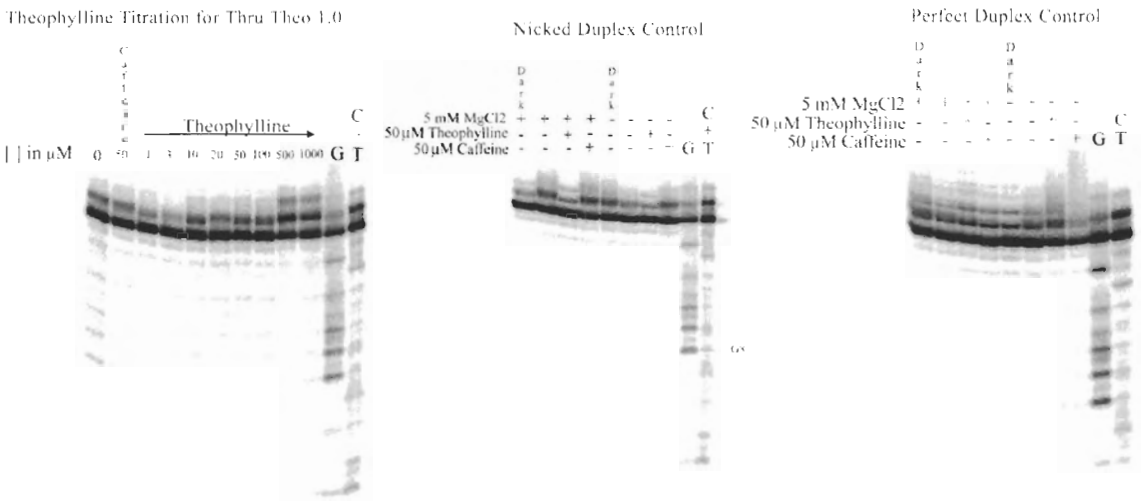

Figure 2-15 Thru Theo 1.0 and control constructs. Gels depicting a theophylline titration, and general charge transport in the control variants.

Other conditions were attempted in efforts to improve the damage signal at G8, including increasing the irradiation time and irradiating at a few different temperatures (namely 4,19 and 35 degrees Celsius). After several attempts to optimize the reaction conditions of Thru Theo 1.0, no improvement in the quality of the data was obtained. In one such experiment, an RNA sequencing method as described by Peattie (Peattie 1979) allowed us to visualize any damage if any occurring at the RNA region (see Materials and Methods). Although the data was messy, the RNA sequencing experiment on the "perfect duplex control" revealed two bands in the RNA region which stood out. Unfortunately the damage at these two bands was the same in the UV irradiated samples as in the dark controls. From this we can confirm that conduction through these RNA/DNA chimeras was very poor, if it was occurring at all.

2.3.4 Further Optimization of the Signal to Noise ratio in ArgA 2.01

Although at this point the signal to noise ratio that we obtained for the ArgA 2.01 construct was reasonably appreciable, we set out to further increase the signal to noise

ratio. The issue was not so much in the actual amount of G damage observed when the ligand bound the aptamer region, but in the amount of G damage even before the ligand was added (background signal). Since the signal for damage at the G8 position is calculated as the "fold increase" in signal over the background, effectively lowering the background signal, even slightly, would proportionally increase the response/fold increase signal. For example; if the background signal is 2.0% and the bound signal is 10%, if we effectively lower the background to 1.0 %, then a five-fold increase in signal becomes a tenfold increase in signal. One way to achieve lowering of the background signal would be by initial disruption of the deoxyribosensor structure such that the path for charge transport between the AQ stem and Detector stems is severely affected. This is what is attempted in this section. The concept was to incorporate a short oligomer, having complementary sequence to the aptamer region, as part of the initial deoxyribosensors construct. This would disrupt the structure of the deoxyribosensor construct and thus the electron path to the detector stem. Varying length of these "interfering-oligos" could then be tested to find the optimal size which would effectively lower the background signal. Upon addition of the true ligand (ArgA) the interfering oligo, would be displaced and a signal would be detected see Figure 2-16 below.

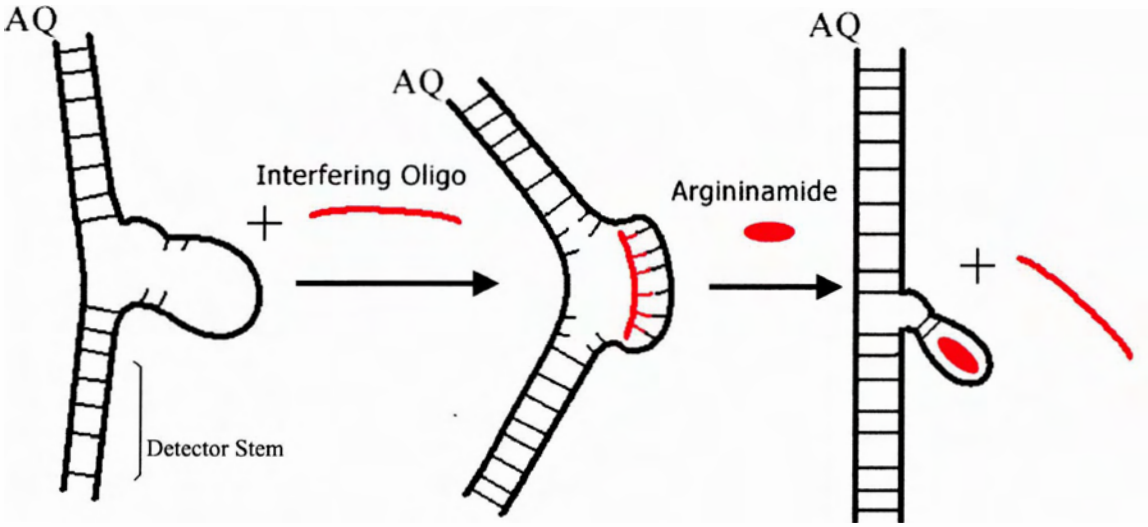

Figure 2-16 A model conceptualizing "Signal Enhancement of Nucleic Acid Biosensors Using Small Oligomers". A short oligonucleotide complementary to the aptamer sequence is added to perturb the initial deoxyribosensor conformation in the absence of the ligand argininamide. The interfering oligo would serve as to minimize the amount of charge transfer to the detector stem in the absence of ligand and thus lower the background signal.

A set of six interfering oligos, (ArgI) were then designed to perturb the initial structure of the ArgA2.01 construct. These oligos range in length from 6 to 17 nucleotides, and their sequences are shown in Figure 2-17 below.

ArgI-6: 5'CGACAC
ArgI-8: 5'GCGACACG
ArgI-10: 5'GGCGACACGT
ArgI-12: 5'AGGCGACACGTT
ArgI-14: 5'GAGGCGACACGTTC
ArgI-17: 5'TTAGAGGCGACACGTTC

Figure 2-17 Arg 2.01 construct and set of Interfering oligomers. The six asterix at the tip of the aptamer region show how ArgI-6 would bind to the Arg 2.01 construct. The rest of the ArgI family variants would then advance towards the junction of the construct in two nucleotide increments.

The idea was to systematically increase the length of the interfering oligonucleotide and progressively "approach" the junction form the aptamer region, where the interfering oligo is designed to bind. An example of this is described in Figure 2-17 where the asterix indicates the bases in the aptamer loop where interfering oligo ArgI-6 is designed to bind. The gels for one set of these experiments are shown in Figure 2-18 below, and Table 2-8 contains the results of 3 replicate experiments of this type.

Table 2-8 Effect of Interfering oligomers on ArgA 2.01 Net Signal. Reported signals contain 5% error. Reported signals contain 5% error.

Set1	Signal before addition of ArgA	Signal after addition of ArgA	Fold Increase in G8 Damage	Set2	Signal before addition of ArgA	Signal after addition of ArgA	Fold Increase in G8 Damage	Set3	Signal before addition of ArgA	Signal after addition of ArgA	Fold Increase in G8 Damage
ArgI-6	1.4	11.8	8.3	ArgI-6	1.8	12.1	6.8	ArgI-6	1.9	13.0	6.7
ArgI-8	1.0	10.5	10.2	ArgI-8	1.6	10.3	6.7	ArgI-8	1.4	10.8	7.5
ArgI-10	1.0	7.3	7.6	ArgI-10	0.9	5.7	6.8	ArgI-10	1.3	6.9	5.4
No ArgI	1.7	10.1	6.1	No ArgI	1.3	12.4	9.3	No ArgI	1.6	15.4	9.7
ArgI-12	1.0	6.7	6.7	ArgI-12	1.0	8.0	8.4	ArgI-12	1.0	8.3	8.6
ArgI-14	1.3	9.0	7.1	ArgI-14	1.2	7.2	5.8	ArgI-14	1.5	8.3	5.5
ArgI-17	0.9	4.2	4.6	ArgI-17	0.9	4.1	4.4	ArgI-17	1.2	5.2	4.3
No ArgI	1.5	10.3	6.7	No ArgI	1.4	13.7	9.9	No ArgI	1.6	14.7	9.1

Looking at set 1 of the results, it appears that all of the interfering oligos have decreased the background signal (signal before the addition of ArgA) to some extent, but as the oligomers got longer the response signal in the presence of ArgA decreased, from a high of 11.9 to 4.2. This effect can be attributed to the increasing amount of energy needed to displace an oligomer of longer length over a shorter one by the binding of the true ligand argininamide. These results show qualitatively the strength of the Watson-Crick base pairing of a small oligomer to the aptamer sequence versus the affinity of the aptamer sequence for its cognate ligand. This phenomenon is not new, as in nature, a similar scenario exists where riboswitches are able to sense the cellular environment for metabolites in this manner (Mandal *et al.* 2003). This is demonstrated most notoriously in this data set by the effect of oligo ArgI-17, the longest interfering oligomer. ArgI-17, perturbs the initial structure the most, reflecting in the lowest signal before the addition of ArgA, but because of its length and thus number of WC base pair interactions it makes with the aptamer region of the deoxyribosensor, it is also the most difficult to displace. From set one ArgI-8 seemed to successfully accomplish the task that we had been

seeking, lowering the initial background signal while maintaining the same response signal.

Unfortunately, this effect was not reproducible as the data from sets 2 and 3 show contrasting results where ultimately the deoxyribosensor ArgA 2.01 worked best in the absence of any interfering oligomer (Table 2-8). Nevertheless, observing all the data sets, a general trend exists; a longer oligomer will disrupt the initial structure best, and thus reduce the background signal, but it will also lower the response signal. The response signal is lowered to an extent which makes the use of these interfering oligos pointless.

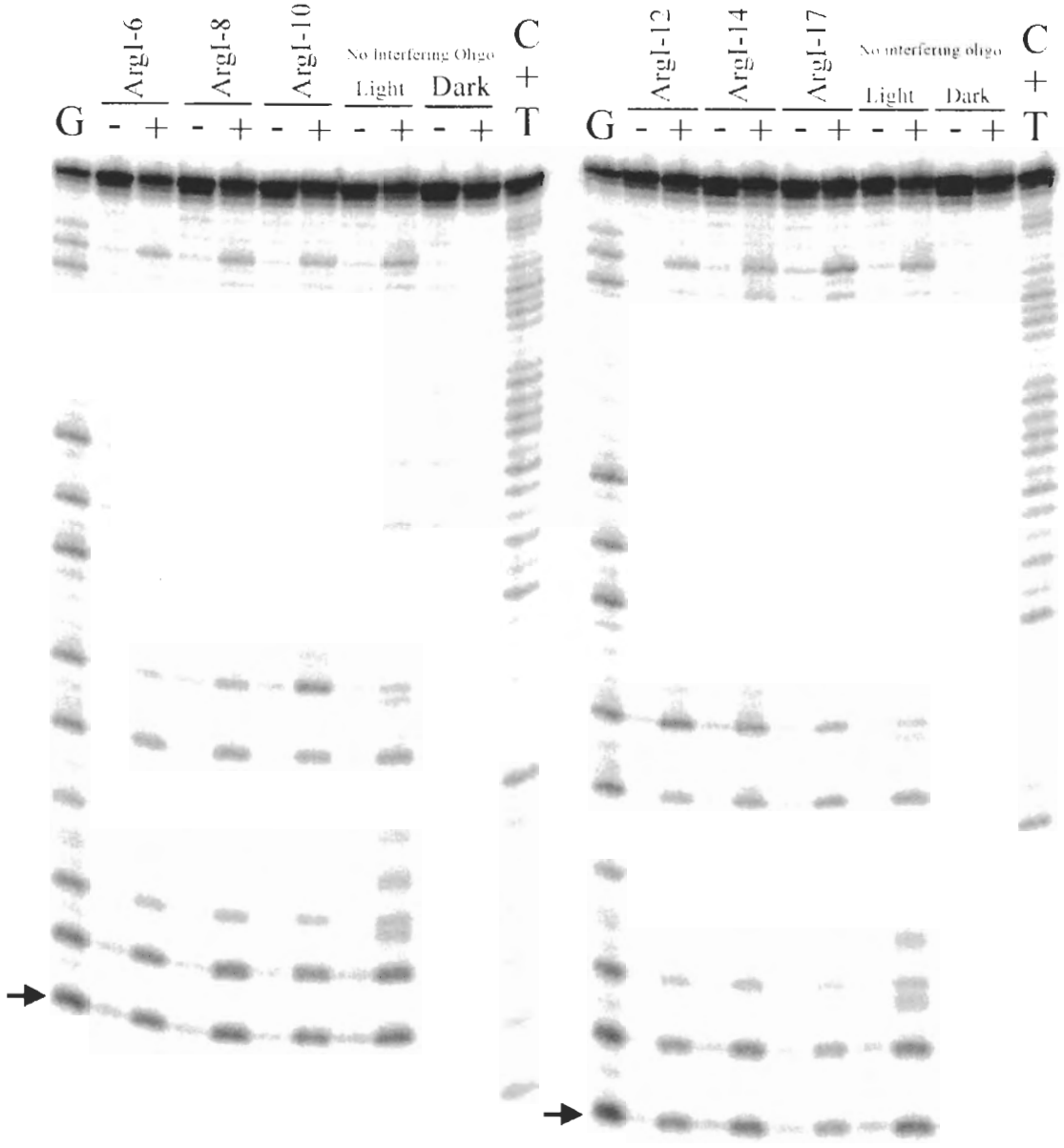

Figure 2-18 Gels depicting the effect of an interfering oligomer on the net signal produced by construct Arg 2.01. The arrow refers to position G8, nucleotide number 8 from the 5'end of the aptamer-containing strand. +/- Refer to the presence or absence of Argininamide.

2.4 Structure Probing of DNAzymes Using Charge Transport

2.4.1 Introduction and Experimental Approach

Working in a lab where several DNA enzymes have been selected, and thoroughly characterized for their enzymatic properties, elucidating the structure of these DNAzymes would aid understanding their mode of action. Out of the many ways there exist to characterize the structure of a complexly folded DNA molecule, such as X-ray crystallography, NMR, or computer based molecular dynamics to name a few, simple low-tech chemical probing can give significant qualitative and quantitative information about the intramolecular interactions of these DNA enzymes.

As we saw earlier, Figure 2-10 depicts a gel showing the titration of argininamide on the ArgA 2.01 deoxyribosensor. This gel not only illustrates the doexyribosensor's affinity for its cognate ligand but also gives us some information in the manner in which the deoxyribosensors is structured. In this gel we see the transition from the initial structure, where the AQ stem and the aptamer stem predominantly stack, to the final structure where the AQ stem and detector stem appear to stack optimally. This effect is seen where at low concentrations of argininamide oxidative damage occurs in the aptamer loop, but as the concentration of argininamide increases this damage attenuates and damage in the detector stem increases. In this fashion we can have a sense of which helical stems are stacking with the oxidant-containing stem in a DNA molecule containing a three-way junction.

In this section, such concepts are utilized to probe for the helical arm stacking partners in the DNAzymes Bipartite (Feldman and Sen 2001), which was selected for in our lab, and the 8-17 DNA enzyme selected by Santoro and Joyce (Santoro and Joyce

1997). Both of these enzymes are DNA molecules whose catalytic ability is to cleave an RNA molecule at its phosphodiester bond. These DNA enzymes recognize their RNA substrates in a Watson-crick base pairing fashion, and by varying the sequence of their recognition arms they can potentially recognize any RNA substrate. Potentially these enzymes may have applications in the pharmaceutical and biotechnology industry as they can be designed to target any messenger RNA of choice. The goal of the work described in these preliminary experiments is to see if probing for helical arm stacking partners in branched DNA by monitoring charge transport can be used as a general tool for gaining structural information from helix containing structures. The secondary structures of these DNAzymes and a control double helix are shown in Figure 2-19. These constructs were designed such that only one anthraquinone labeled DNA oligomer (S-multi) would have to be synthesized. This would serve as a multiple substrate for both of these constructs. For practical considerations, an all DNA substrate is used here in place of the native RNA substrate, as RNA is easily susceptible to breakdown due to its 2'hydroxyl, facilitating phosphodiester cleavage.

These E-Bipartite, E-8-17 and E-comp strands were ^{32}P end labeled and irradiated with UV light at 366 nm in a regular electron transfer experiment. Both of these DNAzymes are, require divalent cations for catalysis, especially for magnesium. When the magnesium concentrations are in the millimolar range (~ 30 mM for Bipartite whereas 8-17 can tolerate magnesium concentrations in 100 mM range with increasing catalytic rate) the DNAzymes display optimal catalytic rates. Therefore we performed a magnesium titration on these constructs to investigate if we could see a transition from an inactive conformation of the DNAzyme to an active one. In contrast to the previous

reaction conditions, the experimental reactions only included 0.5μM DNA (for each strand of a construct) and 50 mM Tris-Cl pH 8.0 to which magnesium was titrated.

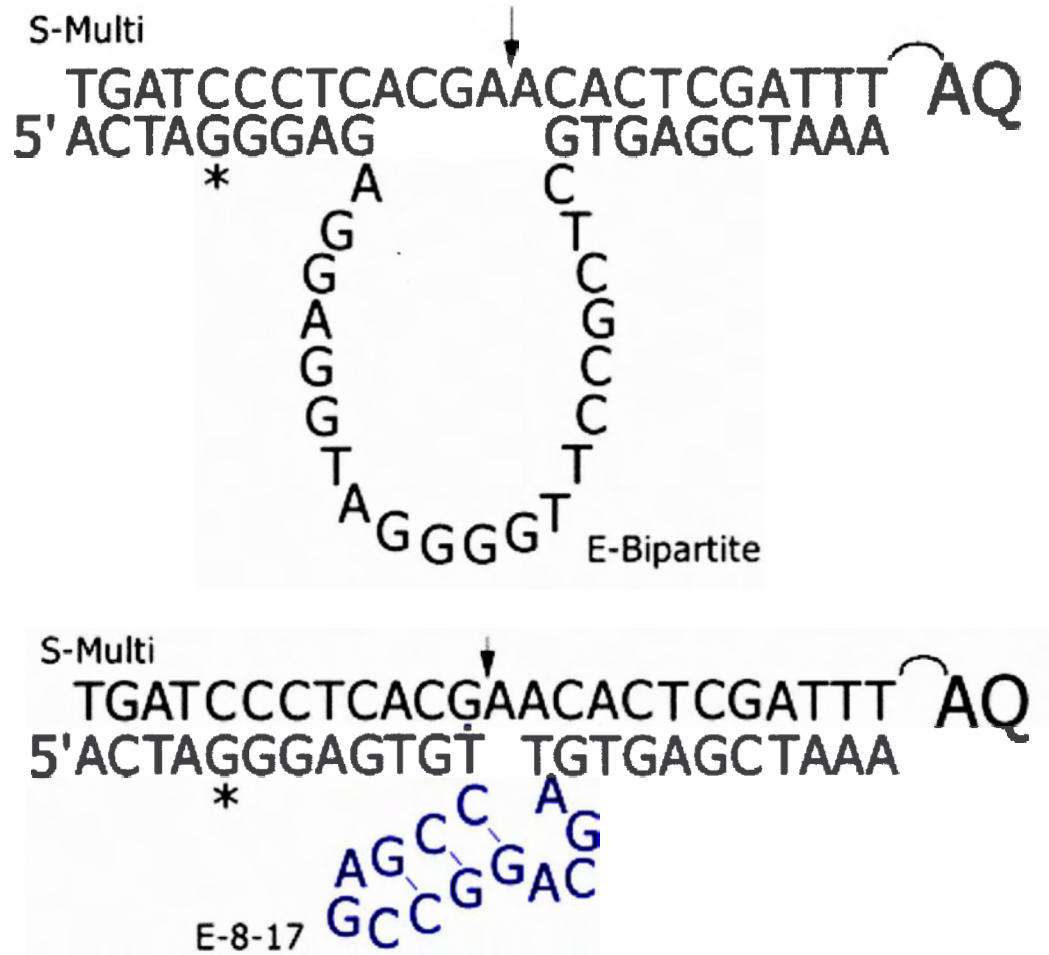

Figure 2-19 Secondary structure of RNA cleaving DNA enzymes. Top: the "Bipartite" DNAzyme, Bottom: the "8-17" DNAzyme. The arrows indicate where the DNAzymes cleave their RNA substrate. The conserved enzymatic core for "8-17" is highlighted in blue, the conserved enzymatic core for "Bipartite" is the entire loop, commencing at A and ending at C.

2.4.2 Probing for Helical-Arm stacking Partners in Bipartite

A gel showing the cleavage patterns of due to oxidative damage caused by charge-transport for the bipartite DNAzyme is shown in Figure 2-20. From this gel we can see that the amount of oxidative damage is getting through to the stem containing the GGG run is quite low and does not fluctuate with changes in magnesium concentration.

This tells us one piece of in formation right away; these two arms are not coaxially stacked in a manner that would permit charge transport. This is evident in the lack of a pronounced damage pattern in the GGG containing stem. Another interesting facet presented by this gel is the damage at nucleotides G33 and G31. Both of these are in this construct's AQ stem and the trend is that with increasing magnesium concentration, we see decreases in the amount of oxidative damage at these positions. From zero to 10 mM magnesium there is a steady drop in the reactivity to these guanines (33 and 31). Beyond 10 mM Magnesium, as the concentration of magnesium increase the reactivity of these guanines plateaus off (Figure 2-21 and Figure 2-22). The results of the densitometry measurements are shown in Table 2-9.

Another marked pattern is observed for guanines 27 and 16 (Figure 2-23 and Figure 2-24). Both of these guanines are in the conserved enzymatic core of this enzyme. For the Bipartite, the conserved enzymatic core is the entire loop as depicted in Figure 2-19, commencing at A on the 5' side and ending at C on the 3' side. The other conserved requirement for the Bipartite is the need for the two adenines where enzymatic cleavage takes place between them; this is shown by the arrow in Figure 2-19. The folded structure of the enzymatic core is not known and is currently being investigated by our laboratory. For guanine 27, from 0 to 100 μM magnesium the signal rapidly drops, and for concentrations exceeding 100 μM magnesium, the damage remains essentially the same. For guanine 16, the reverse of these patterns is observed.

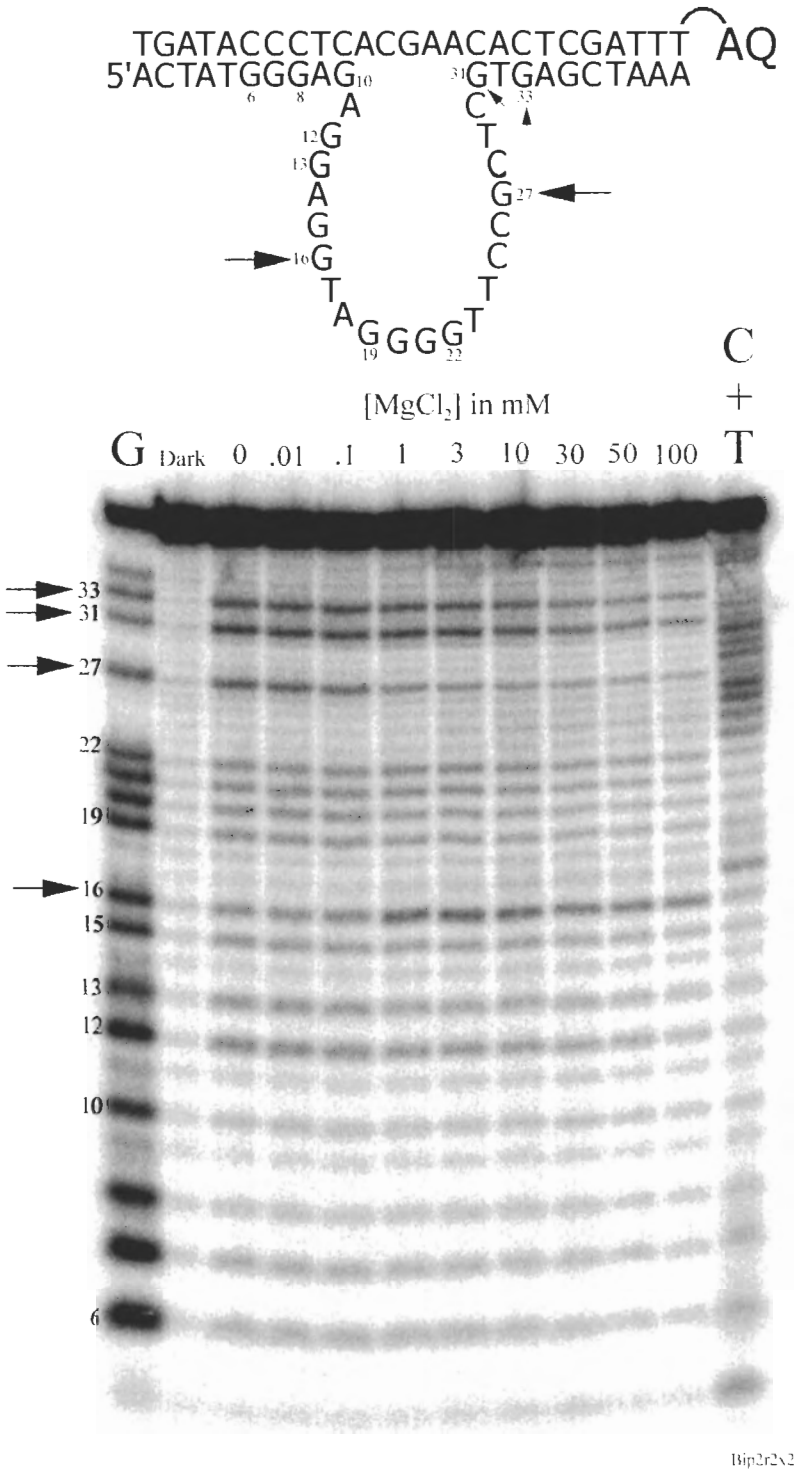

Figure 2-20 Damage Patterns for the Bipartite DNA enzyme. See text for explanation.

For guanine 16 we see a sharp increase in the damage for magnesium concentrations ranging from 0 to 100 μM (Figure 2-20). After this point, concentrations

exceeding 100 μM magnesium do not result in any changes in the reactivity of G16, since the level of damage remains essentially the same. It can be inferred that from this damage pattern a major, abrupt change in structure of the enzymatic core happens between 100 μM and 1.0 mM magnesium chloride. This is notoriously evident just by visual inspection of the gel in Figure 2-20 as the intensities of the bands under go an abrupt change. This implies that at low concentrations of magnesium G27 is to some extent stacked with the AQ containing stem. When concentrations of magnesium increase to > 1.0 mM, G16 is now more coaxially stacked with the oxidant containing arm.

The damage patterns from G31 and G33 also imply that when the concentration of magnesium reaches ~ 30 mM, which is the optimal concentration for multiple turn over (Feldman and Sen 2001), an attenuation in oxidative damage is seen here. This is analogous to G39 in Arg 2.01 where more damage was observed as argininamide concentrations were increased. We argued that argininamide binding was tightening up the helix, leading to increased damage at this nucleotide. Following with the same concept, as we reach the enzyme's most favorable magnesium concentration for multiple turn-over catalysis (~ 30 mM magnesium), we see a "loosening effect" of the strands for the AQ containing stem, which is manifested in its decreasing oxidative reactivity (Figure 2-21 and Figure 2-22). It is important to note that these two residues are in close proximity to the conserved AA in the substrate strand where cleavage of the phosphodiester bond has been shown to occur (Feldman and Sen 2001).

The reactivity of the four guanines in the enzymatic core remain essentially the same as the level of magnesium is varied. The reactivity of one such guanine, G22 is

graphed in Figure 2-25. A more detailed analysis of the reactivity of the guanines in this construct is given in Table 2-9. Replicate experiments also produce the same trends seen in this example for the enzyme Bipartite.

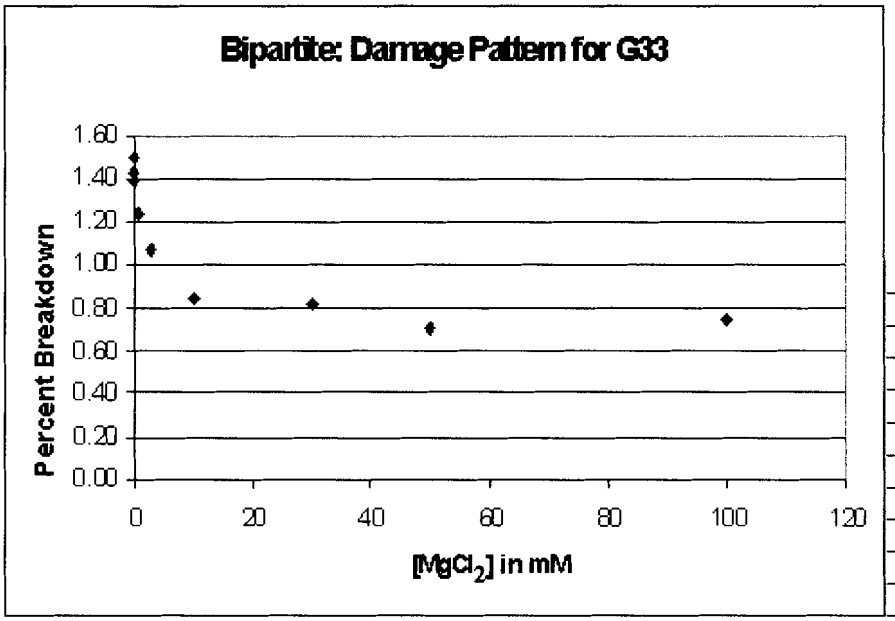

Damage for G33	
[$MgCl_2$] mM	% BrkDwn
0	1.44
0.010	1.50
0.10	1.40
1.0	1.23
3.0	1.07
10	0.84
30	0.82
50	0.70
100	0.75

Figure 2-21 Graphical representation outlining the damage patterns for G33 in Bipartite. Reported signals contain 5% error.

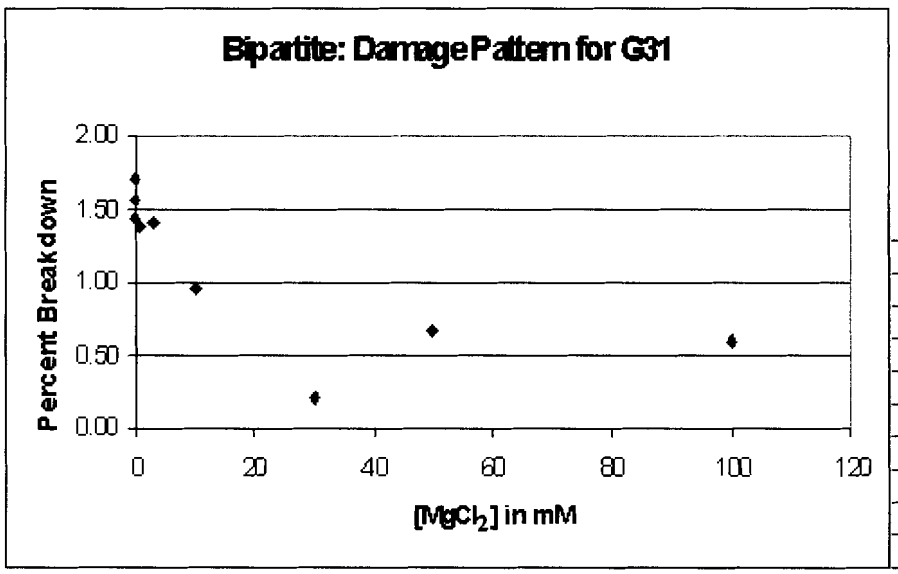

Damage for G31	
[$MgCl_2$] mM	% BrkDwn
0	1.72
0.010	1.57
0.10	1.43
1.0	1.38
3.0	1.41
10	0.96
30	0.22
50	0.67
100	0.59

Figure 2-22 Graphical representation outlining the damage patterns for G31 in Bipartite. Reported signals contain 5% error.

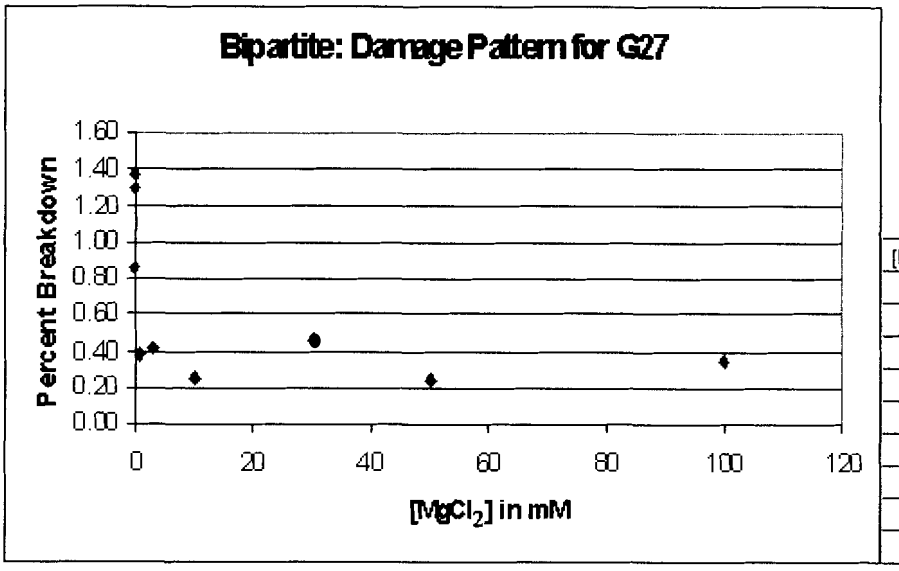

Damage for G27	
$[MgCl_2]$ mM	% BrkDwn
0	1.30
0.010	1.38
0.10	0.86
1.0	0.38
3.0	0.42
10	0.25
30	0.46
50	0.25
100	0.35

Figure 2-23 Graphical representation outlining the damage patterns for G27 in Bipartite. Reported signals contain 5% error.

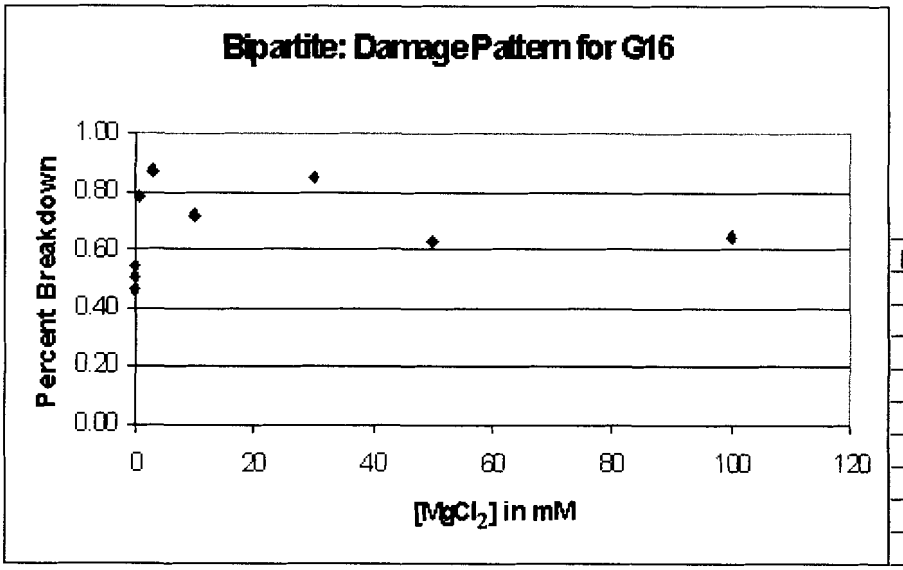

Damage for G16	
$[MgCl_2]$ mM	% BrkDwn
0	0.54
0.010	0.51
0.10	0.46
1.0	0.78
3.0	0.87
10	0.72
30	0.85
50	0.63
100	0.65

Figure 2-24 Graphical representation outlining the damage patterns for G16 in Bipartite. Reported signals contain 5% error.

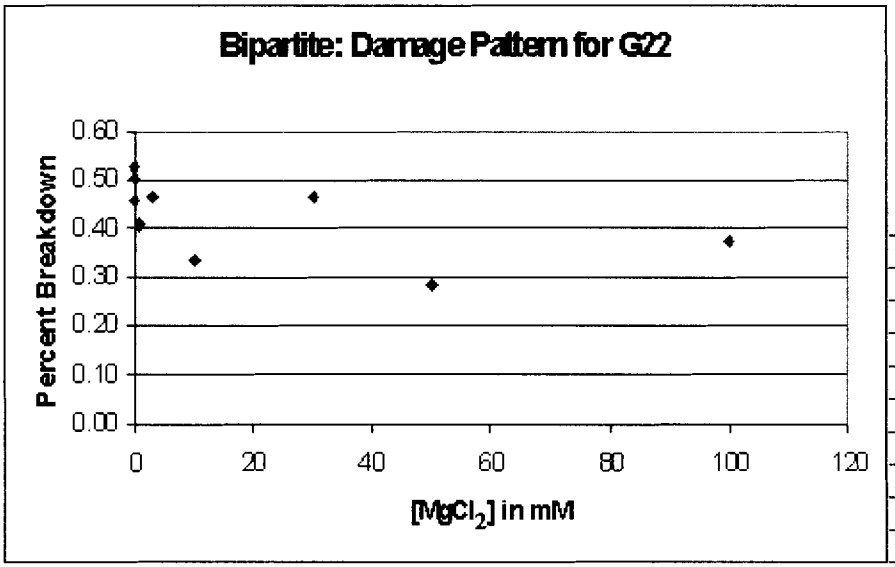

Damage for G22	
[$MgCl_2$] mM	% BrkDwn
0	0.53
0.010	0.51
0.10	0.46
1.0	0.41
3.0	0.47
10	0.34
30	0.47
50	0.28
100	0.38

Figure 2-25 Graphical representation outlining the damage patterns for G22 in Bipartite. Reported signals contain 5% error.

Table 2-9 Quantitation for the Bipartite DNA showing the relative damage to all its guanine residues. Reported signals contain 5% error.

Bipartite	Percent Breakdown at Indicated Magnesium Concentration (mM)								
Guanine	0	0.010	0.10	1.0	3.0	10	30	50	100
33	1.44	1.50	1.40	1.23	1.07	0.84	0.82	0.70	0.75
31	1.72	1.57	1.43	1.38	1.41	0.96	0.22	0.67	0.59
27	1.30	1.38	0.86	0.38	0.42	0.25	0.46	0.25	0.35
22	0.53	0.51	0.46	0.41	0.47	0.34	0.47	0.28	0.38
21	0.47	0.50	0.41	0.36	0.38	0.26	0.35	0.21	0.31
20	0.46	0.48	0.36	0.25	0.30	0.17	0.28	0.16	0.26
19	0.46	0.45	0.33	0.25	0.27	0.17	0.32	0.17	0.27
16	0.54	0.51	0.46	0.78	0.87	0.72	0.85	0.63	0.65
15	0.43	0.42	0.31	0.28	0.30	0.25	0.33	0.21	0.27
13	0.47	0.49	0.38	0.30	0.30	0.25	0.36	0.23	0.28
12	0.59	0.62	0.48	0.40	0.39	0.32	0.39	0.30	0.29
10	0.19	0.22	0.18	0.15	0.15	0.17	0.23	0.16	0.21
8	0.17	0.19	0.16	0.16	0.15	0.17	0.19	0.17	0.17
7	0.31	0.30	0.29	0.27	0.24	0.23	0.26	0.21	0.20
6	0.29	0.29	0.28	0.26	0.28	0.25	0.23	0.20	0.20

2.4.3 Probing for Helical-Arm stacking Partners in 8-17

The second DNA enzyme assayed for helical arm stacking partners was the 8-17 DNAzyme. Under the same conditions, and same range of magnesium concentrations, a

gel showing novel results was obtained. The gel for the probing experiment on 8-17 is shown in Figure 2-26. Graphs showing the results of the densitometry measurements for the various guanines in the 8-17 DNAzyme are shown in Figure 2-27 to Figure 2-39. Looking at the damage patterns for guanines 6,7, 8 and 10 in the GGG containing arm, the reactivity appears noisy with a relatively small spread with respect to the concentration of magnesium administered (Figure 2-36 to Figure 2-39). In general, guanines 30 and 28 on the AQ stem, guanines 25, 22 and 21 in the catalytic core and guanine 12 on the GGG containing stem (G12 is closest to the "junction" of the construct) all see a sharp drop in reactivity under the range of 0-1mM magnesium. For concentrations exceeding 1mM magnesium, the signal stabilizes into a relatively flat line (see corresponding figures below). This flat line effect is most evident in the 10 mM-100 mM, where the DNAzyme structure does not seem to undergo any major structural changes. The sharp drop and decrease in reactivity is also punctuated by a burst-like increase at ~3mM magnesium, thereafter the signal drops and essentially stabilizes. The other two guanines deep in the catalytic core, G16 and G18, show no significant changes in reactivity under all concentrations of magnesium (Figure 2-32 and Figure 2-33 respectively).

From these results it can be inferred that in the absence of, or at lower concentrations of magnesium, both G12 in the detector stem and some guanines in the catalytic core (G25, G22 and G21) are being damaged. This implies that, at zero or small magnesium concentrations, the structure of the 8-17 DNAzyme has a fork like structure, where both the detector arm and the catalytic core are partially stacking with the AQ stem. As magnesium concentrations reach 10mM, the signals in the detector arm and the

catalytic core rapidly drop and stabilize without any further changes in guanine reactivity as magnesium concentration is elevated from 10 to 100mM. This implies that for this magnesium-dependent DNAzyme, when it is fully folded, its GGG-containing stem and the catalytic core are grossly out of plane from the AQ containing stem. This effect can be confirmed by recent work from Liu and Lu where a FRET study on the structure of 8-17 was performed (Liu and Lu 2002). The results revealed the relative orientations of the three arms in transition from an unfolded to a folded state and those results coincide with the damage patterns reported here. A model depicting the relative orientations of these arms is given in Figure 2-40.

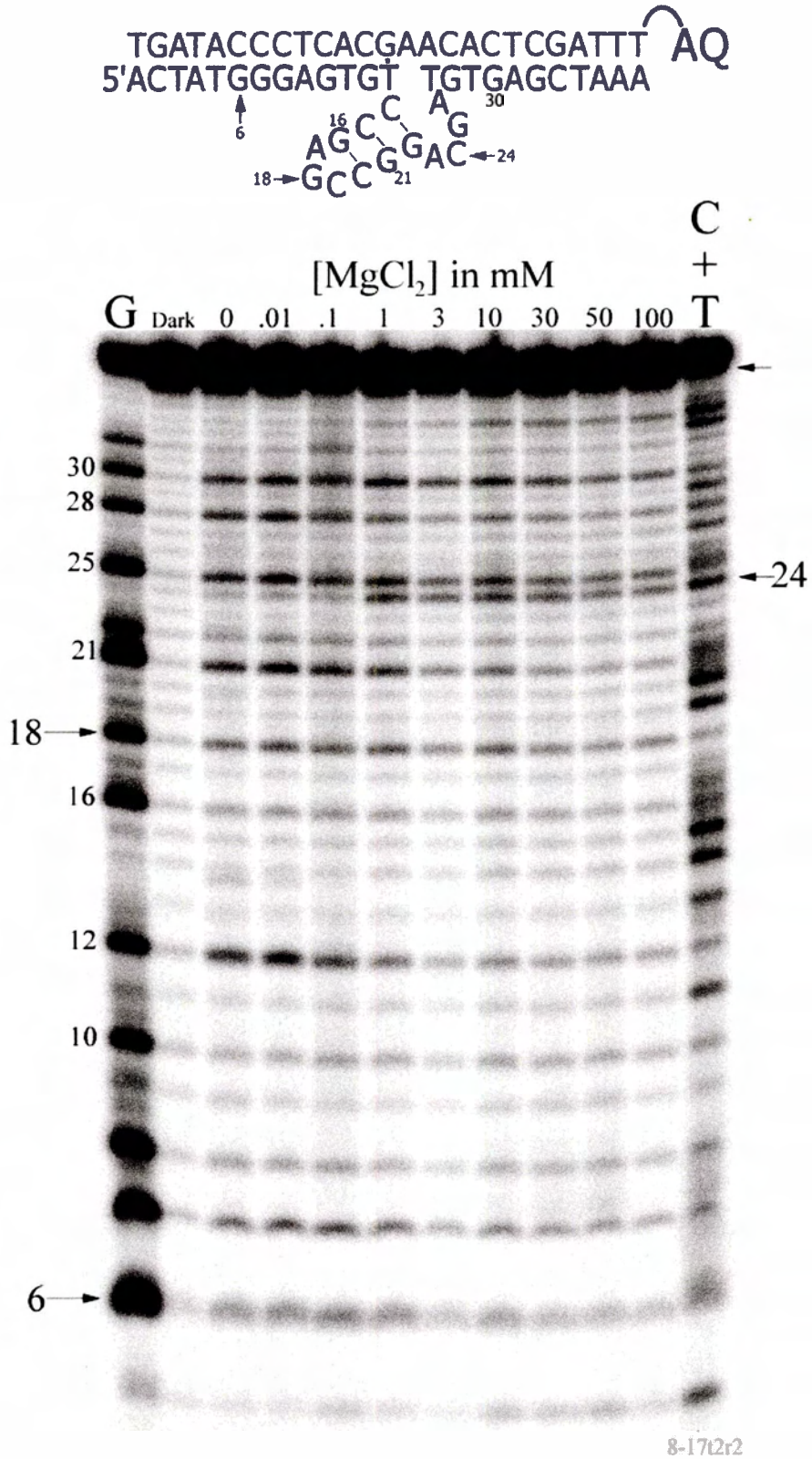

Figure 2-26 Damage Patterns for the 8-17 DNAzyme. See Text for explanation.

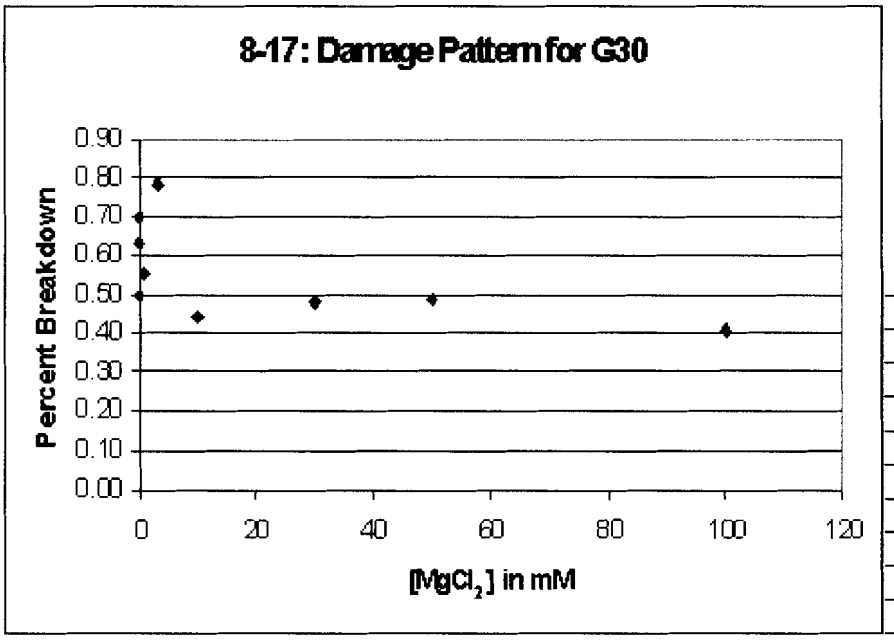

Damage for G30	
[$MgCl_2$] mM	% BrkDwn
0	0.70
0.010	0.63
0.10	0.50
1.0	0.55
3.0	0.78
10	0.44
30	0.48
50	0.48
100	0.41

Figure 2-27 Graphical representation outlining the damage patterns for G30 in the 8-17 DNAzyme. Reported signals contain 5% error.

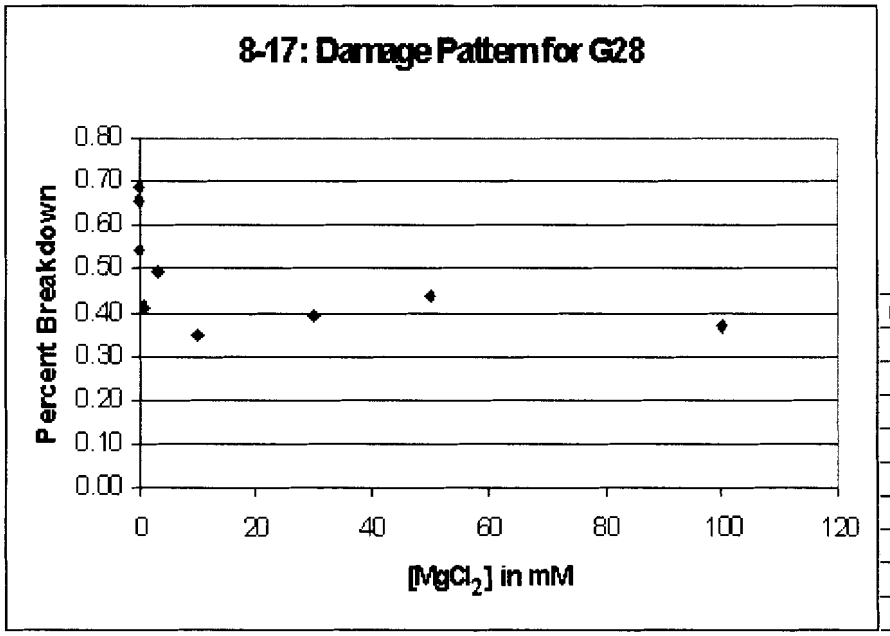

Damage for G28	
[$MgCl_2$] mM	% BrkDwn
0	0.68
0.010	0.66
0.10	0.54
1.0	0.41
3.0	0.49
10	0.35
30	0.39
50	0.44
100	0.37

Figure 2-28 Graphical representation outlining the damage patterns for G28 in the 8-17 DNAzyme. Reported signals contain 5% error.

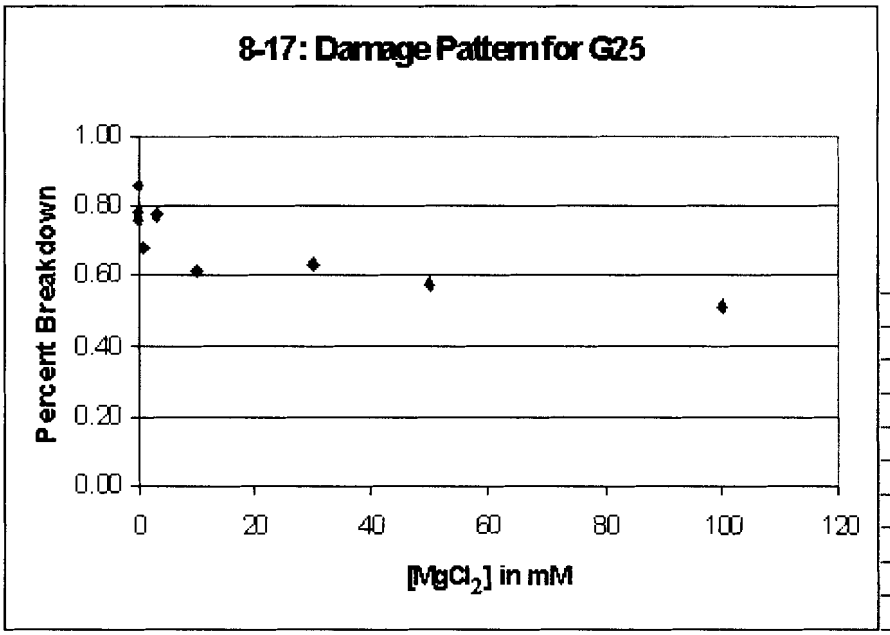

Damage for G25	
[$MgCl_2$] mM	% BrkDwn
0	0.86
0.010	0.77
0.10	0.78
1.0	0.68
3.0	0.78
10	0.62
30	0.63
50	0.58
100	0.51

Figure 2-29 Graphical representation outlining the damage patterns for G25 in the 8-17 DNAzyme. Reported signals contain 5% error.

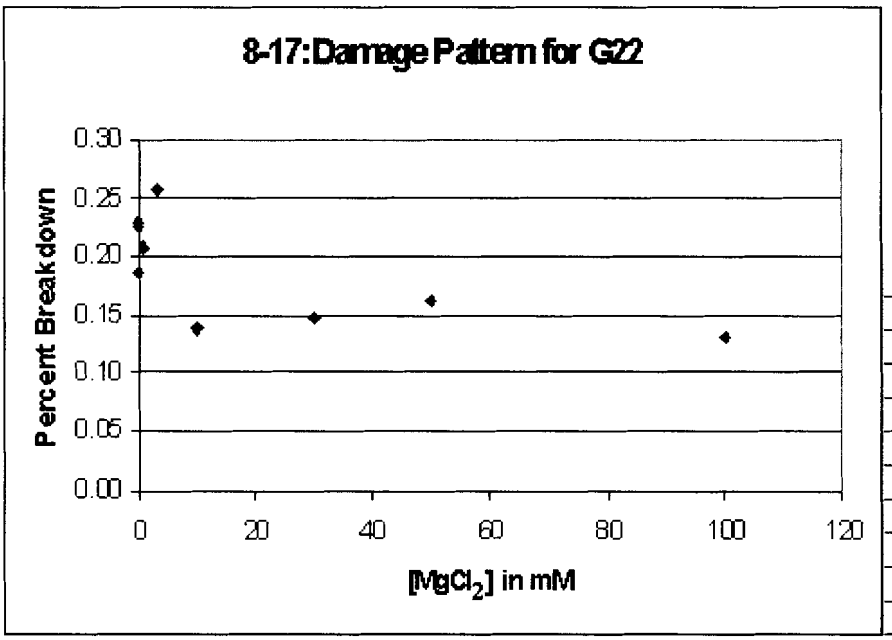

Damage for G22	
[$MgCl_2$] mM	% BrkDwn
0	0.23
0.010	0.19
0.10	0.23
1.0	0.21
3.0	0.26
10	0.14
30	0.15
50	0.16
100	0.13

Figure 2-30 Graphical representation outlining the damage patterns for G22 in the 8-17 DNAzyme. Reported signals contain 5% error.

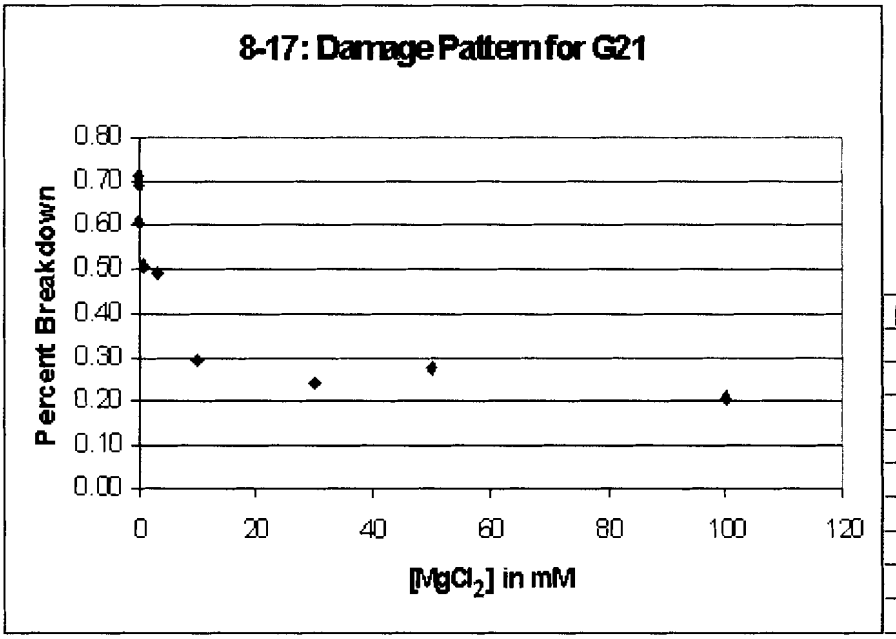

Damage for G21	
[$MgCl_2$] mM	% BrkDwn
0	0.71
0.010	0.60
0.10	0.69
1.0	0.51
3.0	0.49
10	0.29
30	0.24
50	0.27
100	0.21

Figure 2-31 Graphical representation outlining the damage patterns for G21 in the 8-17 DNAzyme. Reported signals contain 5% error.

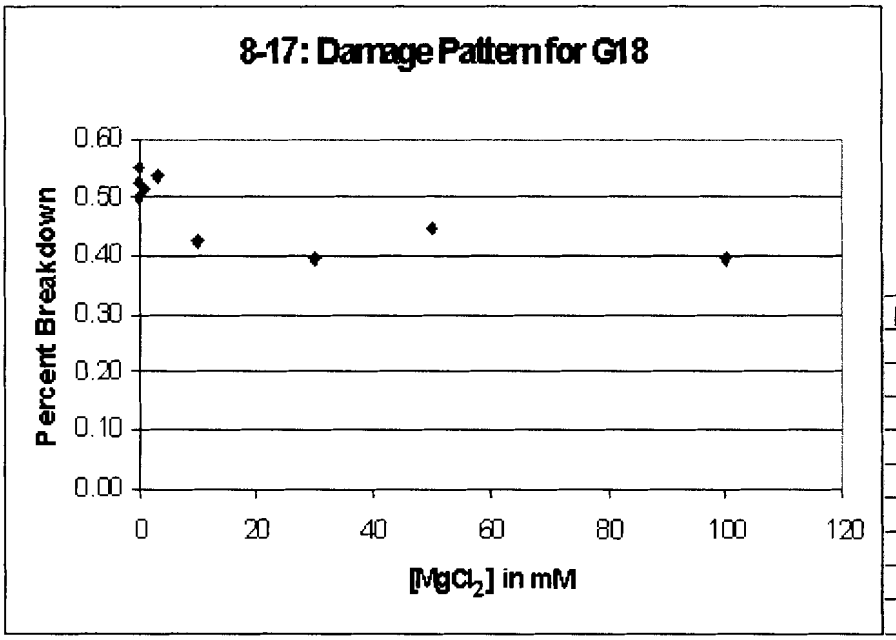

Damage for G18	
[$MgCl_2$] mM	% BrkDwn
0	0.53
0.010	0.50
0.10	0.55
1.0	0.52
3.0	0.54
10	0.43
30	0.39
50	0.45
100	0.40

Figure 2-32 Graphical representation outlining the damage patterns for G18 in the 8-17 DNAzyme. Reported signals contain 5% error.

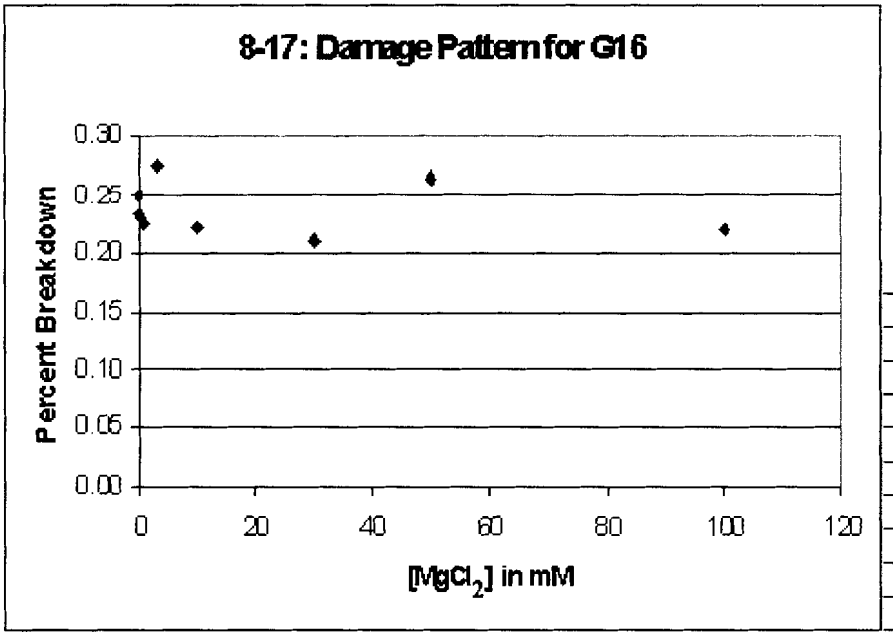

Damage for G16	
[$MgCl_2$] mM	% BrkDwn
0	0.23
0.010	0.25
0.10	0.23
1.0	0.23
3.0	0.27
10	0.22
30	0.21
50	0.26
100	0.22

Figure 2-33 Graphical representation outlining the damage patterns for G16 in the 8-17 DNAzyme. Reported signals contain 5% error.

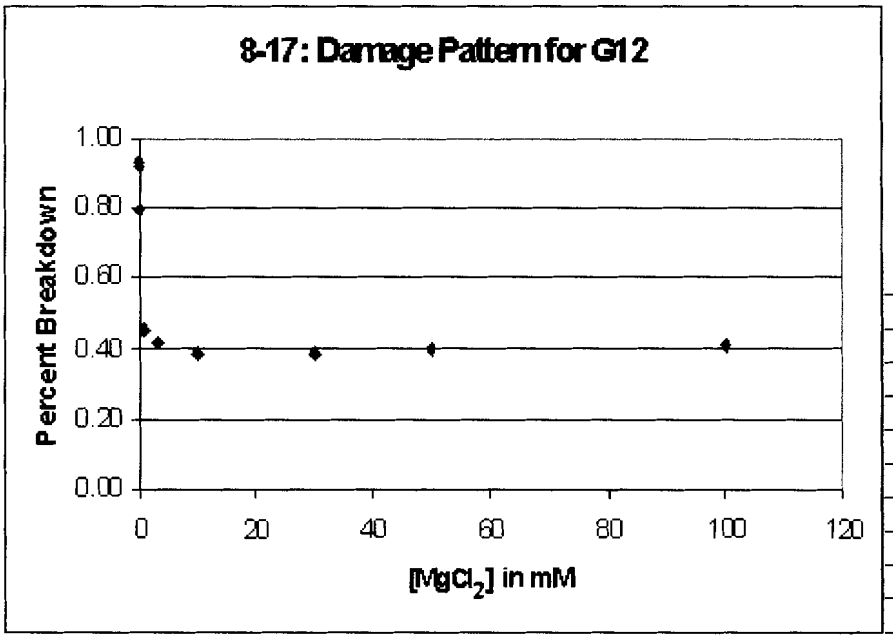

Damage for G12	
[$MgCl_2$] mM	% BrkDwn
0	0.93
0.010	0.92
0.10	0.79
1.0	0.45
3.0	0.42
10	0.39
30	0.38
50	0.40
100	0.41

Figure 2-34 Graphical representation outlining the damage patterns for G12 in the 8-17 DNAzyme. Reported signals contain 5% error.

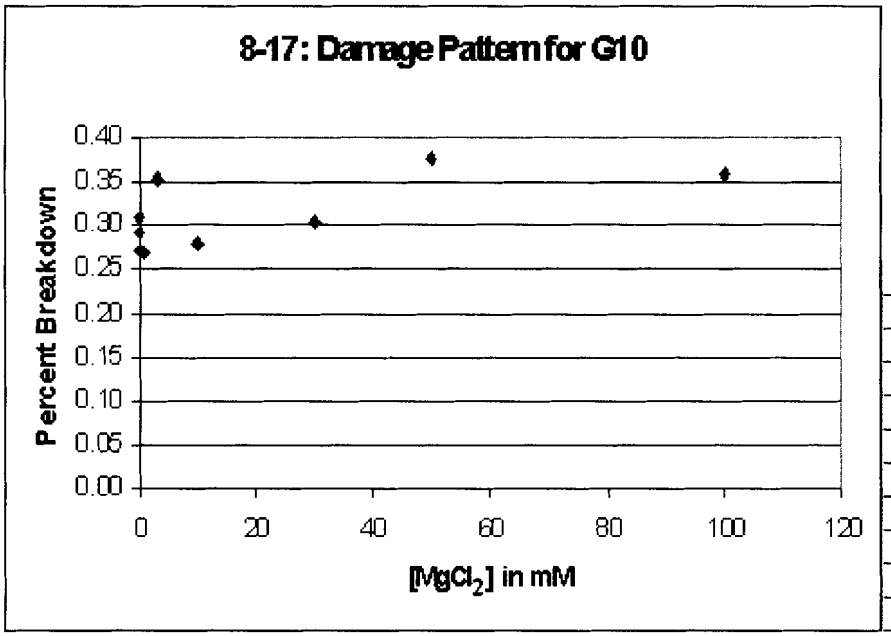

Damage for G10	
[$MgCl_2$] mM	% BrkDwn
0	0.27
0.010	0.31
0.10	0.29
1.0	0.27
3.0	0.35
10	0.28
30	0.30
50	0.38
100	0.36

Figure 2-35 Graphical representation outlining the damage patterns for G10 in the 8-17 DNAzyme. Reported signals contain 5% error.

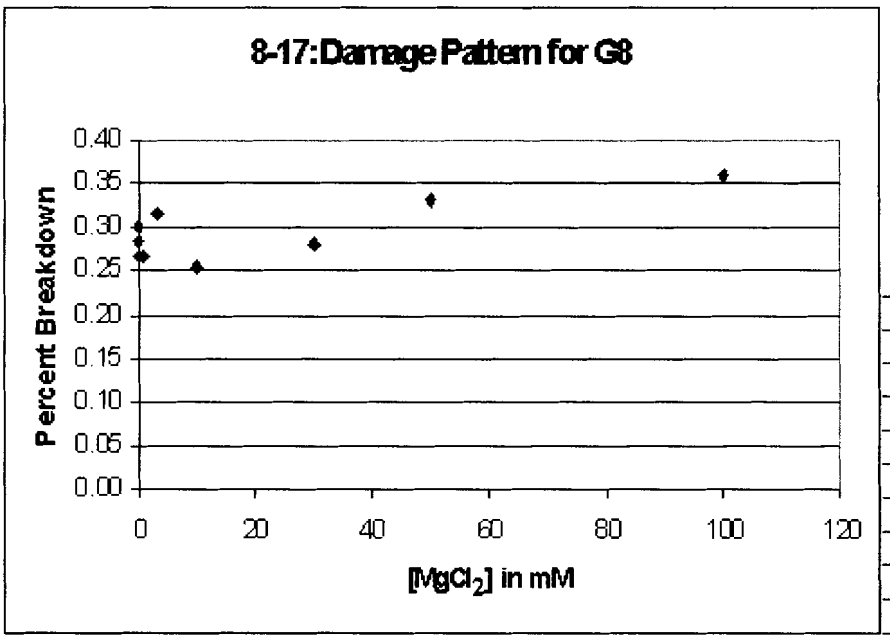

Damage for G8	
[$MgCl_2$] mM	% BrkDwn
0	0.27
0.010	0.30
0.10	0.28
1.0	0.27
3.0	0.32
10	0.25
30	0.28
50	0.33
100	0.36

Figure 2-36 Graphical representation outlining the damage patterns for G8 in the 8-17 DNAzyme. Reported signals contain 5% error.

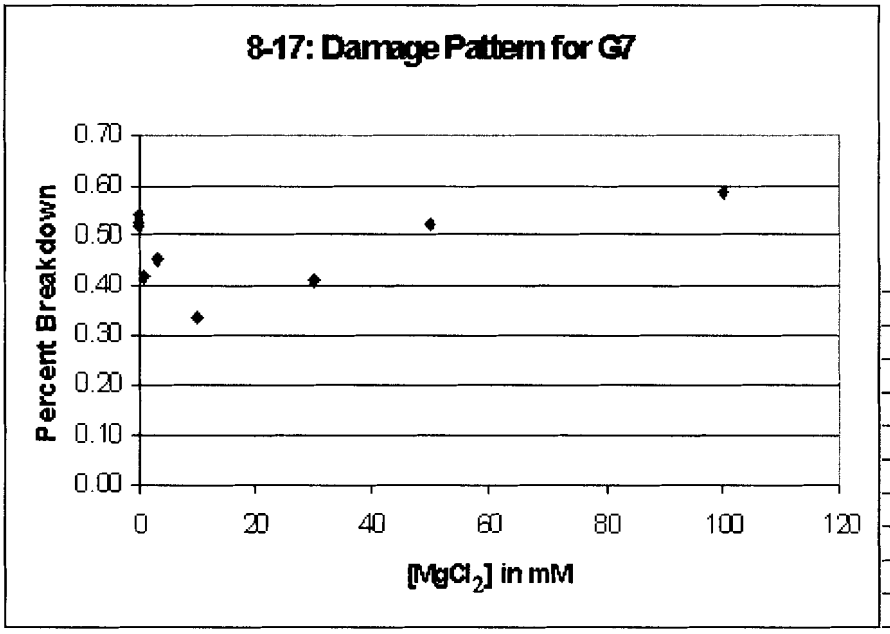

Damage for G7	
$[MgCl_2]$ mM	% BrkDwn
0	0.53
0.010	0.54
0.10	0.52
1.0	0.42
3.0	0.45
10	0.34
30	0.41
50	0.52
100	0.59

Figure 2-37 Graphical representation outlining the damage patterns for G7 in the 8-17 DNAzyme. Reported signals contain 5% error.

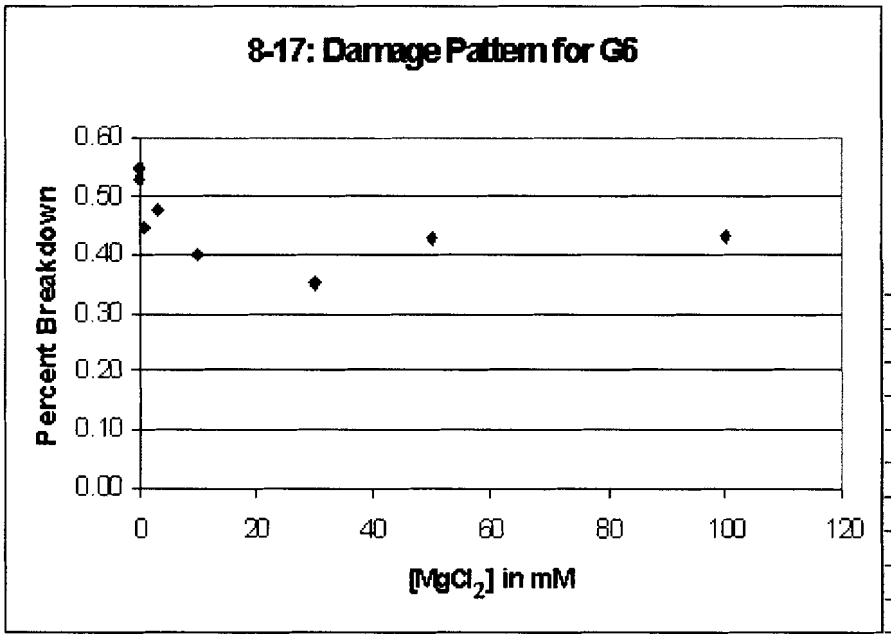

Damage for G6	
$[MgCl_2]$ mM	% BrkDwn
0	0.54
0.010	0.55
0.10	0.53
1.0	0.45
3.0	0.48
10	0.40
30	0.35
50	0.43
100	0.43

Figure 2-38 Graphical representation outlining the damage patterns for G6 in the 8-17 DNAzyme. Reported signals contain 5% error.

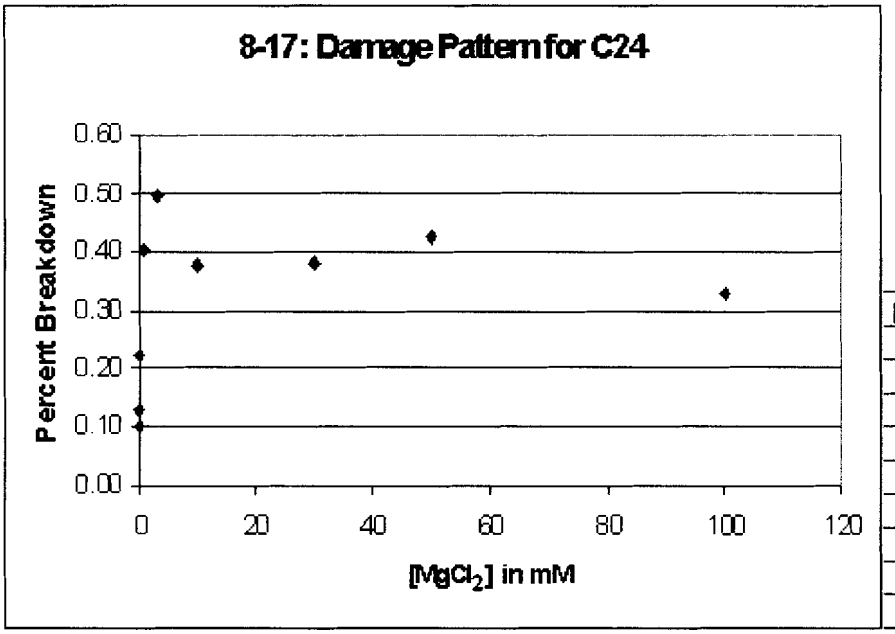

Damage for C24	
[$MgCl_2$] mM	% BrkDwn
0	0.13
0.010	0.10
0.10	0.22
1.0	0.40
3.0	0.50
10	0.38
30	0.38
50	0.42
100	0.33

Figure 2-39 Graphical representation outlining the damage patterns for C24 in the 8-17 DNAzyme. Reported signals contain 5% error.

Another interesting phenomenon is the reactivity of not a guanine but a cytosine in the four base loop between the AQ stem and the catalytic core. This nucleotide, C24, shows the reverse effect in reactivity of all the guanines. For C24, a sharp increase in reactivity is seen from concentrations of 0 to 3.0 mM magnesium, after which, the reactivity stabilizes and does not change appreciably from concentrations of 10 to 100 mM. This is also in agreement with the model proposed by Liu and Lu of a FRET study on 8-17 (Figure 2-40) (Liu and Lu 2002). C24 is situated in the four base bulge between the AQ stem and the catalytic core. In the model presented by Liu and Lu, when the DNAzyme reaches its folded form the four base bulge is directly in-line with the AQ-stem. This unique local conformation of the DNAzyme is thought to permit oxidative damage to a nucleotide having a significantly higher reduction potential than guanine (for C, reduction potential is 1.6 V, where as G is 1.29 V).

This switch in reactivity for this nucleotide (at approximately 3.0 mM) implies a significant structural reorganization. In this case, the reorganization about C24 increases its electron donating ability such that it is able to be damaged; this is consistent with the model proposed by Liu and Lu. This switch in reactivity of key nucleotides at a particular concentration of magnesium was also observed in the Bipartite DNAzyme, particularly for nucleotides G16 and G27.

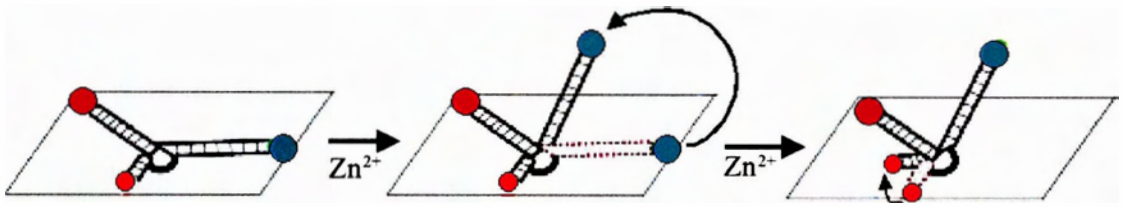

Figure 2-40 FRET model of the 8-17 DNA enzyme. Figure is based on (Liu and Lu 2002). This schematic demonstrates a two-step folding process in the presence of the divalent cation zinc. The magnitude of the conformational change in this DNAzyme reflects the damage patterns of oxidative damage where in place of the green fluorophor, the AQ moiety is covalently tethered.

In all of these experiments, although the magnitude of the damage is not very large, the fluctuations are real effects, as the same trends were observed in three replicate experiments. The extent to which any of the nitrogenous bases in a DNA duplex get oxidized in a stacked DNA molecule depend on many factors, one of these, is its electron donating character, or reduction potential. The unique reduction potential for any given base depends on its local spatial arrangement relative to its neighbouring bases. Changing the local electron density would make a base relatively more oxidizable or more reducible depending on its environment. The unique three-dimensional structure of an enzymatic core provides the nitrogenous bases of DNA with more structural freedom to interact with each other in a non-canonical fashion, giving such bases distinct characteristics from those found in regular duplex DNA. An example of this phenomenon are the diverse tasks that nucleic acid enzymes can accomplish, such as

porphyrin metallation (Li and Sen 1996), and the use of relatively low energy light to repair thymine dimers (Chinnapen and Sen 2004).

It is difficult as yet to solidly ascertain structural information from these patterns, especially for guanines like 16 and 27 in the bipartite enzymatic core and cytosine 24 in the 8-17 enzymatic core, as there needs to be a set of rules established to correlate a damage pattern with a structural feature in a complexly folded nucleic acid molecule. Although it would be a long systematic task to ultimately create a library of structural information based on oxidative damage patterns in DNA, it would serve as a very informative and economical method to discern complex nucleic acid structures. A starting point would be to look at solved nucleic acid crystal structures, FRET models, or NMR structures and compare them with the oxidative damage patterns caused by charge transport. Once rules are established to correlate a structural motif to a damage pattern in DNA, this would serve as very quick and practical method to study the structure of three-dimensional nucleic acid molecules in contrast to the time consuming, low yielding crystallography methods.

In addition, it is important to note that the reactivity of C24 occurs as ionic strength conditions are increased and also occurs below a G residue on a given gel (Figure 2-26 above). These are the same conditions that "trailing bands" appear on other probing gels such as the one for the argininamide titration (Figure 2-10 above). It is possible to argue that since oxidative damage is targeted to these guanines, as the amount of cognate ligand is increased (ArgA), more of the population of the deoxyribosensor will have a conformation where the AQ- stem and detector stem are stacking. This translates into more piperidine labile product being produced at the guanines in the detector stem.

The trailing bands could then be due to partially digested damaged guanines having a different mobility than a cleaved guanine and are perceived as artifacts. Thus it is possible that the reactivity of C24 in Figure 2-26 could be an artifact of gel mobility resulting from G modification. The main difference between the artifacts and C24 is that C24's position on the electrophoretic gel matches up with the position of C24 on the C+T ladders and is a sharp distinct prominent band. This is in contrast the artifact "trailing-bands" which are less well defined. To resolve the issue of whether the reactivity of C24 is a real effect more experimental evidence would be necessary. A key experiment would be to substitute G25 with different nucleobases and observe the reactivity of C24. This would ultimately confirm whether C24 reactivity is genuine and not an artifact.

Table 2-10 Quantitation for the 8-17 DNAzyme showing the relative damage to all its guanine residues and cytosine residue.

8–17	Percent Breakdown at Indicated Magnesium Concentration (mM)								
Guanine	0	0.010	0.10	1.0	3.0	10	30	50	100
30	0.70	0.63	0.50	0.55	0.78	0.44	0.48	0.48	0.41
28	0.68	0.66	0.54	0.41	0.49	0.35	0.39	0.44	0.37
25	0.86	0.77	0.78	0.68	0.78	0.62	0.63	0.58	0.51
C24	0.13	0.10	0.22	0.40	0.50	0.38	0.38	0.42	0.33
22	0.23	0.19	0.23	0.21	0.26	0.14	0.15	0.16	0.13
21	0.71	0.60	0.69	0.51	0.49	0.29	0.24	0.27	0.21
18	0.53	0.50	0.55	0.52	0.54	0.43	0.39	0.45	0.40
16	0.23	0.25	0.23	0.23	0.27	0.22	0.21	0.26	0.22
12	0.93	0.92	0.79	0.45	0.42	0.39	0.38	0.40	0.41
10	0.27	0.31	0.29	0.27	0.35	0.28	0.30	0.38	0.36
8	0.27	0.30	0.28	0.27	0.32	0.25	0.28	0.33	0.36
7	0.53	0.54	0.52	0.42	0.45	0.34	0.41	0.52	0.59
6	0.54	0.55	0.53	0.45	0.48	0.40	0.35	0.43	0.43

CHAPTER 3: CONCLUSIONS

Here we have presented data that shows the general utility of deoxyribosensors for monitoring different small-molecule species. Previous work by Fahlman and Sen (2001) we had described an "integrated" and "coupled" deoxyribosensors for sensing the electrically neutral analyte adenosine (which, being a nucleoside, π-stacks efficiently within the aptamer element (Lin and Patel 1997) and permits charge conduction through itself), here we have demonstrated that the more versatile "coupled" deoxyribosensor design can be used to sense a positively charged amino acid derivative, argininamide, specifically and efficiently. The specificity and the efficiency of our deoxyribosensors generally reflect the corresponding properties of the aptamer used in the sensor. Therefore, newer generations of higher affinity and higher specificity aptamers (whether made of DNA, RNA, or polypeptides) should give rise to correspondingly more sensitive deoxyribosensors.

In attempts to diversify the specificity of the working deoxyribosensor described here (ArgA 2.01), we have replaced the aptamer region specific for argininamide for one specific for Theophylline. In this set of experiments, the Theo 1.0 or the Thru Theo 1.0 constructs did not give desired results. It appeared that no charge transport was occurring in the detector stems of both of these constructs as well as in the aptamer region made of RNA. Due to the nature of the chimeric constructs, damage in the AQ stem could not be visualized. It is suspected that most of the oxidative damage could be occurring in the AQ stem as the RNA region may provide a barrier for charge transport.

Nevertheless, we have monitored charge-transfer generated damage at specific guanine residues to quantify charge conduction within specific DNA elements in the different deoxyribosensors; however, the eventual utility of such sensors will be realized within chip-based technologies, where changes in current flow in response to ligand binding can be measured directly and rapidly, in contrast to the rather cumbersome biochemical detection methods detailed here. Such methodologies might involve the placement of the sensor constructs between nanofabricated electrodes, or the electrochemical measurement, in self assembled monolayers, of the deoxyribosensors (assembled in the presence of an excess of long chain alkyl sulfides). Figure 3-1 illustrates an aspect of the potential versatility of the deoxyribosensors described here, using the self-assembled monolayer methodology. Although all our sensor constructs designated a detector stem within them (such as shown in Figure 3-1), where changes in current flow would be monitored, our guanine-by guanine analysis reported here suggests that in many of the constructs, an optimal and ligand specific "signal" can be obtained from guanine residues not necessarily located in the detector stem (for instance, at G30 in the ArgA 1.3 construct; this guanine residue is located in the AQ stem, flanking the junction itself). It may be possible to monitor oxidation-reduction potentials at sites such as G30 by connecting residues such as this, via short alkyl linkers, to the conductive gold surface of a chip (shown schematically in Figure 3-1) to get indications of conductivity.

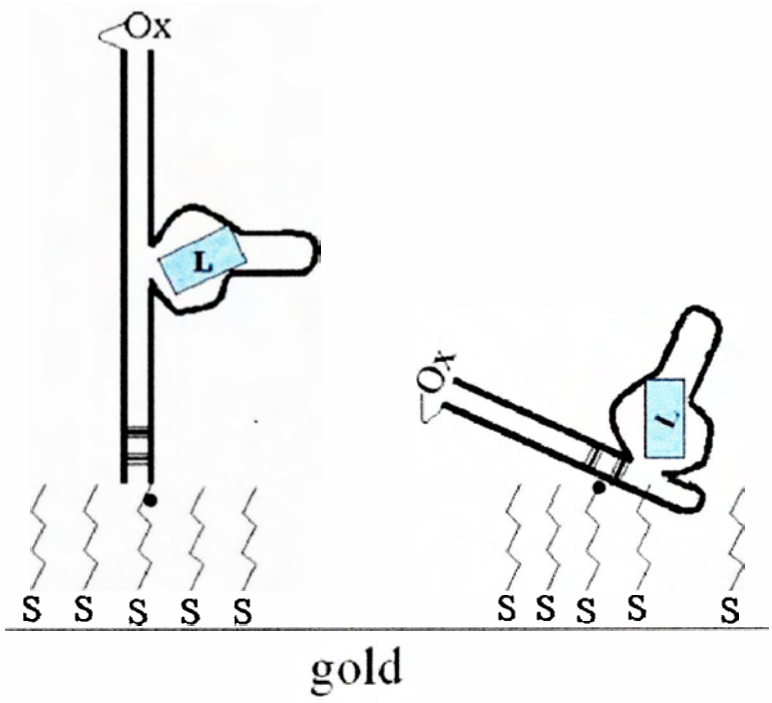

Figure 3-1 A schematic showing two possible modes of attachment of a deoxyribosensor to the conductive surface of a chip (indicated as gold). Ox refers to a tethered redox-active species to initiate charge transfer. Left: this mode would permit the monitoring of charge flow in the designated detector arm of the sensor; however, charge flow through specific guanine residues at other locations in the sensor could be monitored by direct attachment of such guanine residues to the conductive surface (right).

Future work on new deoxyribosensors should focus on further optimization and standardization of the design features of three-way junction based, or coupled-ligand deoxyribosensors. One of the challenges that remain at this stage is the lowering of background (i.e. in the absence of bound ligand) signals in some of these sensors. We have investigated an approach where an interfering oligomer disrupts the initial sensor structure in attempts to lower the background signal. The interfering oligomer had reduced the background signal quite significantly (about 1/3), but it also had lowered the response signal, giving undesired results. Ultimately, *in vitro* selection experiments from partially randomized deoxyribosensor pools will be carried out to obtain directly sensors for defined analyte molecules, especially for molecules for which DNA, RNA, or peptide aptamers have not already been selected.

One of the most promising aspects of charge transport in DNA is its use as a tool to discern complex DNA structures. More specifically, their use to discern helical arm stacking partners in unresolved 3 dimensional DNA structures. We have performed preliminary experiments on two DNA enzymes yielding promising results. In the Bipartite DNAzyme, a switch in reactivity is observed for guanines 16 and 27 in the conserved catalytic loop between the concentrations of 0.10 and 1.0 mM Magnesium. This implies that in this range of magnesium concentrations, the enzyme must undergo a gross structural change. For Bipartite we have discerned that regardless of magnesium concentration, the GGG containing arm is not in enough electronic overlap with the AQ containing stem as to produce oxidative damage to the guanines situated there. For the 8-17 DNAzyme we have obtained results that resemble those of a FRET study on the structure of 8-17. In the presence of very little or no magnesium, 8-17 adopts a conformation such that both the GGG containing stem and the enzymatic core exhibit some degree of stacking with the AQ- containing stem. When 8-17 reaches its mature folded state, the GGG containing arm and the catalytic loop become out of electronic overlap and this is reflected in the attenuated damage patterns observed by gel electrophoresis.

A huge potential exists here for exploring unresolved nucleic acid structures by interpreting the oxidative damage patterns left on the DNA. Future experiments should aim at establishing a set of rules to correlate a certain damage pattern in DNA with a structural motif. One approach would investigate the damage patterns produced in structurally characterized nucleic acid molecules and compare them with their known three-dimensional structures. In this way, some rules or a library of structural

information based on oxidative damage patterns in DNA could be created. This would serve as a very quick and practical technique to study the three-dimensional structure of nucleic acid molecules in solution in contrast to the time consuming crystallographic methods, which address solid-state structures.

Although this method of exploring unresolved nucleic acid structures has a lot of promise there are certainly foreseeable limitations. For instance, the work shown in this thesis only outlines the use of charge transfer for discerning helical arm stacking partners and not for exploring fine local structure of complexly folded nucleic acids. This limits the "resolution" and the type of the structure that one is trying to study, to a level where only structures containing helical arms can be studied. Limitations may also exist on size of the DNA structure one is trying to study, the bigger and longer a DNA molecule becomes, the electron transfer process becomes less efficient and the DNA structure also becomes more dynamic. Structures being studied must contain at least one helical stem for the purpose of injecting the radical cation from the photo activated AQ moiety. Also, it is important to be able to assess which nucleic acid structures would be good candidates for probing in this manner; since charge transfer through DNA highly depends on π-orbital overlap and base stacking, the higher the degree of unpredictable folding or regions of single stranded character may impede the radical cation from being able to migrate from the injecting helical arm. The more ambiguous the nucleic acid structure is, the greater chance that it would contain a low degree of π-orbital overlap from region to region, thus reducing the chance that one would be able to see appreciable oxidative damage due to charge transport.

Although certain criteria must be present for studying nucleic acid structures in this fashion, it is these very constraints on charge transport through DNA that generate the distinctive damage patterns for a particular structure. More research is required to understand the intricacies of using this method to discern fine local conformations of nucleic acid structures. As a starting point, the structure of a DNA hairpin with a 4 base loop (tetra loop) can be studied for fine local structure by systematically varying the identity of the bases in the loop. Correlating the changes in base sequence to changes in damage patterns would then start to unveil the potential of this technique for studying nucleic acid structure.

REFERENCES

Anderson, R. and G. Wright (1999). "Energetics and rate of electron transfer in DNA from base radical anions to electron-affinic intercalators in aqueous solution." Phys. Chem. Chem. Phys. **1**: 4827-31.

Basti, M. M., J. W. Stuart, et al. (1996). "Design, biological activity and NMR-solution structure of a DNA analogue of yeast tRNA(Phe) anticodon domain." Nat Struct Biol **3**(1): 38-44.

Beveridge, D. L. and K. J. McConnell (2000). "Nucleic acids: theory and computer simulation, Y2K." Curr Opin Struct Biol **10**(2): 182-96.

Boone, E. and G. B. Schuster (2002). "Long-range oxidative damage in duplex DNA: the effect of bulged G in a G-C tract and tandem G/A mispairs." Nucleic Acids Res **30**(3): 830-7.

Braun, E., Y. Eichen, et al. (1998). "DNA-templated assembly and electrode attachment of a conducting silver wire." Nature **391**(6669): 775-8.

Burrows, C. J. and J. G. Muller (1998). "Oxidative Nucleobase Modifications Leading to Strand Scission." Chem Rev **98**(3): 1109-1152.

Cadet, J., M. Berger, et al. (1997). "Oxidative damage to DNA: formation, measurement, and biological significance." Rev Physiol Biochem Pharmacol **131**: 1-87.

Camerini-Otero, R. D. and P. Hsieh (1993). "Parallel DNA triplexes, homologous recombination, and other homology-dependent DNA interactions." Cell **73**(2): 217-23.

Chinnapen, D. J. and D. Sen (2004). "A deoxyribozyme that harnesses light to repair thymine dimers in DNA." Proc Natl Acad Sci U S A **101**(1): 65-9.

Debije, M. G., M. T. Milano, et al. (1999). "DNA Responds to Ionizing Radiation as an Insulator, Not as a "Molecular Wire"." Angew Chem Int Ed Engl **38**(18): 2752-2756.

Delaney, S. and J. K. Barton (2003). "Long-range DNA charge transport." J Org Chem **68**(17): 6475-83.

Duarte, V., D. Gasparutto, et al. (2001). "Repair and mutagenic potential of oxaluric acid, a major product of singlet oxygen-mediated oxidation of 8-oxo-7,8-dihydroguanine." Chem Res Toxicol **14**(1): 46-53.

Duarte, V., J. G. Muller, et al. (1999). "Insertion of dGMP and dAMP during in vitro DNA synthesis opposite an oxidized form of 7,8-dihydro-8-oxoguanine." Nucleic Acids Res **27**(2): 496-502.

Duckett, D. R. and D. M. Lilley (1990). "The three-way DNA junction is a Y-shaped molecule in which there is no helix-helix stacking." Embo J **9**(5): 1659-64.

Eley, D. D. and D. I. Spivey (1962). "Semiconductivity of organic substances. IX. Nucleic acid in the dry state." Transactions of the Faraday Society **58**: 411-415.

Fahlman, R. P. and D. Sen (2001). "DNA Conformational Switches as Sensitive Electronic Sensors of Analytes." J Am Chem Soc **124**: 4610-16.

Feldman, A. R. and D. Sen (2001). "A new and efficient DNA enzyme for the sequence-specific cleavage of RNA." J Mol Biol **313**(2): 283-94.

Fink, H. W. and C. Schonenberger (1999). "Electrical conduction through DNA molecules." Nature **398**(6726): 407-10.

Gasper, S. M. and G. B. Schuster (1997). "Intramolecular Photoinduced Electron Transfer to Anthraquinones Linked to Duplex DNA: The Effect of Gaps and Traps on Long-Range Radical Cation Migration." J Am Chem Soc **119**: 12762-71.

Giese, B. (2000). "Long-distance charge transport in DNA: the hopping mechanism." Acc Chem Res **33**(9): 631-6.

Giese, B. (2002). "Electron transfer in DNA." Curr Opin Chem Biol **6**(5): 612-8.

Giese, B. (2002). "Long-distance electron transfer through DNA." Annu Rev Biochem **71**: 51-70.

Giese, B., J. Amaudrut, et al. (2001). "Direct observation of hole transfer through DNA by hopping between adenine bases and by tunnelling." Nature **412**(6844): 318-20.

Giese, B., S. Wessely, et al. (1999). "On the Mechanism of Long-Range Electron Transfer through DNA." Angewandte Chemie International Edition **38**(7): 996-998.

Gold, L., B. Polisky, et al. (1995). "Diversity of oligonucleotide functions." Annu Rev Biochem **64**: 763-97.

Grinstaff, M. W. (1999). "How Do Charges Travel through DNA?-An Update on a Current Debate." Angew Chem Int Ed Engl **38**(24): 3629-3635.

Hagerman, P. J. (1988). "Flexibility of DNA." Annu Rev Biophys Biophys Chem **17**: 265-86.

Harada, K. and A. D. Frankel (1995). "Identification of two novel arginine binding DNAs." Embo J **14**(23): 5798-811.

Hendeles, L. and M. Weinberger (1983). "Theophylline. A "state of the art" review." Pharmacotherapy **3**(1): 2-44.

Herbert, A. and A. Rich (1999). "Left-handed Z-DNA: structure and function." Genetica **106**(1-2): 37-47.

Hermann, T. and D. J. Patel (2000). "Adaptive recognition by nucleic acid aptamers." Science **287**(5454): 820-5.

Huizenga, D. E. and J. W. Szostak (1995). "A DNA aptamer that binds adenosine and ATP." Biochemistry **34**(2): 656-65.

Jenison, R. D., S. C. Gill, et al. (1994). "High-resolution molecular discrimination by RNA." Science **263**(5152): 1425-9.

Jortner, J., M. Bixon, et al. (1998). "Charge transfer and transport in DNA." Proc Natl Acad Sci U S A **95**(22): 12759-65.

Kan, Y. and G. B. Schuster (1999). "Long-Range Guanine Damage in Single-Stranded DNA: Charge Transport through a Duplex Bridge and in a Single-Stranded Overhang." J Am Chem Soc **121**: 10857-64.

Kino, K., I. Saito, et al. (1998). "Product Analysis of GG-Specific Photooxidation of DNA via Electron Transfer: 2-Aminoimidazolone as a Major Guanine Oxidation Product." J Am Chem Soc **120**: 7373-74.

Kino, K. and H. Sugiyama (2001). "Possible cause of G-C-->C-G transversion mutation by guanine oxidation product, imidazolone." Chem Biol **8**(4): 369-78.

Leontis, N. B., W. Kwok, et al. (1991). "Stability and structure of three-way DNA junctions containing unpaired nucleotides." Nucleic Acids Res **19**(4): 759-66.

Li, Y. and D. Sen (1996). "A catalytic DNA for porphyrin metallation." Nat Struct Biol **3**(9): 743-7.

Lilley, D. M. (1995). "Kinking of DNA and RNA by base bulges." Proc Natl Acad Sci U S A **92**(16): 7140-2.

Lilley, D. M. (2000). "Structures of helical junctions in nucleic acids." Q Rev Biophys **33**(2): 109-59.

Lin, C. H. and D. J. Patel (1997). "Structural basis of DNA folding and recognition in an AMP-DNA aptamer complex: distinct architectures but common recognition motifs for DNA and RNA aptamers complexed to AMP." Chem Biol **4**(11): 817-32.

Liu, C. S., R. Hernandez, et al. (2004). "Mechanism for radical cation transport in duplex DNA oligonucleotides." J Am Chem Soc **126**(9): 2877-84.

Liu, J. and Y. Lu (2002). "FRET study of a trifluorophore-labeled DNAzyme." J Am Chem Soc **124**(51): 15208-16.

Lu, M., Q. Guo, et al. (1991). "Effect of sequence on the structure of three-arm DNA junctions." Biochemistry **30**(24): 5815-20.

Mandal, M., B. Boese, et al. (2003). "Riboswitches control fundamental biochemical pathways in Bacillus subtilis and other bacteria." Cell **113**(5): 577-86.

Mao, C., W. Sun, et al. (1999). "A nanomechanical device based on the B-Z transition of DNA." Nature **397**(6715): 144-6.

Meggers, E., M. E. Michel-Beyerle, et al. (1998). "Sequence Dependent Long Range Hole Transport in DNA." J. Am. Chem. Soc. **120**: 12950-55.

Mirkin, C. A., R. L. Letsinger, et al. (1996). "A DNA-based method for rationally assembling nanoparticles into macroscopic materials." Nature **382**(6592): 607-9.

Murphy, C. J., M. R. Arkin, et al. (1993). "Long-range photoinduced electron transfer through a DNA helix." Science **262**(5136): 1025-9.

Osborne, S. E. and A. D. Ellington (1997). "Nucleic Acid Selection and the Challenge of Combinatorial Chemistry." Chem Rev **97**(2): 349-370.

Paukstelis, P. J., J. Nowakowski, et al. (2004). "Crystal structure of a continuous three-dimensional DNA lattice." Chem Biol **11**(8): 1119-26.

Peattie, D. A. (1979). "Direct chemical method for sequencing RNA." Proc Natl Acad Sci U S A **76**(4): 1760-4.

Razskazovskii, Y., S. G. Swarts, et al. (1997). "Competitive Electron Scavenging by Chemically Modified Pyrimidine Bases in Bromine-Doped DNA: Relative Efficiencies and Relevance to Intrastrand Electron Migration Distances." J. Phys. Chem. B. **101**: 1460-67.

Robertson, S. A., K. Harada, et al. (2000). "Structure determination and binding kinetics of a DNA aptamer-argininamide complex." Biochemistry **39**(5): 946-54.

Saito, I., T. Nakamura, et al. (1998). "Mapping of the hot spots for DNA damage by one-electron oxidation: Efficacy of GG doublets and GGG triplets as a trap in long-range hole migration." Journal of the American Chemical Society **120**(48): 12686-12687.

Saito, I., M. Takayama, et al. (1995). "Photoinduced DNA Cleavage Via Electron-Transfer - Demonstration That Guanine Residues Located 5' to Guanine Are the Most Electron-Donating Sites." Journal of the American Chemical Society **117**(23): 6406-6407.

Sanii, L. and G. B. Schuster (2000). "Long-Distance Charge Transport in DNA: Sequence-Dependent Radical Cation Injection Efficiency." J. Am. Chem. Soc. **122**: 11545-46.

Sankar, C. G. and D. Sen (2004). "DNA helix-stack switching as the basis for the design of versatile deoxyribosensors." J Mol Biol **340**(3): 459-67.

Santini, G. P., C. Pakleza, et al. (2003). "DNA tri- and tetra-loops and RNA tetra-loops hairpins fold as elastic biopolymer chains in agreement with PDB coordinates." Nucleic Acids Res **31**(3): 1086-96.

Santoro, S. W. and G. F. Joyce (1997). "A general purpose RNA-cleaving DNA enzyme." Proc Natl Acad Sci U S A **94**(9): 4262-6.

Sartor, V., P. T. Henderson, et al. (1999). "Radical Cation Transport and Reaction in RNA/DNA Hybrid Duplexes: Effect of Global Structure on Reactivity." J Am Chem Soc **121**(48): 11027-11033.

Sassanfar, M. and J. W. Szostak (1993). "An RNA motif that binds ATP." Nature **364**(6437): 550-3.

Schuster, G. B. (2000). "Long-range charge transfer in DNA: transient structural distortions control the distance dependence." Acc Chem Res **33**(4): 253-60.

Schwögler, A., L. Burgdorf, et al. (2000). "Self-Repairing DNA Based on a Reductive Electron Transfer through the Base Stack." Angewandte Chemie International Edition **39**(21): 3918-20.

Seeman, N. C. (1999). "DNA engineering and its application to nanotechnology." Trends Biotechnol **17**(11): 437-43.

Seeman, N. C. (2003). "At the crossroads of chemistry, biology, and materials: structural DNA nanotechnology." Chem Biol **10**(12): 1151-9.

Seeman, N. C. (2003). "DNA in a material world." Nature **421**(6921): 427-31.

Seidel, C. A. M., A. Schulz, et al. (1996). "Nucleobase-Specific Quenching of Fluorescent Dyes. 1. Nucleobase One-Electron Redox Potentials and Their Correlation with Static and Dynamic Quenching Efficiencies." J. Phys. Chem. **100**: 5541-53.

Sheu, C. and C. S. Foote (1995). "Reactivity toward Singlet Oxygen of a 7,8-Dihydro-8-oxoguanosine ("8-Hydroxyguanosine") Formed by Photooxidation of a Guanosine Derivative." J Am Chem Soc **117**: 6439-42.

Shibutani, S., M. Takeshita, et al. (1991). "Insertion of Specific Bases During DNA-Synthesis Past the Oxidation-Damaged Base 8-Oxodg." Nature **349**(6308): 431-434.

Soukup, G. A. and R. R. Breaker (2000). "Allosteric nucleic acid catalysts." Curr Opin Struct Biol **10**(3): 318-25.

Steenken, S. and S. V. Jovanovic (1997). "How Easily Oxidizable Is DNA? One-Electron Reduction Potentials of Adenosine and Guanosine Radicals in Aqueous Solution." J. Am. Chem. Soc. **119**: 617-18.

Stuhmeier, F., J. B. Welch, et al. (1997). "Global structure of three-way DNA junctions with and without additional unpaired bases: a fluorescence resonance energy transfer analysis." Biochemistry **36**(44): 13530-8.

Sugiyama, H. and I. Saito (1996). "Theoretical studies of GC-specific photocleavage of DNA via electron transfer: Significant lowering of ionization potential and 5'-localization of HOMO of stacked GG bases in B-form DNA." Journal of the American Chemical Society **118**(30): 7063-7068.

Travascio, P., A. J. Bennet, et al. (1999). "A ribozyme and a catalytic DNA with peroxidase activity: active sites versus cofactor-binding sites." Chem Biol **6**(11): 779-87.

Turro, N. and J. K. Barton (1998). "Paradigms, supermolecules, electron transfer and chemistry at a distance. What's the problem? The science or the paradigm?" Journal of Biological Inorganic Chemistry **3**(2): 201 - 209.

van Buuren, B. N., F. J. Overmars, et al. (2000). "Solution structure of a DNA three-way junction containing two unpaired thymidine bases. Identification of sequence features that decide conformer selection." J Mol Biol **304**(3): 371-83.

Watson, J. D. and F. H. Crick (1953). "Molecular structure of nucleic acids; a structure for deoxyribose nucleic acid." Nature **171**(4356): 737-8.

Welch, J. B., D. R. Duckett, et al. (1993). "Structures of bulged three-way DNA junctions." Nucleic Acids Res **21**(19): 4548-55.

Welch, J. B., F. Walter, et al. (1995). "Two inequivalent folding isomers of the three-way DNA junction with unpaired bases: sequence-dependence of the folded conformation." J Mol Biol **251**(4): 507-19.